UNIVERSITA' DI PADOVA FACOLTA' DI INGEGNERIA

Dipartimento di Ingegneria dell'Informazione

Scuola di Dottorato di Ricerca in Ingegneria dell'Informazione
Indirizzo: Bioingegneria

Ciclo XX

PET PARAMETRIC IMAGING OF ACETYLCHOLINE ESTERASE ACTIVITY WITHOUT ARTERIAL BLOOD SAMPLING IN NORMAL SUBJECTS AND PATIENTS WITH NEURODEGENERATIVE DISEASE

Dottorando: Ioana Florea

Supervisori: Ch.mo Prof. Claudio Cobelli
Ch.mo Prof. Maria Carla Gilardi

Direttore della Scuola: Ch.mo Prof. Silvano Pupolin

Gennaio 2008

To my family

"From the brain and the brain alone arise our pleasures, joys, laughter and jests, as well as our sorrows, pains and griefs"

(Hippocrates)

Contents

List of Figures

List of Tables

Summary

Assessment of the integrity of the cortical cholinergic system is of primary interest in dementia because of its crucial role for memory and attention.

The use of PET (Positron Emission Tomography) and tracers that are hydrolysed specifically by acetylcholine esterase (AChE) permits measurement and imaging of local AChE activity in humans. Carbon-11-labelled *N*-methyl-4 piperidyl-acetate (^{11}C-MP4A) is a PET tracer that is highly specific for AChE and has kinetic properties that are favorable for measuring cortical AChE activity. Kinetic analysis of these images provides the quantification of AChE activity; the analysis can be performed both at pixel and region of interest (ROI) level.

The standard method to estimate regional hydrolysis rate of ^{11}C-MP4A by AChE is to identify by nonlinear least squares (NLLS) the parameter estimates of the model using the arterial concentration of tracer as input function. However, the measurement of the arterial input function is an invasive procedure for the patients and requires considerable technical expertise, which may restrict widespread use of this method in daily clinical practice. To overcome this drawback, in the last years, different methods have been proposed for non-invasive quantification of AChE activity at region of interest level: shape analysis, firstly proposed by Koeppe et al.; reference tissue linear least squares (RLS) proposed by Nagatsuka et al. (2001); reference ratio exponential (RRE) approach proposed by Herholz and coworkers in 2001. Nevertheless, only few attempts have been made in order to quantify no invasively AChE activity at pixel level: Zundorf et al. in 2002 which implemented a basis function approach (RRE_BF) to Herholz technique in

order to reduce unnecessary bias, while estimating the parameters of interest. The methods available in literature, based on reference region input, do not consider the reliability and the accuracy of all the parameter estimates.

The purpose of this study is to propose and develop a Bayesian method, based on maximum *a posteriori* information (MAP), to quantify ^{11}C-MP4A activity at pixel level in patients with neurodegenerative diseases and in normal subjects. The main goal is to accurately estimate AChE activity in brain regions with low (neocortex) and moderate (thalamus) enzymatic expression taking into account the reliability of all estimates. Bayesian estimator allows to quantify model parameters maximizing the conditional probability of data given parameters: it uses information contained in the data, the so called *a posteriori* information and consider also *a priori* probability information of all or some of the parameters. In our study, *a priori* information is obtained for each subject who participates at the study from a preliminary reference weighted non linear least squares (R_NLLS) analysis implemented at ROI level. R_NLLS analysis, as already confirmed by the literature, evidences a low inter-region variability within subject of the parameter that characterize the unmetabolized tracer washout from tissue to blood. Therefore, it can be assumed that this parameter has *a priori* a Gaussian probability density function with mean and standard deviation obtained from R_NLLS at ROI level. This additional probabilistic information is used to estimate tracer kinetic indexes at pixel level applying MAP procedure to PET dynamic images.

Another intent of this work is to compare the performance of the Bayesian estimator with the other few methods already propose in the literature for AChE activity quantification implemented at pixel level. The comparison between methods is based on the precision of estimates.

A new method for an automatic extraction of ROIs is also proposed in this study. Automatic extraction is preferred to the often used manual technique: first, because of the lack of subjects MRI scans that are usually

used as anatomical reference in identifying brain regions of interest; second, in order to avoid errors sampling during a manual position of ROIs on the dynamic or parametric ^{11}C-MP4A PET images.

Bayesian method, as well as already published methods, is based on the same compartmental model that describes tracer kinetics: reference region described by one tissue-one rate constant, while the target tissue is described by a two tissue compartment - three rate constant model. This kinetic model is actually considered the best model to quantify ^{11}C-MP4A data. AChE activity is measured in terms of the rate constant for hydrolysis of ^{11}C-MP4A, k_3. Striatum (basal ganglia) is chose as reference structure to be used as input function for all models, because of its very high AChE activity. All methods have been applied at both pixel and ROI level (except for RRE_BF proposed only for pixel level). Only estimates with good precision are accepted for the comparison study. The consistence of estimates obtained by each mathematical approach for both analysis levels is also investigated.

The automatic extraction of anatomical areas and the comparison study of the different methodologies for AChE activity quantification at pixel level confirm that in cortex area with low enzyme activity the models have similar performance. However, for RRE and RRE_BF approaches inaccurate estimates of the parameter that describes the unmetabolized tracer washout from tissue to blood is observed. Thus, in order to have only reliable estimates for these two methods, a threshold of inaccurate parameter was calculated for each PET study and applied as acceptability condition for estimates. Anyway, this correction does not improve RRE_BF performance. However, from computational point of view, RLS linear calculation is faster for pixel by pixel parameter estimation respect to non linear quantification methods (R-NLLS, MAP) and the results are in good agreement with published neocortex values.

On the contrary, RLS approach shows some difficulties in estimating k_3 index in area with moderate enzyme activity, such as thalamus and brainstem. The use of Bayesian (MAP) estimator helps to

overcome these drawbacks and allows the quantification of AChE activity in regions with moderate enzyme expression, like thalamus and brainstem. At pixel level, this procedure presents results consistent with the scientific literature. MAP technique is more time consuming respect to the other methods because it implicates a previous analysis at ROI level in order to obtain the *a priori* information, but improve the precision of estimates. Actually, pixel and ROI estimates obtain applying the Bayesian estimator are more similar respect to the ones obtained with published methods.

In conclusion, MAP method is the best quantification approach, in terms of precision and accuracy, for AChE activity in both area with low and moderate enzyme expression. Pixel level estimates, even if it's a procedure more time consuming, are more reliable because conserve all the information contained in the cortical map respect to the ROI approach where loss of resolution is a major drawback.

An European project finalized to validate on a bigger dataset the best method to be applied to ^{11}C-MP4A/PET images is going to start soon. Its aim will be the confirmation of the clinical applicability of the chosen technique in the discrimination of different neurodegenerative pathologies as AD, Lewy body dementia (DLB), mild cognitive impairment (MCI). MAP procedure as well as another Bayesian method under development will be taken into account. Simulation study based on real plasma input are going to be considered for best method validation.

Sommario

La valutazione dell'integrità del sistema colinergico, considerato il suo ruolo cruciale nei meccanismi cerebrali che regolano la memoria e l'attenzione, è di grande interesse nelle malattie neurodegenerative come la demenza.

L'utilizzo della PET (tomografia ad emissione di positroni) e dei traccianti che sono idrolizzati in modo specifico dall'acetilcolinesterase (AChE) permette di misurare l'attività enzimatica cerebrale *in vivo* nell'uomo. In particolare, il N-metil-4 piperidil-acetato (MP4A) marcato con carbonio 11 (^{11}C) è un tracciante PET molto specifico per AChE ed ha delle proprietà cinetiche che favoriscono lo studio dell'attività corticale dell'AChE. Più precisamente, l'analisi quantitativa delle immagini acquisite tramite PET e ^{11}C-MP4A permette di stimare l'attività dell'AChE in termini di velocità di metabolismo (per idrolisi) del ^{11}C-MP4A; l'analisi può essere effettuata al livello di pixel o al livello di regione di interesse (ROI).

Il metodo standard per la stima dell'attività dell'AChE si basa sull'uso dei minimi quadrati non lineari ed utilizza come funzione d'ingresso la concentrazione plasmatica del tracciante. La misura della concentrazione plasmatica, però, è invasiva, richiede un'ampia esperienza tecnica e costituisce un fattore importante di limitazione all'uso dell'indagine PET con ^{11}C-MP4A nella pratica clinica di routine. Per superare questo inconveniente, negli ultimi anni sono stati proposti vari metodi per la quantificazione non invasiva dell'attività dell'AChE al livello di ROI: la *shape* analisi (SA) proposta da Koeppe et al; il metodo a tessuto

di riferimento proposto da Nagatsuka et al (2001) basato sui minimi quadrati lineari (RLS); il metodo del quoziente esponenziale (RRE) proposto da Herholz e collaboratori (2001). I tentativi di stima dell'attività enzimatica al livello di pixel sono stati, invece, pochi tra cui il più interessante è stato sviluppato e proposto da Zundorf e colleghi nel 2002 (RRE_BF). Comunque, tutti i metodi proposti per la quantificazione senza funzione di ingresso arteriale non prendono in considerazione l'affidabilità e l'accuratezza di tutti parametri stimati.

Uno degli obbiettivi di questo studio è di proporre e sviluppare un nuovo metodo basato sull'utilizzo dello stimatore Bayesiano di probabilità massima *a posteriori* (MAP) per la quantificazione non invasiva al livello di pixel dell'attività enzimatica dell'AChE in individui normali e in soggetti affetti da malattie neurodegenerative. Lo scopo principale è di stimare in modo accurato e preciso l'attività dell'AChE in regioni cerebrali con espressione enzimatica bassa (neocortex) e media (talamo) considerando l'affidabilità di tutti parametri. Lo stimatore MAP utilizza sia le informazioni contenute nei dati – le cosiddette informazioni *a posteriori* – che le informazioni statistiche *a priori* disponibili su alcuni o tutti i parametri incogniti. Nel corso di questo studio, le informazioni *a priori* sono state ricavate per ogni soggetto che ha partecipato allo studio tramite un'analisi preliminare a tessuto di riferimento basata sui minimi quadrati non lineari (R_NLLS) implementata al livello di ROI. L'analisi R_NLLS, come già confermato in letteratura, evidenzia una bassa variazione del parametro che caratterizza l'eliminazione del tracciate non metabolizzato dal tessuto nel sangue. Di conseguenza, questo parametro è stato assunto avere una distribuzione di probabilità Gaussiana *a priori*, con media e deviazione standard pari a quella ottenuta con R_NLLS al livello di ROI. Questa informazione probabilistica addizionale costituisce l'informazione *a priori* fornita allo stimatore MAP.

Un altro obbiettivo di questo studio è rappresentato dalla messa a confronto e selezione del metodo più affidabile per la quantificazione dell'attività corticale.

Per limitare il più possibile gli errori di posizionamento delle ROI sulle immagini dinamiche e/o parametriche e limitare al contempo l'effetto di volume parziale, si è fatto uso di un nuovo metodo automatico disponibile in rete per la generazione di ROI.

Sia il metodo MAP che gli altri metodi considerati si basano sullo stesso modello compartimentale a tessuto di riferimento (due compartimenti tessutali e tre costanti di trasferimento), considerato attualmente il miglior modello per la quantificazione dei dati ^{11}C-MP4A PET. L'attività dell'AChE è stata misurata in termini di costante di trasferimento per l'idrolisi dell'^{11}C-MP4A, k_3. Data l'alta espressione di AChE al livello dello striato (gangli della base), questa regione è stata scelta come regione di riferimento da utilizzare come funzione d'ingresso in tutti gli approcci matematici. Tutti i metodi sono stati applicati sia a livello di ROI che a livello di pixel. Solo i parametri stimati con una buona precisione sono stati considerati per lo studio comparato.

L'estrazione automatica delle ROI e lo studio di confronto tra le varie metodologie matematiche applicate al livello di pixel hanno confermato che in aree con espressione enzimatica bassa la performance dei modelli è simile. Comunque, per i metodi RRE e RRE_BF sono state identificate delle stime non fisiologiche per il parametro che caratterizza il *washout* del tracciante dal tessuto nel sangue. Di conseguenza, per questi due metodi è stato calcolato un valore soglia del parametro tale da considerare solo le stime affidabili. Nonostante questa correzione, l'accuratezza delle stime RRE e RRE_BF non migliora.

Dal punto di vista computazionale, il metodo lineare RLS applicato al livello di pixel è molto più veloce rispetto ai metodi non lineari (R_NLLS a MAP). Al contrario, l'approccio RLS ha difficoltà a stimare l'indice k_3 in area con attività enzimatica media come il talamo e il brainstem. L'utilizzo dello stimatore MAP aiuta a superare questo inconveniente e permette la quantificazione dell'attività enzimatica dell'AChE nelle regioni con espressione enzimatica media con risultati consistenti con la letteratura scientifica. Nonostante il metodo MAP sia

molto più impegnativo perché implica un'analisi preliminare al livello di ROI per ottenere l'informazione *a priori*, migliora la precisione e l'affidabilità della stima. In particolare, le stime MAP al livello di pixel e al livello di ROI sono molto simili in confronto alle stime ottenute con i metodi pubblicati in letteratura.

In conclusione, la quantificazione delle immagini di ^{11}C-MP4A tramite MAP risulta essere il metodo con i risultati più affidabili sia nelle regioni con attività enzimatica bassa che nelle aree con attività media. Inoltre, la stima a livello di pixel, nonostante richieda un tempo computazionale indubbiamente maggiore, permette di ottenere mappe parametriche con la stessa risoluzione spaziale delle immagini dinamiche originali, cosa questa, invece, non possibile se l'analisi viene condotta a livello di ROI.

Nell'ambito di un progetto finanziato dalla UE, nei prossimi mesi sarà disponibile un data-base con un ampio numero di studi ^{11}C-MP4A/PET. Il progetto europeo è finalizzato alla validazione del modello migliore per la quantificazione e l'applicabilità clinica del modello scelto per la discriminazione delle varie patologie neurodegenerative quale Alzheimer, demenza dei corpi di Lewy e Mild Cognitive Impairement. Il metodo MAP assieme ad un altro approccio Bayesiano in sviluppo sono tra i primi metodi che verranno considerati per la validazione. Studi di simulazione basati su dati plasmatici reali saranno utilizzati per la scelta del metodo migliore per la quantificazione delle immagini.

Chapter 1

Introduction

Degeneration of the cortical cholinergic system is one of the most consistent neurochemical changes in degenerative diseases like Alzheimer disease (AD). In particular, hystochemical studies indicate that cholinergic dysfunction is associated with decreased choline acetyltransferase (ChAT) and acetylcholine esterase (AChE) (and consequently acetylcholine) activity associated with basal forebrain cholinergic degeneration, found in the cortex and hippocampus of AD patients. The most specific marker, expressed by cholinergic neurons for neurotransmitter synthesis, is acetylcholine transferase, but there is no tracer available for in-vivo imaging of this enzyme. The most recent studies indicate that AChE activity in cerebral cortex is mainly due to expression of this enzyme in cholinergic neurons and their axons [10, 49-51]. The same studies revealed that the hippocampus and cortex are the primary sites of the amyloidal deposits and the neurofibrillary tangles, which characterize AD [16].

The quantitative knowledge of the AChE activity is of fundamental importance not only to understand the physiological mechanisms acting in the brain but also to comprehend the pathogenesis of important diseases, with high social impact, such as Alzheimer diseases.

It has been shown that impairment of AChE activity is significantly correlated with the severity of dementia. Therefore, quantitative knowledge of AChE activity in the living brain is highly desirable. Use of tracers that

are hydrolyzed specifically by AChE permits measurement and imaging of local AChE activity in humans. The N-methylpiperidyl esters have been extensively characterized as synthetic substrates for AChE [1-6].

During the last two decays, the development of positron emission tomography (PET) and tracers that are hydrolyzed specifically by AChE permitted measurement and imaging of local AChE activity in humans. Currently ^{11}C-labeled analogs of these two esters, 1-[^{11}C]methyl-4-piperidinyl acetate (^{11}C-AMP or ^{11}C-MP4A) and 1-[^{11}C]methyl-4-piperidinyl-propionate (^{11}C-PMP or ^{11}C-MP4P) are used as radiopharmaceuticals for in vivo studying AD using PET [7-20] and are classified as irreversible tracer.

The AChE selectivity of ^{11}C-MP4A and ^{11}C-MP4P in human cortical homogenates was estimated to be 94% [8] and 86%, respectively, and the hydrolysis rate is four or five times larger for ^{11}C-MP4A then for ^{11}C-MP4P [2]. PET studies using ^{11}C-MP4A and ^{11}C-MP4P have demonstrated significant reduction of cerebral regional AChE activity in patients with Alzheimer disease (AD), Parkinson's disease (PD), and Lewy body dementia (DLB) compared with the seen age-matched healthy subjects [7, 9-11].

^{11}C-MP4A is a PET tracer that is highly specific for AChE and has kinetic properties that are favorable for measuring cortical AChE activity. Measurement of regional AChE activity by ^{11}C-MP4A/PET usually requires arterial blood sampling and correction for hydrolyzed tracer that cannot pass the blood-brain barrier. ^{11}C-MP4A, as a radiolabeled lipophilic acetylcholine analogue, readily enters the brain via the blood-brain barrier. A portion of the ^{11}C-MP4A that reaches the brain tissue diffuses back across the blood-brain barrier, while the rest is hydrolyzed selectively by AChE to produce the hydrophilic radioactive product, ^{11}C-N-methyl-4-piperidinol (^{11}C-MP4OH), which has very limited permeability through the blood-brain barrier and essentially becomes trapped in the brain at the site of the enzymatic reaction. Analysis of radioactivity in brain tissue and plasma yields a functional parameter corresponding to AChE activity: k_3 [3, 7, 8]. The standard method to estimate regional hydrolysis rate of ^{11}C-

MP4A by AChE (k_3) is to fit the regional time-activity curve (TAC) obtained by PET to the theoretical function derived from the kinetic model and the arterial input function using nonlinear least squares (NLLS) optimization. In NLLS analysis, however, the procedure involves measurement of the arterial input function that is invasive to patients and requires considerable technical expertise, which may restrict widespread use of this method in daily clinical practice. Recent studies employed a special feature of AChE distribution in brain, namely its very high activity in basal ganglia and cerebellum and the relatively fast rate of ^{11}C-MP4A hydrolysis by AChE, to devise the non-invasive technique for the measurement of cortical AChE activity [12-14]: because of the very high metabolism rate of ^{11}C-MP4A by AChE in striatum and cerebellum, all ^{11}C-MP4A molecules entered these regions would be trapped there completely. This assumption allows the use of these brain regions as reference region to obtain input function data in the form of single integral with respect to PET scan time.

As far as we know there are only several methods published to quantify ^{11}C-MP4A images without arterial sampling: shape analysis (SA) proposed for the first time for AChE quantification by Koeppe et al [48] and re-proposed then by Tanaka et al [25] for ^{11}C-MP4A PET images, the reference tissue linear least squares (RLS) proposed by Nagatsuka et al 2001 [12], the reference ratio exponential (RRE) approach proposed by Herholz and coworkers in 2001 [13], Zundorf et al. 2001 that proposed basis function mathematical approach (RRE_BF) for Herholz method [14]. SA is a method for direct estimation of the rate constant describing an irreversible process based solely on the shape of tissue TAC that proved to be too much sensitive to noise level in the data and give no reliable results. The other approaches, RLS, RRE, and RRE_BF are based on the same model structure but used different estimation methods.

Positron Emission Tomography quantification can be performed at region of interest (ROI) levels and pixel level. ROI advantages are the good signal to noise ratio of the time activity curves to be identified with the kinetics model and the existence of well-established techniques for the

estimation of unknown parameters (NLLS). One major drawback of this approach is the loss of resolution of the original PET image.

Kinetic analysis at pixel-by-pixel level of ^{11}C-MP4A images provides to quantify the activity of AChE enzyme. However, pixel-by-pixel kinetic analysis has two major drawbacks: one is the noise level in a pixel-based time activity curve (pTAC) and the second is the large number of pixel involved. The noise level leads to instability in the estimated parameters. The large number of pixels leads to considerable long time for parametric image generation. In the last years, different methods have been proposed for non-invasive quantification of AChE activity at ROI level but only very few attempts have been made in order to quantify AChE activity at pixel level [14, 22].

AChE quantitation at pixel and ROI level by ^{11}C-MP4A/PET are two investigation approaches not only useful but complementary, in order to obtain a clear picture of the cholinergic system.

The aim of the present work is twofold: first, the development of a Bayesian method to quantify ^{11}C-MP4A images at both pixel and ROI level in patients with neurodegenerative diseases and in normal subjects in order to accurately estimate AChE activity in brain regions with low and moderate enzymatic expression. The second objective is to compare the performance of the Bayesian method with the other few methods already propose in the literature for AChE activity quantification at pixel level: reference NLLS, RLS, RRE, RRE_BF [8, 12-14].

The thesis is articulated as follows:

- Chapter 2 describes the cholinergic system with main events underlying the chemistry and metabolism of acetylcholine (ACh) with the distribution of ACh receptor in the brain; a further subsection of neuropharmacology follows and finally a brief section on PET tracer ^{11}C-MP4A.
- Chapter 3 presents details about ^{11}C-MP4A experimental protocol and image acquisition and processing; it is also presented an automatic method for masking the PET dynamic images in order to

extract TACs characteristic for different brain areas with low, moderate and high AChE activity.

- Chapter 4 is the modeling chapter and describes the compartmental model structure of ^{11}C-MP4A kinetics that represents the base of all the mathematical approaches used to analyze the dataset. Details about each estimation procedure and identification process are reported for each mathematical technique as sub-sections. Finally, the processing flowchart of the obtained functional parametric image is described.
- Chapter 5 presents the results obtained applying the techniques described in the previous chapter at pixel and ROI level. A subsection is dedicated to each mathematical method.
- Chapter 6 is focused on the assessment and comparison of the Bayesian method performance at pixel level respect to the methods already proposed in the literature for AChE activity quantification that were implemented at pixel-by-pixel level. A discussion follows.
- Chapter 7 discusses results obtained in this study as well as emerged open questions.
- Chapter 8 presents the conclusions of this work and the future direction of the research.

Chapter 2

Cholinergic System

Impairment of cholinergic neurotransmission in the central nervous system leads to severe cognitive impairment. The brain contains a network of cholinergic neurons (FIGURE 2.1). Those with cell bodies in the basal forebrain project to areas of the brain linked with cognitive function, memory and learning. Degeneration of neurons in the cholinergic system occurs in Alzheimer's disease and this may contribute to impaired cognitive function and learning, characteristics of the disease. Acetylcholine is an important neurotransmitter in both the peripheral nervous system (PNS: skeletal and smooth muscle, autonomic sympathetic and parasympathetic ganglia), and in the central nervous system (CNS).

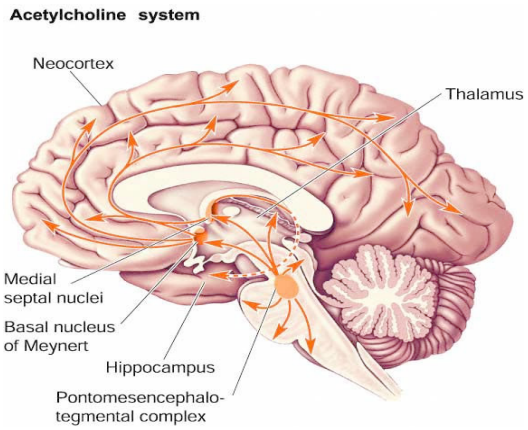

FIGURE 2.1 Acetylcholine system: network of cholinergic neurons [38]

2.1. Biosynthesis and Metabolism of ACh.

The chemical compound acetylcholine, often abbreviated as ACh, was the first neurotransmitter to be identified. It is a chemical transmitter in both the PNS and CNS in many organisms including humans. [35].

Acetylcholine is an ester of acetic acid and choline with chemical formula $CH_3COOCH_2CH_2\ N+(CH_3)_3$. This structure is reflected in the systematic name, 2-acetoxy-N,N,N-trimethylethanaminium [35].

Acetylcholine is synthesized from its two immediate precursors, choline (Ch) and acetyl coenzyme A (ACoA). The synthesis reaction is a single step catalyzed by the enzyme cholin acetyltransferase (ChAT) [23, 35, 36].

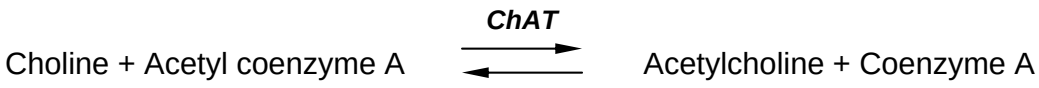

Choline present in tissues has two origins: exogenous, in food, and endogenous.

The acetyl CoA used for ACh synthesis in mammalian brain comes from pyruvate formed from glucose. It is uncertain how the acetyl CoA, generally thought to be formed at the inner membrane of the mitochondria, accesses the cytoplasmic ChAT, and it is possible that this is a rate-limiting step

ChAT, first assayed in a cell-free preparation in 1943, subsequently has been purified and cloned from several sources. The purification of ChAT has allowed production of specific antibodies. ChAT is found in the nervous system specifically at sites where ACh synthesis takes place. Within cholinergic neurons, ChAT is concentrated in nerve terminals, although it is also present in axons, where it is transported from its site of synthesis in the soma. When subcellular fractionation studies are carried out, ChAT is recovered in the synaptosomal fraction, and within synaptosomes it is primarily cytoplasmic. It has been suggested that ChAT also binds to the outside of the storage vesicle under physiological

conditions and that ACh synthesized in that location may be situated favorably to enter the vesicle. [23].

Acetylcholine formation is limited by the intracellular concentration of choline, which is determined by uptake of choline into the nerve ending [23].

While ChAT catalysis the formation of ACh, acetylcholinesterase (AChE) is the enzyme responsible for degradation of ACh and is produced by cells containing cholinoreceptive sites as well as in cholinergic neurons. Normally, the enzyme acetylcholinesterase converts acetylcholine into the inactive metabolites choline and acetate. This enzyme is abundant in the synaptic cleft, and its role in rapidly clearing free acetylcholine from the synapse is essential for proper muscle function [35].

ACh metabolism is synthesized in FIGURE 2.2 [40] and consists in different stages [39]:

1. The neurotransmitter – ACh - is made by the *pre-synaptic neurone* in presence of ChAT and is stored in *synaptic vessels* at the end of the axon.
2. An action potential arrives at presynaptic membrane. Voltage gated calcium channels in the presynaptic membrane open, calcium ions enter the presynaptic neurone
3. Calcium ions cause synaptic vesicles to fuse with the presynaptic membrane, releasing acetylcholine into the synaptic cleft.
4. ACh diffuses cross the synaptic cleft and binds to specific neuroreceptor sites in the post synaptic membrane. The membrane of the *post-synaptic neurone* has chemical-gated ion channels called *neuroreceptors*. These have specific binding sites for neurotransmitters.
5. Sodium channels open. Sodium ions diffuse into the postsynaptic membrane causing depolarisation, which may initiate an action potential.

6. Acetylcholinesterase breaks down acetylcholine. The products diffuse back into the presynaptic neurone where ACh is resynthesised using ATP from the mitochondria.

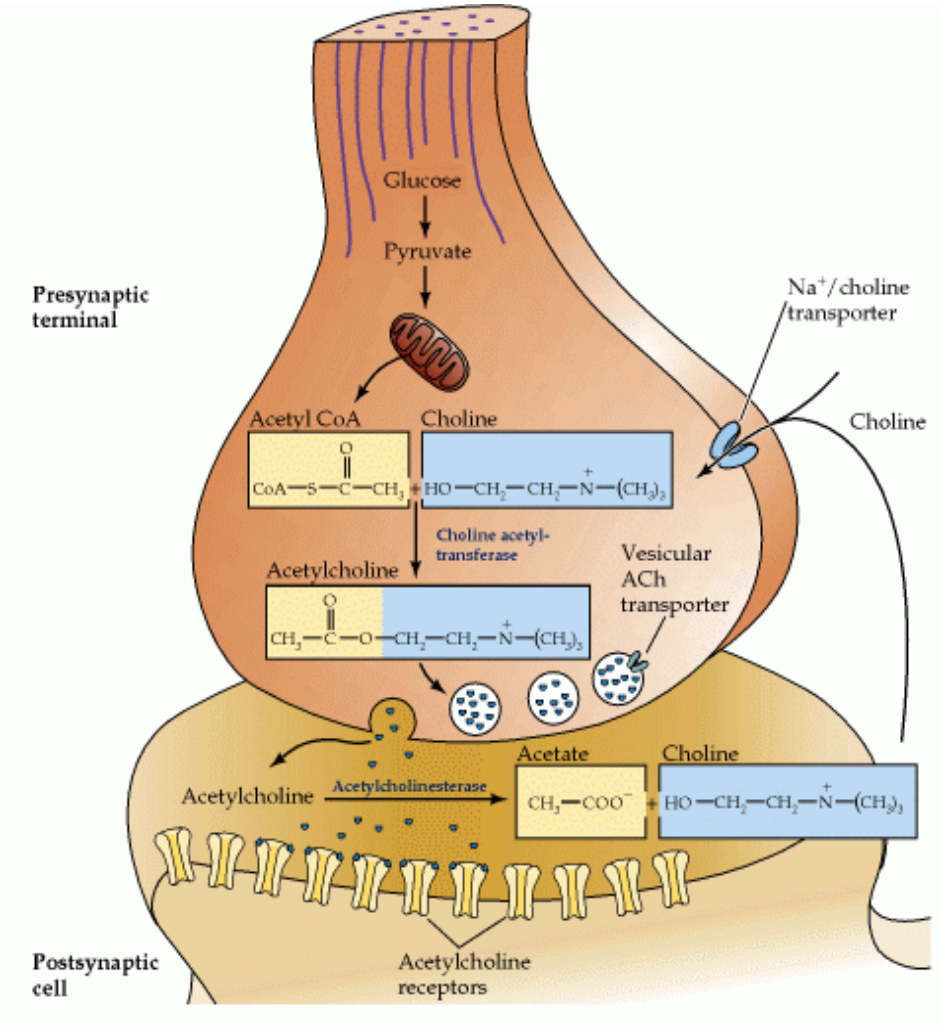

FIGURE 2.2 Acetylcholine metabolism in cholinergic nerve terminals. The synthesis of acetylcholine from choline and acetyl CoA requires choline acetyltransferase. Acetyl CoA is derived from pyruvate generated by glycolysis, while choline is transported into the terminals via a Na^+-dependent transporter. After release, acetylcholine is rapidly metabolized by acetylcholinesterase and choline is transported back into the terminal [40].

2.2. Acetylcholinesterase and the Termination of Acetylcholine Action.

Cholinesterases are widely distributed throughout the body in both neuronal and non-neuronal tissues. Based largely on substrate specificity,

the cholinesterases are subdivided into the acetylcholinesterases (AChEs) and the butyryl or pseudocholinesterases (BuChE). Acetylcholines with an acyl group the size of butyric acid or larger are hydrolyzed very slowly by the former enzyme; selective inhibitors for each enzyme have been identified. BuChE is made primarily in the liver and appears in plasma; however, it is highly unlikely that appreciable concentrations of ACh diffuse from the locality of the synapse and elicit a systemic response. In general, AChE distribution correlates with innervation and development in the nervous system. The AChEs also exhibit synaptic localization upon synapse formation. Acetyl- and butyrylcholinesterases are encoded by single, but distinct, genes. [23]

Acetylcholinesterase is an enzyme which deesterifies the ubiquitous neurotransmitter ACh, thus inactivating it. AChE is a serine esterase and has an anionic binding site which attracts the positively charged quaternary ammonium group of ACH. A serine then attacks and cleaves the ester. This is an example of general base catalysis, since serine must first be deprotonated by a neighboring hystidine (HIS). Following ester hydrolysis, the enzyme is quickly regenerated. [24]

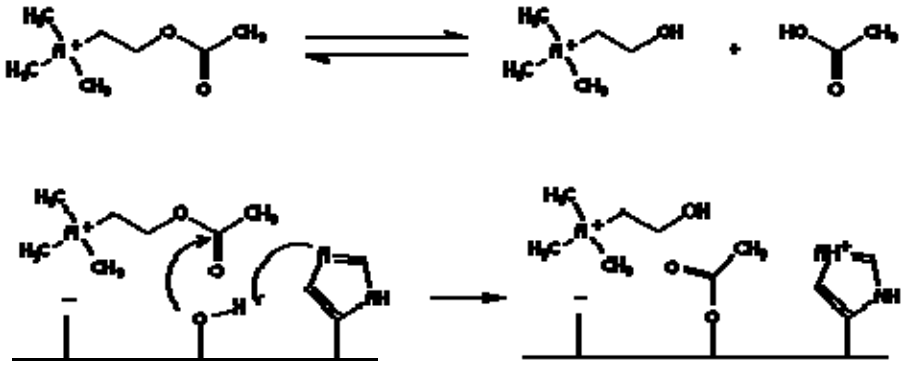

Acetylcholinesterases exist in several molecular forms: these forms differ in solubility and mode of membrane attachment rather than in catalytic activity. One class of molecular forms exists as a homomeric assembly of catalytic subunits that appear as monomers, dimers or tetramers .These forms also differ in their degree of hydrophobicity, and their amphiphilic character arises from a post-translational addition of a glycophospholipid on the carboxyl-terminal amino acid. The

glycophospholipid allows the enzyme to be tethered on the external surface of the cell membrane. Soluble globular forms of the enzyme have been identified in brain.

The second class of AChEs exists as heteromeric assemblies of catalytic and structural subunits. One form consists of up to 12 catalytic subunits linked by a disulfide bond to filamentous, collagen-containing structural subunits. These forms are often termed asymmetric, since the tail unit imparts substantial dimensional asymmetry to the molecule. The asymmetric species are localized to synaptic areas. The collagenous tail unit is responsible for this molecular form being associated with the basal lamina of the synapse rather than the plasma membrane. Asymmetric forms are particularly abundant in the neuromuscular junction. A second type of structural subunit, to which a tetramer of catalytic subunits is linked by disulfide bonds, has been characterized in brain. This subunit contains covalently attached lipid, enabling this form of the enzyme to associate with the plasma membrane. The different subunit assemblies and post-translational modifications lead to distinct localization of AChE on the cell surface but appear not to affect the intrinsic catalytic activities of the individual forms [23].

2.3. Pharmacology

ACh acts using two different types of cholinergic receptors (AChRs) that are widely distributed throughout brain (FIGURE 2.3). These receptors are classified as muscarinic and nicotinic receptors and are named for the ligands used to discover the receptors [35]. In certain regions of the brain only the muscarinic subtype is found eg midbrain, medulla, and pons while in other regions eg substantia nigra, locus coeruleus and septum only the nicotinic receptor subtype is found. Both sub-types are located in the corpus striatum, cerebral cortex, hippocampus, thalamus, hypothalamus and cerebellum [24].

Nicotinic AChRs are ionotropic receptors permeable to sodium, potassium, and chloride ions. They are stimulated by nicotine and acetylcholine. They are of two main types, muscle type and neuronal type. The main location of nicotinic AChRs are on muscle end plates, autonomic ganglia (both sympathetic and parasympathetic), and in the CNS [35]. These receptors are made up of 5 sub-units surrounding a central pore. Each sub-unit comprises a polypeptide that spans the membrane 4 times, and the N- and C- terminals are outside the cell (FIGURE 2.4, Panel A). The number of alpha and beta sub-units vary.

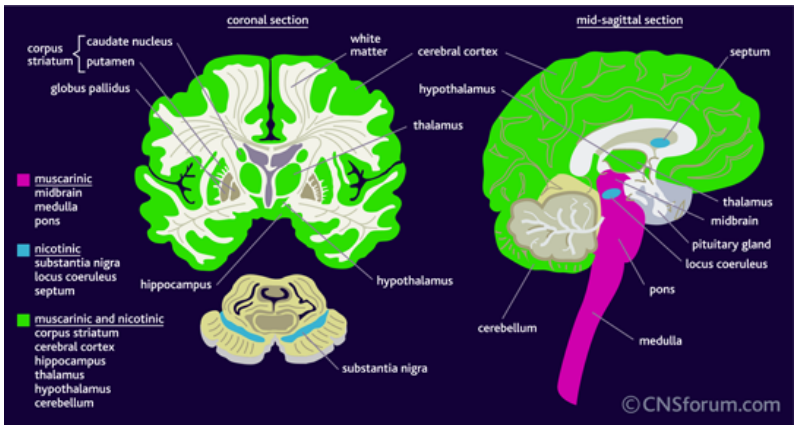

FIGURE 2.3 Distribution of the cholinergic receptors [24].

Nicotine is an agonist and either hexamethonium or tubocurarine are antagonists for all these types of receptor [38].

Muscarinic receptors are metabotropic and affect neurons over a longer time frame. They are stimulated by muscarine and acetylcholine, and blocked by atropine.

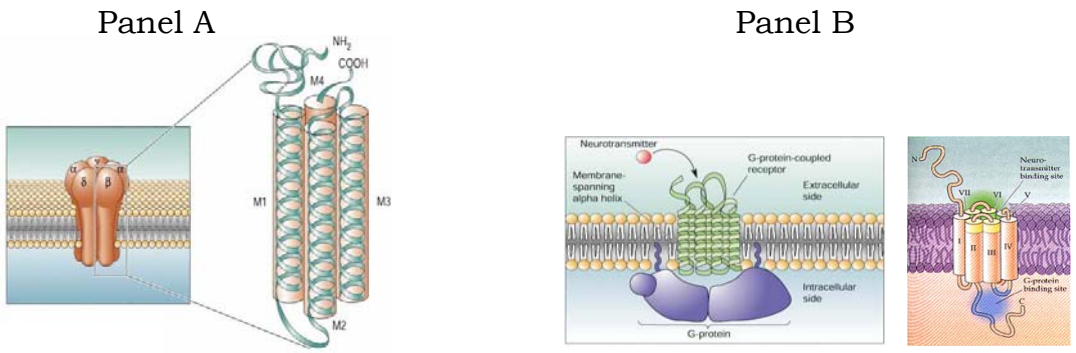

FIGURE 2.4 Types and structure of cholinergic receptors: nicotinic (Panel A) and muscarinic (Panel B) receptors [38].

Muscarinic receptors are found in both the central nervous system and the peripheral nervous system, in heart, lungs, upper GI tract and sweat glands. These receptors are made up of a single sub-unit and there is no channel directly associated with the receptor. The receptor comprises a polypeptide that spans the membrane 7 times, and the N-terminus is outside and the C- terminus is inside the cell (FIGURE 2.4., Panel B). The inside contains a G-protein binding site, which is activated when ACh binds to the receptor. Muscarine is an agonist and atropine is an antagonist for all types of muscarinic ACh receptor [38].

Cholinergic System in Alzheimer Disease.

Alzheimer's disease is associated with a reduction of all cholinergic neurones in the subcortical areas of the brain, leading to reduced availability of acetylcholine. In Alzheimer's disease ChAT is less active than in a non-Alzheimer's brain resulting in a reduction in the synthesis of ACh. As ChAT activity declines, less ACh is packaged into the synaptic vesicles and released at the nerve terminal. This deficit in ACh leads to decreased neurotransmission and is implicated in the pathogenesis of Alzheimer's disease [37]. Therefore ChAT might be considered the specific marker, expressed by cholinergic neurons for neurotransmitter synthesis, but there is no tracer available for in-vivo imaging of this enzyme [11].

Several studies developed in the last decades showed that that impairment of AChE activity is significantly correlated with the severity of dementia. There were individuated several possible mechanisms for the floor effect in AChE measurement in AD recalled and described by Shinotoh and its colleagues [11]: first, AChE is associated with not only the presynaptic cholinergic neurons but also with the postsynaptic cholinoceptive neurons. Second, AChE is not only associated with the cholinergic system but is also found in noncholinergic structure. Therefore, much of the AChE associated with the cholinergic system is lost early in the course of the disease, and the remainder may be associated largely with the noncholinergic structure. Third, AChE is associated with

the increased number of neuritic plaques and neurofibrillary tangles in the AD brain. Thus, the increased number of neuritic plaques and neurofibrillary tangles may contribute to the stabilization of cortical AChE activity. Fourth, AChE may be downregulated early in the course of the disease in the response to diminished ACh synthesis as a means of maintaining levels of ACh in the synapses.

Therefore, quantitative knowledge of AChE activity in the living brain is highly desirable. The N-methylpiperidyl esters have been extensively characterized as synthetic substrates for AChE [1-6].

2.4. PET Tracer: ^{11}C-MP4A.

In the last years several tracers have been developed for in vivo imaging of cerebral AChE activity with PET. More then 20 years ago a first description of the reduction of cerebral glucose metabolism in association areas for AD patients has been identify in vivo by 2-deoxy-2-[^{18}F]fluoro-D-glucose(FDG)-PET [41]. However, impairment of local FDG uptake is not specific for AD pathology: even if high sensitivity in order of 90% to 95% has been documented in different studies, the specificity for discrimination from other neurodegenerative diseases is lower and in the order of 65% to 75% [41].

In the recent years have been developed piperidine analogues for the in vivo imaging of AChE with PET: 1-[^{11}C]methyl-4-piperidinyl acetate (^{11}C-MP4A) and 1-[^{11}C]methyl-4-piperidinyl-propionate(^{11}C-MP4P) are used as radiopharmaceuticals for in vivo studying AD using PET [7-20] and are classified as irreversible tracer. Significant reduction of cerebral regional AChE activity in patients with Alzheimer disease (AD), Parkinson's disease (PD), and dementia with Lewy bodies (DLB) compared with the seen age-matched healthy subjects have demonstrated by PET studies using ^{11}C-MP4A and ^{11}C-MP4P [7, 9-11]. Thus, imaging of cholinergic neurotransmission could become an important tool for differentiation between types of dementia [41].

^{11}C-MP4A is a PET tracer that is highly specific for AChE and has kinetic properties that are favorable for measuring cortical AChE activity. The tracer is freely diffusible in the brain and is distributed in proportion to the blood flow; it is hydrolyzed by AChE and accumulates depending on enzyme expression because the hydrolyzed product is trapped in the brain. With the impaired function and neurodegeneration of the cholinergic axons, the amount of cortical AChE is reduced and can be detected by the reduced accumulation of MP4A.

Radioligand ^{11}C-MP4A is characterized by rapid metabolism in human plasma (FIGURE 2.5) and its higher accumulation in the basal ganglia and cerebellum (FIGURE. 2.6) regions where post mortem study demonstrate a very high concentration of AChE. Neocortex (e.g. temporal lobe) area is characterized by a low enzyme expression, while thalamus (TH) has a moderate enzyme activity (FIGURE 2.6).

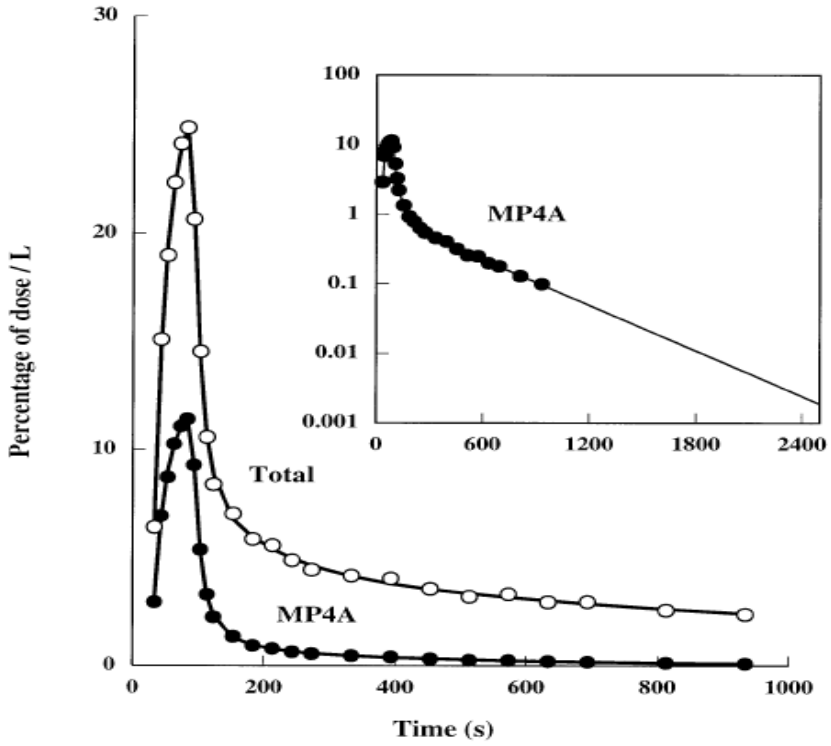

FIGURE 2.5 Total and metabolite-corrected radioactivity of the arterial plasma in a subject after intravenous injection of ^{11}C-MP4A. Time 0=start of intravenous tracer infusion. Inset: Semilogarithmic plot of the metabolite-corrected radioactivity up to 15 min after intravenous injection of ^{11}C-MP4A and a fitted curve up to 40 min [8].

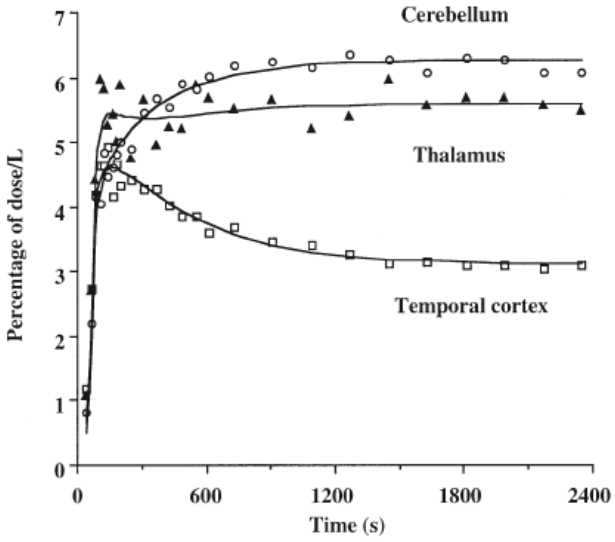

FIGURE 2.6 Time-activity curves in the cerebral (temporal) cortex, thalamus and cerebellar cortex in a subject after intravenous injection of ^{11}C-MP4A [8].

In recent PET studies has been shown that AChE activity was reduced in AD subjects respect to controls in neocortex area [7-12, 17, 19, 20, 22, 33, 34], thalamus [8, 11, 12, 15, 33, 34], hippocampus [11, 12, 16, 33, 34], and amygdala [19] but not in nucleus basalis Meynert (nbM) [19]. Average images with stereotactic normalization of AChE distribution amoung the brain in NC and AD subjects respect to MRI scans is also shown (FIGURE 2.7).

Imaging of cholinergic neurotransmission might become an important tool for differentiation between different types of dementia. Validation of different mathematical approaches for a reliable quantitation of ^{11}C-MP4A PET images as a measure of AChE activity is on going in the DiMI European network.

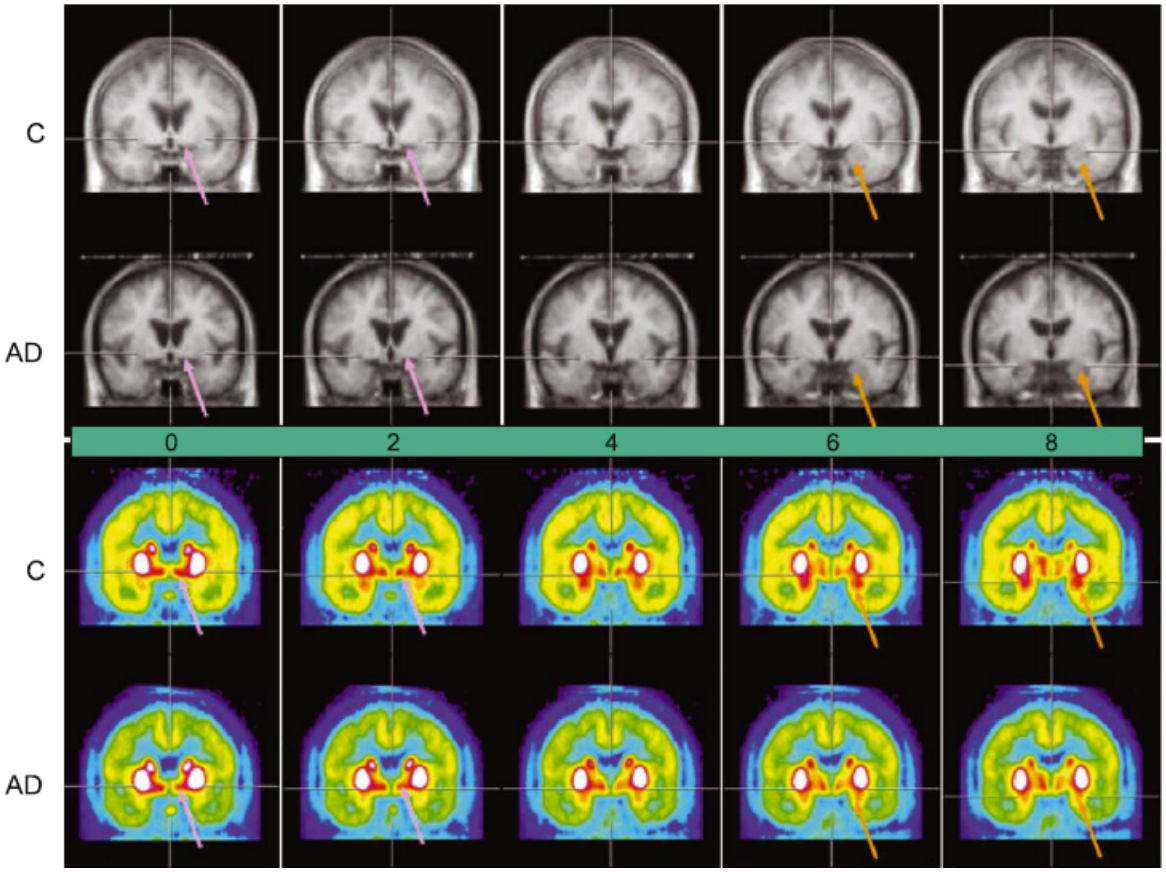

FIGURE 2.7 Average images of controls (C) and AD patients (AD) with stereotactic normalization. Coronal slices (perpendicular to the AC–PC line) are shown, starting at the AC and progressing in 2 mm steps caudally (distance from AC shown in the middle of the figure). MRI images are shown on top, ^{11}C-MP4A PET scaled to 65% of maximum brain activity at bottom. The anteromedial and anterolateral parts of the nbM are marked by a pink arrow (the posterior part is located just below the putamen with its very high activity and cannot be separated). The amygdalae are marked by an orange arrow. Please note the progression of the distance between the left and right optic tract from 0 to 8 mm caudal to the AC. This serves as a landmark to compare the anatomical site with the histochemical studies (Hedreen et al., 1984; Mesulam and Geula, 1988b). In AD (bottom row), AChE activity was reduced in cortex and amygdala, but not in nbM.[19].

Chapter 3

Image Acquisition and Processing

3.1. Subjects

Two groups of subjects, normal control group (NC group – 4 subjects) and Alzheimer disease group (AD group – 7 subjects) participated at the study. The NC group ages ranged from 58 to 68 years (64. ± 4). AD group ages ranged from 61 to 85 years (76 ± 9). The study was approved by the Ethics and Radiation Safety Committee of the San Raffaele Hospital. Written informed consent was obtained from each subject and/or a family member prior to the study in accordance with the declaration of Helsinki.

3.2. ^{11}C-MP4A PET

To assess local AChE activity, 500-700 MBq ^{11}C-MP4A that were synthesized according to the methods of Irie et al [2] with modification as recently described by Carpinelli et al [42] were solved in 2-5mL saline solution with physiological pH and injected intravenously as a bolus. PET studies were performed with an 18 ring PET/CT tomograph (GE Discovery LS NXI) with 35 slices and matrix acquisition dimension of 128x128 pixels. The protocol includes a CT scan at 140mV over a 15.7cm axial field of view, followed by PET scan acquired over a period of 60 minutes in 3D mode, using the following dynamic sequence:6x30s, 2x60s, 2x150s, 10x300s. PET images were corrected for geometric effect (rebinning), dead time, decay, random coincidences (real time subtraction of delayed

coincidences), scattered coincidences, attenuation. Images reconstruction was performed using filtered back projection algorithm: transaxial images were reconstructed using a Shepp - Logan filter (cutoff 5 mm filter width) in the transaxial plane, and a Shepp - Logan filter (cutoff 8.5 mm) in the axial direction. The resolution of the reconstructed image is 5.3 mm FWHM and the voxel size is 2.5x2.5x4.25 mm.

All PET scans were done under resting condition in a quite scanner room. No MRI scan was performed for the subjects who participated in this study.

3.3. Automatic generation of ROIs

Quantification of ^{11}C-MP4A images was made both at pixel and region of interest (ROI) level. ROIs were automatically determined in the temporal lobe (TE), parietal lobe (PA), occipital lobe (OC), frontal lobe (FR), Rolandic operculum (R), insula (I), thalamus (TH), hippocampus (HP), striatum (BG). Automatic extraction was preferred to the often used manual technique one because of the lack of MRI scans and two in order to avoid errors sampling during a manual position of ROIs on the dynamic or integrated ^{11}C-MP4A PET images.

To automatically derive the ROIs, SPM2 (Wellcome Institute of Cognitive Neuroscience, London, U.K.) and MARINA - MAsks for Region of INterest Analysis (Bertram Walter Bender Institute of Neuroimaging University of Giessen, Germany) software for image registration and ROI drawing were used. SPM2 is well known software that refers to the construction and assessment of spatially extended statistical processes used to test hypotheses about functional imaging data.

MARINA software allows one to create, edit, and save ROIs in an SPM-ANALYZE format (FIGURE 3.1). The creation of ROIs is aided by the anatomical parcellation of the brain published by Tzourio-Mazoyer et al. (2002). MARINA is based on the single subject MRI brain template with a voxel size of 2 mm that comes from the Montreal Neurological Institute

and is included in the SPM2-package as canonical/single_subj_T1.img. This program allows creating, smooth, threshold, edit, and save masks of different ROIs in an SPM-ANALYZE format [26].

In particular, in order to automatically extract the TAC for different regions of interest, image processing proceeded with the following steps:

1. PET dynamic image (4D PET image) was decomposed in 3D volumes each representing a corresponding time acquisition volume.
2. Integrated images of the first ten minutes of acquisition ("early images" which are representative for tracer delivery and distribution) were created for each subject.
3. For each subject, the "early images" was used to check visually in sagittal view the AC-PC line orientation using Analyze software (Mayo Clinic). No correction for position or movement was needed. Integrated images have been normalized to the Montreal Neurological Institute (MNI) stereotactic space (PET.mnc) and then coregistered to the single subject canonical template (MNI) by mutual information using SPM2 software. Mean "early image" was created both for normals and AD group and are shown in coronal (Panel A) and transversal view (Panel B) in FIGURE 3.2.
4. Each 3D frame was normalized and coregistered with the same procedure described in step 3 by using the identified integrated image parameters for normalization and coregistration. 4D PET image is recomposed. The voxel size in the new image is 2 mm.
5. Mask ROIs are generated with Marina software [26]. The following ROIs have been selected: frontal (FR), parietal (PA), occipital (OC), and temporal cortex (TE), hippocampus (HP) for the brain area with low enzyme activity, thalamus (TH) with moderate AChE activity and the striatum or basal ganglia (BG) with high enzymatic concentration. Marina software, as described in the previous page, is based on single subject MRI with voxel size of 2 mm that comes from Montreal Neurological Institute and is included in SPM2 as canonical/single_subject image.

6. The dynamic PET images (obtained in step 4) are masked with the mask ROIs previously obtained – step 5 – in order to generate time activity curves (TACs). Typical ^{11}C-MP4A time activity curves in a normal subject are shown in FIGURE 3.3.
7. Finally, In order to obtain quantitative information, different mathematical techniques are applied at TAC_ROI level.

The flowchart of dynamic image processing for ROI level analysis is presented in FIGURE 3.4

Panel A

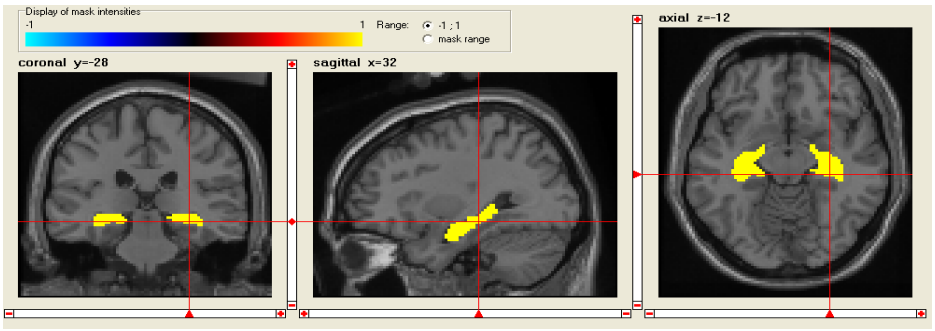

Panel B

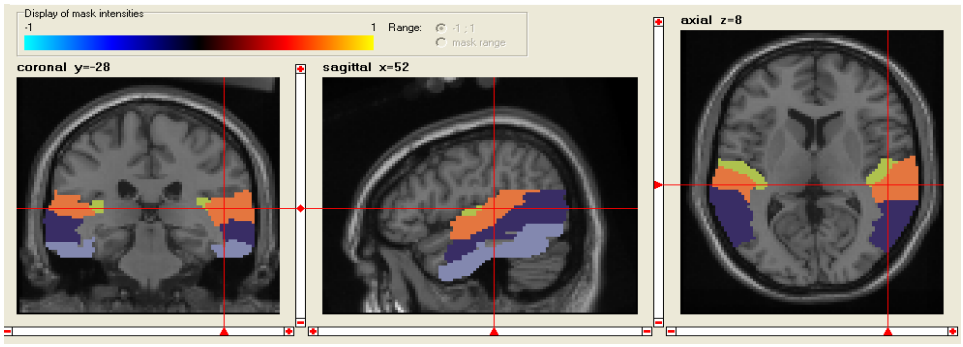

Panel C

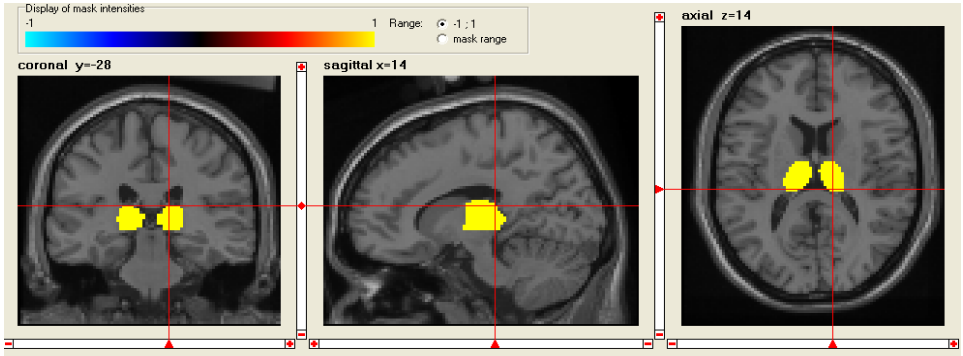

FIGURE 3.1. Examples of mask ROI generation with Marina software: region with low enzyme activity like temporal lobe (TE) and HP in Panel B and respectively Panel A, and moderate enzyme expression as and TH in Panel C. From left to right, in each panel are represented coronal, sagittal and transversal view.

Panel A

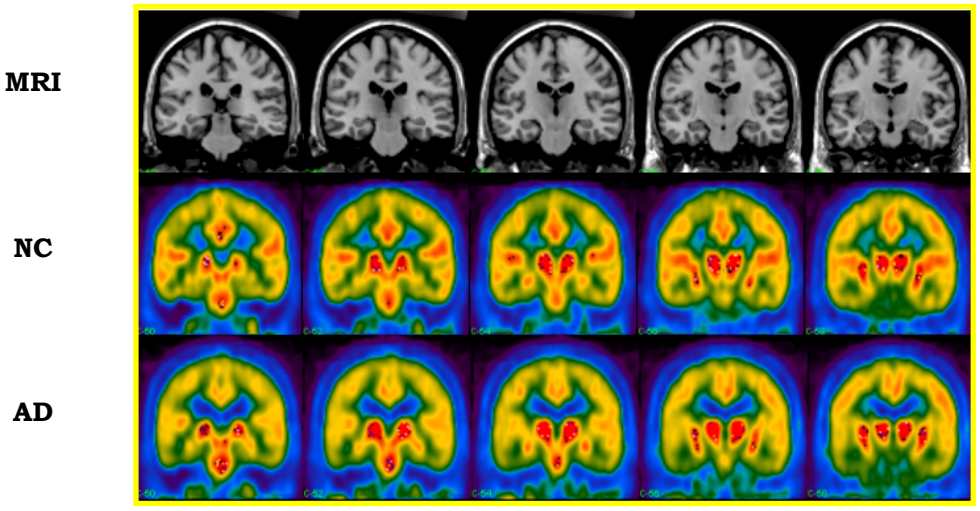

Panel B

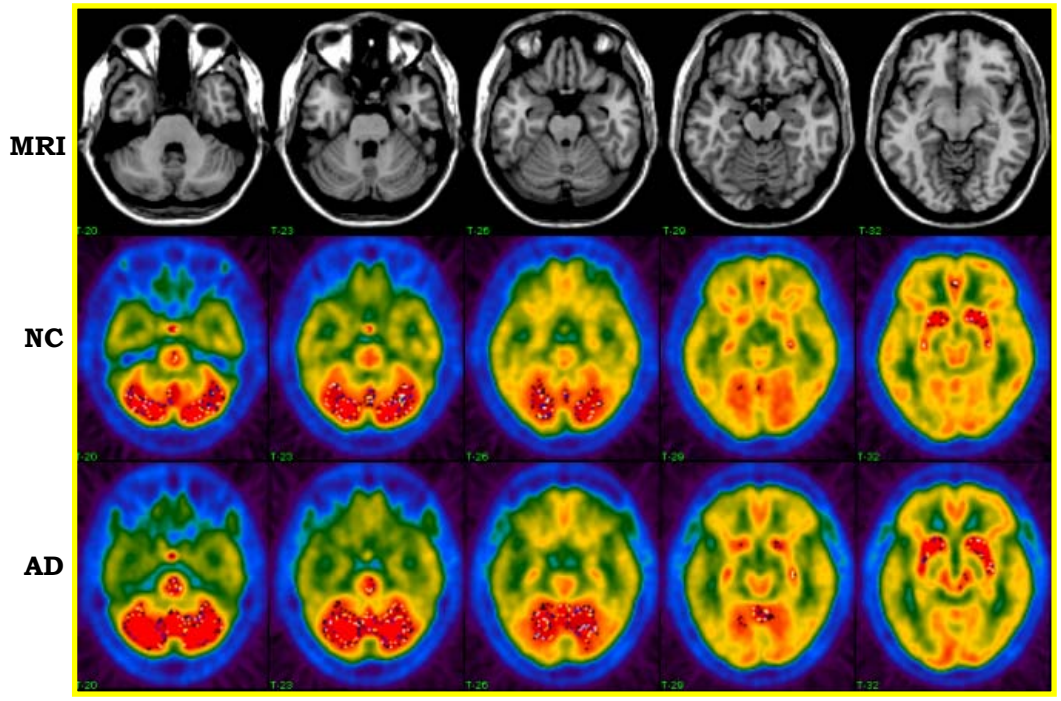

FIGURE 3.2 ^{11}C-MP4A average 1-10 "early" image of controls (NC) middle line and AD patients (AD) bottom line normalized to stereotactic space and coregistered to the single-subject (MRI) canonical template of SPM (bottom line) shown in each panel. Coronal view-Panel A and transversal view –Panel B.

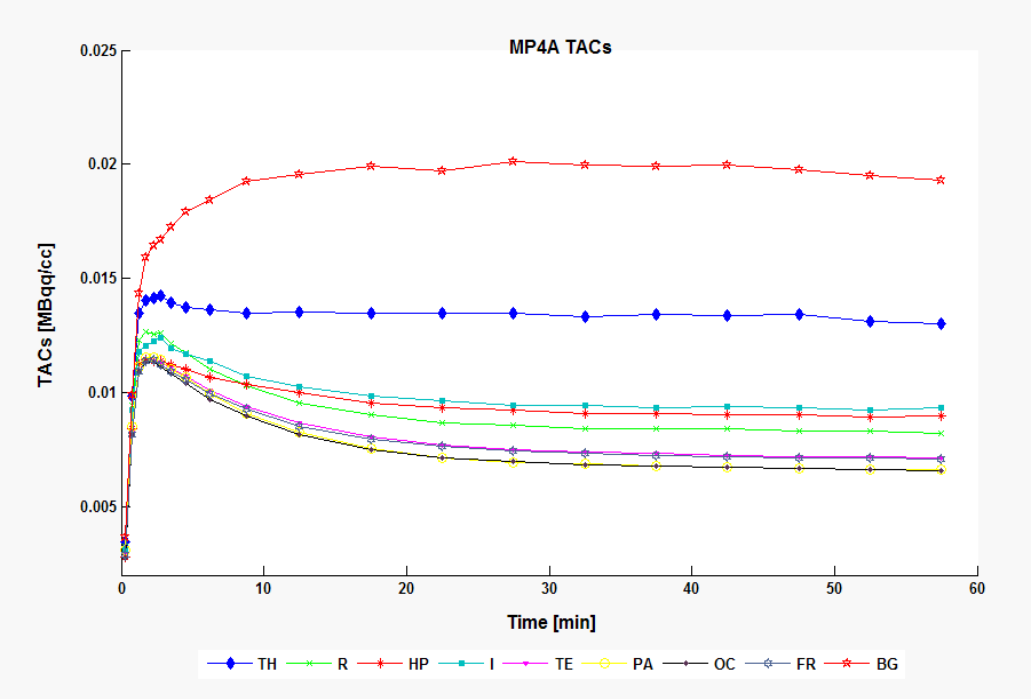

FIGURE 3.3 ^{11}C-MP4A time activity curves e.g. in NC Image Processing

Image Processing

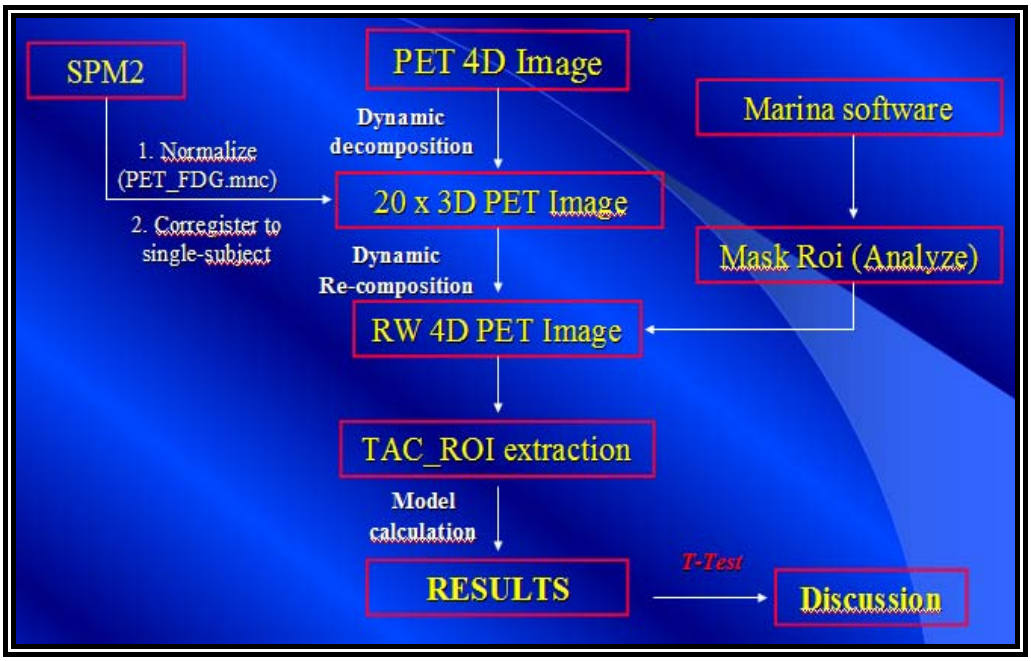

FIGURE 3.4 The flowchart of 4D ^{11}C-PET images processing at TAC_ROI level

Chapter 4

Models and Methods for ^{11}C-MP4A Quantification

^{11}C-MP4A is a lipophilic acetylcholine analogue that readily enters the brain via the blood-brain barrier. In the brain tissue, ^{11}C-MP4A partly diffuses back across the blood-brain barrier, while the rest is hydrolyzed selectively by AChE to produce the hydrophilic radioactive product, ^{11}C-*N*-methyl-4-piperidinol (^{11}C-MP4OH), which has very limited permeability through the blood-brain barrier (BBB) and essentially becomes trapped in the brain at the site of the enzymatic reaction. BBB does not allow the plasma metabolites of ^{11}C-MP4A to enter the brain [8].

The gold-standard in PET quantification is to estimate the kinetic rate constants using the relationship between tissue data measured with the PET scanner and the input function, usually derived from arterial blood samples corrected for metabolites [8]. However, approaches have been developed to avoid the measurement of the arterial input function and still estimate kinetic parameters by comparison of the time–activity curve in the region of interest to that in a reference region. Usually, in PET receptor modeling the reference input function is derived from a brain region void of a specific receptor system [45].

For this study, since arterial tracer activity was not available, a reference region was used as input function. However, in case of ^{11}C-MP4A the reference input function is derived from regions having very high

AChE activity, such as striatum and cerebellum [27; 12-14], for which it is possible to assume that all ^{11}C-MP4A molecules entered these regions would become trapped there completely. In particular, in this study the reference region was identified with the striatum.

Mathematically, ^{11}C-MP4A kinetics can be described in brain region having low and intermediate AChE activity by a two-tissue three-rate constant compartmental model (Figure 4.1).

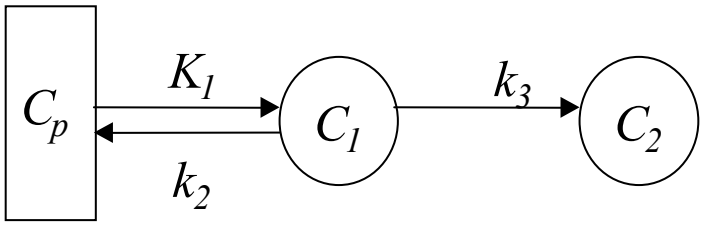

FIGURE 4.1 The two-tissue three-rate constant compartmental model of ^{11}C-MP4A in brain region having low or intermediate AChE activity. C_p is the unmetabolized free tracer concentration curve in plasma, C_1 the ^{11}C-MP4A tracer concentration in tissue, C_2 the ^{11}C-MP4OH metabolite concentration in tissue, K_1 [ml/ml/min] the rate of tracer inflow into the brain, k_2 [min^{-1}] the rate of unmetabolized tracer washout, and k_3 [min^{-1}] the rate of tracer hydrolysis by AChE.

The model equations are:

$$\begin{aligned} \dot{C}_1(t) &= K_1 C_p(t) - (k_2 + k_3) C_1(t) & C_1(0) &= 0 \\ \dot{C}_2(t) &= k_3 C_1(t) & C_2(0) &= 0 \end{aligned} \qquad (4.1)$$

$$C_T(t) = (1 - V_b)\left[C_1(t) + C_2(t)\right] + V_b C_b(t) \qquad (4.2)$$

where C_p is the unmetabolized free tracer concentration curve in plasma, C_b the whole blood tracer concentration including the metabolite, C_1 the ^{11}C-MP4A tracer concentration in tissue, C_2 the ^{11}C-MP4OH, i.e. hydrolyzed tracer, concentration in tissue, C_T the ^{11}C concentration in the target tissue, K_1 [ml/ml/min] the rate of tracer inflow into the brain, k_2 [min^{-1}] the rate of unmetabolized tracer washout, k_3 [min^{-1}] the rate of

tracer hydrolysis by AChE, and V_b [unitless] is the fraction of the measured volume occupied by blood. Because V_b in humans is around 5%, the blood term is often omitted. Thus, by assuming negligible blood volume presence, i.e. $V_b \cong 0$, Eq. 4,2 becomes:

$$C_T(t) = C_1(t) + C_2(t) \tag{4.3}$$

AChE activity was measured in terms of the rate constant for hydrolysis of ^{11}C-MP4A, k_3.

In brain region having high AChE acitivty, it is normally assumed that ^{11}C-MP4A is so rapidly transformed into the hydrophilic metabolites [^{11}C]MP4OH that elimination of [^{11}C]MP4OH from the brain can be ignored [8] and, thus, ^{11}C-MP4A kinetics can be described by a one-tissue one-rate constant compartmental model [13] (Figure 4.2).

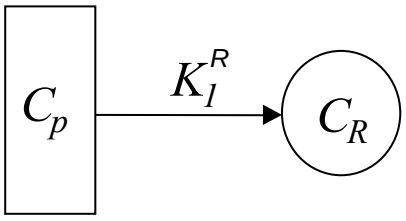

FIGURE 4.2 The one-tissue one-rate constant compartmental model of ^{11}C-MP4A in brain region having high AChE activity. C_p is the unmetabolized free tracer concentration curve in plasma, C_R the ^{11}C-MP4A tracer concentration in the target tissue, K_1^R [ml/ml/min] the joint rate constant of both tracer inflow into the tissue brain and tracer hydrolysis activity.

By assuming also in this region negligible blood volume presence, the model equation is:

$$\dot{C}_R(t) = K_1^R C_p(t) \qquad C_R(0) = 0 \tag{4.4}$$

where C_p is the unmetabolized free tracer concentration curve in plasma, C_R the ^{11}C-MP4A tracer concentration in the target tissue, K_1^R

[ml/ml/min] the joint rate constant of both tracer inflow into the tissue brain and tracer hydrolysis activity.

The Reference Tissue Model for ^{11}C-MP4A.

A reference model. i.e. a mathematical relationship for the region-of-interest concentration in terms of the reference region data and the kinetic parameters of both reference and target regions, can be derived by combining Eqs. 4.1, 4.3, and 4.4. In fact, from Eq. 4.1, taking Laplace transform:

$$\begin{aligned} (s + k_2 + k_3) \cdot C_1(s) &= K_1 C_p(s) \\ s \cdot C_2(t) &= k_3 C_1(s) \end{aligned} \tag{4.5}$$

and, from Eq. 4.4:

$$C_p(s) = \frac{1}{K_1^R} s \cdot C_R(s) \tag{4.6}$$

Substituting Eq. 4.6 in Eq. 4.3, one obtains:

$$\begin{aligned} C_1(s) &= \frac{K_1}{K_1^R} \frac{s}{(s + k_2 + k_3)} \cdot C_R(s) \\ C_2(t) &= \frac{K_1}{K_1^R} \frac{k_3}{(s + k_2 + k_3)} \cdot C_R(s) \end{aligned} \tag{4.7}$$

and, from Eq. 4.3:

$$C_T(s) = C_1(s) + C_2(s) = \frac{K_1}{K_1^R} \frac{s + k_3}{(s + k_2 + k_3)} \cdot C_R(s) \tag{4.8}$$

Finally, in temporal space, Eq. 4.8 returns:

$$\boxed{C_T(t) = K_R \cdot C_R(t) - K_R k_2 \cdot \int_0^t C_R(t) \cdot e^{-(k_2+k_3)(t-\tau)} d\tau} \tag{4.9}$$

where $K_R = \frac{K_1}{K_1^R}$ [unitless]. Eq. 4.9 describes the reference model of ^{11}C-MP4A. The three-model parameter K_R, k_2, k_3 can be estimated together

with their precision by using nonlinear weighted least squares (NLLS). However, since NNLS is computational demanding when pixel-wise quantification is performed, it is also possible to linearize the model of Eq. 4.9 and resort to less computational demanding algorithms. Up to now, several different methods and linearized version of the model of Eq. 4.9 have been proposed for ^{11}C-MPA4 quantification at pixel levels. Among all, the three most promising have been used and compared together with an additional novel method, developed during my Ph.D [33, 34] course: the reference tissue linear least squares (RLS) proposed for ^{11}C-MP4A by Nagatsuka et al 2001 [12], the reference ratio exponential (RRE) approach proposed by Herholz et al [13] and its version based on the use of a different estimation approach (RRE_BF) [14]; the comparison technique is the novel reference maximum a posteriori method (MAP). Results have been also compared to those obtained by using the "standard" NNLS estimator with model of Eq. 4.9.

4.1. RLS (Reference Tissue Based Linear Least Square Method)

In the early eighties (1984), Blomqvist [46] developed an innovative linear algorithm for the rapid calculation of the local rate constants for the category of the irreversible tracers. Nagatsuka et al.[12], implemented Blomqvist approach in case of ^{11}C-MP4A.

By combining equation 4.1 and 4.3, one has:

$$C_T(t) = K_1\int_0^t C_p(\theta)d\theta + K_1k_3\int_0^t\int_0^\theta C_p(\tau)d\tau d\theta - (k_2+k_3)\int_0^t C_T(\theta)d\theta \qquad (4.10)$$

Substituting Eq. 4.4 into Eq. 4.10:

$$C_T = K_R C_R(t) + K_R k_3\int_0^t C_R(\tau)d\tau - (k_2+k_3)\int_0^t C_T(\tau)d\tau \qquad (4.11)$$

and assuming:

$$\begin{aligned} p_1 &= \frac{K_1}{K_1^R} \equiv K_R \\ p_2 &= K_R \cdot k_3 \\ p_3 &= -(k_2 + k_3) \end{aligned} \tag{4.12}$$

one has:

$$C_T = p_1 C_R(t) + p_2 \int_0^t C_R(\tau)d\tau + p_3 \int_0^t C_T(\tau)d\tau \tag{4.13}$$

Once obtained the estimates of p_1, p_2, p_3, the original K_R, k_2, k_3 parameters can be derived from:

$$\begin{aligned} K_R &= p_1 \\ k_3 &= \frac{p_2}{p_1} \\ k_2 &= -p_3 - \frac{p_2}{p_1} \end{aligned} \tag{4.14}$$

The three p_1, p_2, p_3 unknown parameters can be estimated by linear least squares:

$$\begin{bmatrix} p_1 \\ p_2 \\ p_3 \end{bmatrix} = (\mathbf{X}^T\mathbf{X})^{-1}\mathbf{X}^T\mathbf{y} \tag{4.15}$$

where X is a N x 3 matrix, with N equal to the number of total frames, i.e. measurements, built in this way:

$$\mathbf{X} = \begin{bmatrix} C_R(t_1) & \int_0^{t_1} C_R(\tau)d\tau & \int_0^{t_1} C_T(\tau)d\tau \\ \vdots & \ddots & \vdots \\ C_R(t_N) & \int_0^{t_N} C_R(\tau)d\tau & \int_0^{t_N} C_T(\tau)d\tau \end{bmatrix} \tag{4.12}$$

$\mathbf{X}^T$ is the transpose of $\mathbf{X}$, and

$$\mathbf{y} = \begin{bmatrix} C_i(t_1) \\ \vdots \\ C_i(t_N) \end{bmatrix} \tag{4.13}$$

the vector of the measurements. Precision of parameter estimates can be derived from the covariance matrix given by:

$$\begin{bmatrix} V(p_1) & Cov_{12} & Cov_{13} \\ Cov_{12} & V(p_2) & Cov_{23} \\ Cov_{13} & Cov_{23} & V(p_3) \end{bmatrix} = \phi \cdot (\mathbf{X}^T\mathbf{X})^{-1} \qquad (4.14)$$

where $\phi = \frac{RSS}{N-m}$ with m the number of unknown parameters (3 in this case), and RSS representing the residual sum of squares evaluated at the minimum, i.e.

$$RSS = \sum_{i=1}^{N}\left[C_T(t_i) - C_T^{Obs}(t_i)\right]^2 \qquad (4.15)$$

with $C_T(t_i)$ and $C_T^{obs}(t_i)$ the model predicted and measured PET activity. The variances of K_R, k_2, k_3 estimates can be obtained by [12]:

$$\begin{aligned} V(K_R,k_2,k_3) = &\left(\frac{\partial \mathbf{y}}{\partial p_1}\right)^2 \cdot V(p_1) + \left(\frac{\partial \mathbf{y}}{\partial p_2}\right)^2 \cdot V(p_2) + \left(\frac{\partial \mathbf{y}}{\partial p_3}\right)^2 \cdot V(p_3) + \\ &2\left(\frac{\partial \mathbf{y}}{\partial p_1}\right)\left(\frac{\partial \mathbf{y}}{\partial p_2}\right)Cov_{12} + 2\left(\frac{\partial \mathbf{y}}{\partial p_1}\right)\left(\frac{\partial \mathbf{y}}{\partial p_3}\right)Cov_{13} + 2\left(\frac{\partial \mathbf{y}}{\partial p_2}\right)\left(\frac{\partial \mathbf{y}}{\partial p_3}\right)Cov_{23} \end{aligned} \qquad (4.16)$$

Of note is that RLS method proposed in [12] does not use weights.

4.2. RRE (Reference Ratio Exponential Approach)

A different approach for ^{11}C-MP4A quantification have been developed by Namba et al. [8]. The regional brain time-radioactivity curves $C_T(t)$ is again described by using the two-tissue three-rate constant compartmental model of Fig. 4.1, arterial input function and the Eq.4.1 and Eq. 4.3 solved to give:

$$C_T(t) = \frac{K_1 k_2}{k_2 + k_3}\int_0^t C_p(\tau)e^{-(k_2+k_3)(t-\tau)}d\tau + \frac{K_1 k_3}{k_2 + k_3}\int_0^t C_p(\tau)d\tau \qquad (4.17)$$

Assuming that the reference region is described by the model of Eq. 4.4:

$$C_R(t) = K_1^R \int_0^t C_p(\tau)d\tau \qquad (4.18)$$

and considering the mathematical approach proposed by Herholz and his colleagues [13]one can obtain C(t):

$$C(t) = \frac{C_T(t)}{C_R(t)} = A\frac{\int_0^t C_p(\tau)e^{-K(t-\tau)}d\tau}{\int_0^t C_p(\tau)d\tau} + B \tag{4.19}$$

where

$$\begin{aligned} A &= \frac{K_1}{K_1^R}\cdot\frac{k_2}{k_2+k_3} \quad [\text{unitless}] \\ B &= \frac{K_1}{K_1^R}\cdot\frac{k_3}{k_2+k_3} \quad [\text{unitless}] \\ K &= k_2 + k_3 \quad [\text{min}^{-1}] \end{aligned} \tag{4.20}$$

By assuming, now, that there is a very rapid fall of non-hydrolyzed tracer activity in plasma, the arterial input function, $C_p(t)$, can be described by a mono-exponential function:

$$C_p(t) = \alpha\cdot e^{-k_p t} \tag{4.21}$$

with $k_p >> K$ due to very rapid hydrolysis [13] of the tracer in plasma. Thus, by substitution of Eq. 4.21 in Eq. 4.19:

$$\begin{aligned} C(t) &= A\frac{\alpha\int_0^t e^{-k_p\tau}e^{-K(t-\tau)}d\tau}{\alpha\int_0^t e^{-k_p\tau}d\tau} + B = A\frac{e^{-Kt}\int_0^t e^{(K-k_p)\tau}d\tau}{\int_0^t e^{-k_p\tau}d\tau} + B \\ &= A\frac{e^{-Kt}\,\frac{1}{K-k_p}\left[e^{(K-k_p)t}-1\right]}{\frac{1}{k_p}\left[1-e^{-k_p t}\right]} + B \end{aligned} \tag{4.22}$$

Since $k_p >> K$, $e^{(K-k_p)t} \approx e^{-k_p t}$ and, thus, Eq. 4.22 becomes:

$$\boxed{C(t) = A\cdot e^{-Kt} + B} \tag{4.23}$$

The three model parameters, A, B, K, can be estimated by nonlinear least squares minimizing the weighted residuals sum of squares:

$$\mathrm{WRSS}(\mathbf{p}) = \sum_{i=1}^{N} \frac{\left[C(t_i) - C^{Obs}(t_i)\right]^2}{\sigma_i^{\,2}} \tag{4.24}$$

with $\mathbf{p} = [A, B, K]^T$ vector of model parameters, N = number of total frames, $C(t_i)$ and $C^{obs}(t_i)$ the model predicted and measured ratio (i.e. $C_T(t)/C_R(t)$) PET activity. σ_i^2 is the variance of the measurements errors assumed to be uncorrelated and normally distributed with zero mean and known with the exception of a term γ. The values $1/\sigma_i^2$ are occasionally referred to as weights. As *C(t)* expressed in Eq. 4.23 is obtained from the ratio of two observed noise corrupted measures, the error propagation must be consider during the parameters estimation process. Therefore, variance δ^2 was chosen to be equal to:

$$\delta_i^2 = \gamma\left(\frac{C_T(t_i)}{\Delta t(t_i)}\right) + \gamma\left(\frac{C_R(t_i)}{\Delta t(t_i)}\right) = \gamma \cdot \sigma_i^2 \tag{4.25}$$

where $\Delta t(t_i)$ is the scan interval at time t_i. The scale factor γ is estimated *a posteriori* [28] as:

$$\gamma = \frac{WRSS(\hat{p})}{N - m} \tag{4.26}$$

where $\mathrm{WRSS}(\hat{p})$ is the value of the sum of squares of residuals evaluated at the minimum.

The precision of estimates is obtained from the inverse of Fisher information matrix *F* by approximate measures of the covariance matrix Σ of estimation error $\hat{\mathbf{p}} - \mathbf{p}$:

$$\mathbf{\Sigma} = \mathbf{F}^{-1} = \begin{bmatrix} V(A) & Cov_{12} & Cov_{13} \\ Cov_{21} & V(k) & Cov_{23} \\ Cov_{31} & Cov_{32} & V(B) \end{bmatrix} \tag{4.27}$$

where **F** is the Fisher information matrix:

$$\mathbf{F}(p)\,|_{p=\hat{p}} = \mathbf{S}^T\mathbf{R}^{-1}\mathbf{S} \tag{4.28}$$

with **S** the sensitivity matrix of the model of Eq. 4.23, given by:

$$\mathbf{S}(k,i)=\begin{bmatrix} \frac{\partial C(p,t_1)}{\partial A} & \frac{\partial C(p,t_2)}{\partial A} & \dots & \dots & \frac{\partial C(p,t_N)}{\partial A} \\ \frac{\partial C(p,t_1)}{\partial B} & \frac{\partial C(p,t_2)}{\partial B} & \dots & \dots & \frac{\partial C(p,t_N)}{\partial B} \\ \frac{\partial C(p,t_1)}{\partial K} & \frac{\partial C(p,t_2)}{\partial K} & \dots & \dots & \frac{\partial C(p,t_N)}{\partial K} \end{bmatrix} \tag{4.29}$$

and *R* the known N x N weighted matrix:

$$R=\mathrm{diag}(1/\delta_i^2), \qquad i=1,..,N \tag{4.30}$$

Then the percent coefficient of variation of the estimates $\hat{p}$=[A, K, B], $CV(\hat{p}_k)$, is given by:

$$CV(\hat{p}_k)=\frac{\sqrt{\Sigma(k,k)}}{\hat{p}_k}\times 100, \quad k=1,...,m\ (m=3) \tag{4.31}$$

Finally, k_2 and k_3 values obtained from:

$$\begin{aligned} k_3 &= \frac{B}{A+B}\cdot K \quad [\mathrm{min}^{-1}] \\ k_2 &= \frac{A}{A+B}\cdot K \quad [\mathrm{min}^{-1}] \end{aligned} \tag{4.32}$$

The variance of k_3, i.e. the most interesting parameter, can be derived by using linear error transfer function as follows:

$$\begin{aligned} V(k_3) = &\left(\frac{\partial k_3}{\partial A}\right)^2\cdot V(A)+\left(\frac{\partial k_3}{\partial K}\right)^2\cdot V(K)+\left(\frac{\partial k_3}{\partial B}\right)^2\cdot V(B) \\ &+2\left(\frac{\partial k_3}{\partial A}\cdot\frac{\partial k_3}{\partial K}\right)\cdot Cov_{12}+2\left(\frac{\partial k_3}{\partial A}\cdot\frac{\partial k_3}{\partial B}\right)\cdot Cov_{13}+2\left(\frac{\partial k_3}{\partial B}\cdot\frac{\partial k_3}{\partial K}\right)\cdot Cov_{23} \end{aligned} \tag{4.33}$$

4.3. RRE_BF model (Reference Ratio Exponential based on Basis Function Approach)

Recently, Zundorf and his colleagues [14] extended and modified the non-invasive technique proposed by Herholz [13] based on reference ratio exponential (RRE) for the quantitation of AChE activity by ^{11}C-MP4A PET. They extend and modify this method in order to generate parametric images for analysis of local AChE activity without need for definition of

region of interest and to further improve the numerical representation of the input function by eliminating off the unnecessary mono-exponential approximation.

The method in based on the compartmental kinetic model of the tracer described in Eq. 4.19 (Figure 4.1) where Eq.4.18 is used to substitute C_p:

$$\begin{aligned} C(t) = \frac{C_T(t)}{C_R(t)} &= A\frac{\int_0^t \dot{C}_R(\tau)e^{-K(t-\tau)}d\tau}{C_R(t)} + B = A\frac{e^{-Kt}\int_0^t \dot{C}_R(\tau)e^{K\tau}d\tau}{C_R(t)} + B \\ &= A\frac{e^{-Kt}\left\{C_R(t)e^{Kt} - K\int_0^t C_R(\tau)e^{K\tau}d\tau\right\}}{C_R(t)} + B \\ &= A\frac{C_R(t) - K\int_0^t C_R(\tau)e^{K(t-\tau)}d\tau}{C_R(t)} + B \end{aligned} \qquad (4.34)$$

And, finally, one has:

$$\boxed{C(t) = A\left[1 - K\frac{\int_0^t C_R(\tau)e^{K(t-\tau)}d\tau}{C_R(t)}\right] + B = A\cdot W_K(t) + B} \qquad (4.35)$$

As seen for REE method, the three model parameters, A, B, K, can be estimated by nonlinear least squares, which is a time consuming approach above all if pixel-by-pixel quantification is required. In order to speed up the quantification process, a basis function approach [14] can be used. Following this approach, $W_K(t)$ is calculated by numeric integration for a set of different K that covers the entire range of interest. Subsequently, for each K values, A and B are estimated by weighted linear least square estimator. In particular, having K fixed to a specific value:

$$\begin{bmatrix} A \\ B \end{bmatrix} = (\mathbf{X}^T\mathbf{R}\mathbf{X})^{-1}\mathbf{X}^T \cdot \mathbf{R} \cdot \mathbf{y} \tag{4.36}$$

where X is a N x 2 matrix, with N equal to the number of total frames, i.e. measurements, built in this way:

$$\mathbf{X} = \begin{bmatrix} 1 & W_K(t_1) \\ \vdots & \vdots \\ 1 & W_K(t_N) \end{bmatrix} \tag{4.37}$$

$\mathbf{X}^T$ is the transpose of $\mathbf{X}$, and

$$\mathbf{y} = \begin{bmatrix} C(t_1) \\ \vdots \\ C(t_N) \end{bmatrix} = \begin{bmatrix} C_T(t_1)/C_R(t_1) \\ \vdots \\ C_T(t_N)/C_R(t_N) \end{bmatrix} \tag{4.38}$$

the vector of the measurements. *R* is the known N x N weighted matrix:

$$R = \mathrm{diag}(1/\sigma_i^2), \qquad i = 1,..,N \tag{4.39}$$

with σ_i^2 as in 4.24. The covariance matrix for A and B is given by:

$$\begin{bmatrix} V(p_1) & Cov_{12} \\ Cov_{12} & V(p_2) \end{bmatrix} = \gamma(X^TRX)^{-1} \tag{4.40}$$

with γ as in Eq.4.26.

Final optimum estimates of A, B, and K will coincide with the parameters set for which the weighted sum of residuals is smallest.
Finally, k_3 and k_2 estimates are obtained from equations 4.32 and an underestimation of the variance of k_3 from:

$$V(k_3) = \left(\frac{\partial k_3}{\partial A}\right)^2 \cdot V(A) + \left(\frac{\partial k_3}{\partial B}\right)^2 \cdot V(B) + 2\left(\frac{\partial k_3}{\partial A} \cdot \frac{\partial k_3}{\partial B}\right) \cdot Cov_{12} \tag{4.41}$$

In order to estimate a physiological grid for parameter K variation, i.e. the K minimum and maximum values, no information is giving about the range choose and about the number of values considered for the range interval, the so called basis function. Therefore, based on the information already published on k_2 and k_3 estimates we calculate K_{min} and a K_{max} as:

$$K_{\min} = k_{2\min} + k_{3\min}$$
$$K_{\max} = k_{2\max} + k_{3\max} \quad (4.42)$$

We choose the range interval for K such that:

$$K'_{\min} < K_{\min} \quad and \quad K'_{\max} > K_{\max} \quad (4.43)$$

Three different assumptions for K have been made:

1. K range between 0.05 and 0.5 with NBF=100 (C1);
2. K range between 0.01 to 1 with NBF=100 (C2);
3. K range between 0.01 to 1 with NBF=200 (C3);

where NBF denotes the basis function number.

4.4. R-NLLS (Reference Tissue based Non Linear Least Square Method)

The standard method to estimate regional hydrolysis rate of AChE using ^{11}C-MP4A images is to fit the regional time-activity curve (TAC) obtained by PET to the theoretical function derived from the kinetic model and the arterial input function using weighed nonlinear least squares (NLS) optimisation. In this study we also evaluated the results obtained by using model of Eq. 4.9 and the weighted nonlinear least squares estimator. Thus, the three rate constants, i.e. K_R, k_2, k_3 , are estimated by minimizing the following objective function:

$$\mathrm{WRSS}(\mathrm{p}) = \sum_{\mathrm{i}=1}^{\mathrm{N}} \frac{[\mathrm{C}_\mathrm{T}^{\mathrm{obs}}(\mathrm{t}_\mathrm{i}) - \mathrm{C}_\mathrm{T}(\mathrm{p}, \mathrm{t}_\mathrm{i})]^2}{\sigma_\mathrm{i}^2} \quad (4.44)$$

with $\mathbf{p} = [\mathrm{K}_\mathrm{R}, \mathrm{k}_2, \mathrm{k}_3]^\mathrm{T}$ vector of model parameters, N = number of total frames, $\mathrm{C}_\mathrm{T}(\mathrm{t}_\mathrm{i})$ and $\mathrm{C}_\mathrm{T}^{\mathrm{obs}}(\mathrm{t}_\mathrm{i})$ the model predicted and measured PET activity. σ_i^2 is known as the variance of the measurements errors assumed to be uncorrelated and normally distributed with zero mean. The total error variance δ^2 was chosen to be equal to:

$$\delta_i^2 = \gamma\left(\frac{C_T(t_i)}{\Delta t(t_i)}\right) = \gamma \cdot \sigma_i^2 \qquad (4.45)$$

where $\Delta t(t_i)$ is the scan interval at time t_i. The scale factor γ is estimated *a posteriori* [28] as in Eq. 4.26. The precision of estimates is obtained from Eq. 4.27 , i.e. from the inverse of Fisher information matrix and the percent coefficient of variation of the estimates obtained from Eq. 4.31.

4.5. MAP (Reference Tissue based Maximum a Posteriori Parameter Estimation)

The maximum *a posteriori* (MAP) estimator is closely related to the Fisherian method of maximum likelihood (ML). The ML estimator maximize the likelihood function, which is the conditional probability of data given the parameter vector [30, 31]. The MAP estimator expands this concept and considers not only the likelihood function but also the known a priori probability of the parameters [47]. MAP estimation is a Bayesian approach since a priori available statistical information on the unknown parameters is also exploited for their estimation. The updated probability, the so called a posteriori probability, is obtained according to the Bayes' theorem:

$$f(\mathbf{p} \mid \mathbf{C}_T^{obs}) = \frac{f(\mathbf{C}_T^{obs} \mid \mathbf{p}) f(\mathbf{p})}{f(\mathbf{C}_T^{obs})} \qquad (4.46)$$

where $f(\mathbf{p})$ is the prior probability of model parameters $\mathbf{p}$, $f(\mathbf{C}_T^{obs})$ is the prior probability of measurements $\mathbf{C}_T^{obs}$, and $f(\mathbf{C}_T^{obs} \mid \mathbf{p})$ is the conditional probability of measurements $\mathbf{C}_T^{obs}$ given the parameter vector $\mathbf{p}$. The denominator in Eq. 4.46 is called the normalization factor and is independent of the paramaters.. Thus, ignoring the denominator in Eq. 4.46, which is independent on $\mathbf{p}$, Eq. 4.46 can be rewritten as:

$$f(\mathbf{p} \mid \mathbf{C}_T^{obs}) \propto f(\mathbf{C}_T^{obs} \mid \mathbf{p}) f(\mathbf{p}) \qquad (4.47)$$

Finally, parameter estimates can be obtained by using a MAP estimator maximizing:

$$\hat{\mathbf{p}}_{MAP} = \arg\max_{\mathbf{p}}[f(C_T^{obs} \mid \mathbf{p}) f(\mathbf{p})] \tag{4.48}$$

A preliminary reference weighted non linear least squares (R-NLLS) analysis at TAC_ROI level was implemented in SAAM II software that is a general purpose modelling tool with a user friendly interface based on compartmental models; SAAM II software allows a fast kinetic analysis - for TAC_ROIs - in order to identify the parameters of interest(K_R, k_2, k_3). k_2 showed a low inter-region variability within subject (as already confirmed in the literature by Namba[8] and Herholz [10, 13] in a range of 0.08-0.12); it was assumed that k_2 has a priori Gaussian probability density function with mean and standard deviation equal to k_2 mean and SD estimates obtained with R-NLLS at TAC_ROI level for each subject. This additional probabilistic information was used to estimate tracer kinetic indexes at pixel and TAC_ROI level in MAP approach. In particular, assuming that k_2 model parameter and its measurement error have a Gaussian distribution, Eq. 4.48 can be shown to become:

$$\begin{aligned}\hat{\mathbf{p}}_{MAP} = \arg\min_{p}[C_T^{obs} - C_T]^T R^{-1}[C_T^{obs} - C_T] \\ + (k_2 - \mu_{k_2})^T \Omega_{k_2}^{-1} (k_2 - \mu_{k_2})\end{aligned} \tag{4.49}$$

where p is the parameter vector $p=[K_R, k_2, k_3]^T$, C_T^{obs} is the measurement vector, C_T is the vector prediction of the model of Eq. 4.9, μ_{k_2} is the a priori mean vector and $\Omega_{k_2}^{-1}$ the respective inverse of the covariance matrix. R^{-1} represents the inverse of the measurement error variance: the measurements has been chosen Gaussian, with zero mean and variance equal to $\delta^2 = \gamma C_T(t_i)/\Delta t(t_i)$ where $\Delta t(t_i)$ is the scan interval at time t_i. The scale factor γ is estimated *a posteriori* [28] as:

$$\gamma = \frac{WRSS(\hat{p})}{N-m} \tag{4.50}$$

where $WRSS(\hat{p})$ is the value of the cost function evaluated at the minimum, i.e., for p equal to the vector of estimated model parameters $\hat{p}$.

The precision of MAP estimates can be obtained from the covariance matrix of the estimation error [30]:

$$\Sigma_{MAP} = (SR^{-1}S^{T} + \Omega_{k_2}^{-1})^{-1} \tag{4.51}$$

where S is the sensitivity matrix of the model equation 4.9, the matrix with entries given by:

$$S(k,i) = \left.\frac{\partial C_i(p,t)}{\partial p_k}\right|_{\substack{t=t_i \\ p=\hat{p}}} \quad \text{for } k = 1,..,m; \qquad i = 1,...,N \tag{4.52}$$

Then the percent coefficient of variation of the estimates $\hat{p}_k$ (K_R, k_2, k_3), $CV(\hat{p}_k)$ is calculates using the same approach as in R-NLLS technique by:

$$CV(\hat{p}_k) = \frac{\sqrt{\Sigma_{MAP}(k,k)}}{\hat{p}_k} \times 100, \quad k = 1,...,m \ (m = 3) \text{ and } \hat{p}_1 = K_R \tag{4.63}$$

The name MAP just reflects the fact that point estimates are those which maximize the *a posteriori* probability density function, or equally minimize the cost function, given the *a priori* probability density function, the model structure, and the measurement error statistical description.

4.6. Parametric Images Processing

In order to obtain functional parametric images of K_R, k_2 and k_3, the mathematical methods previously described were implemented in Matlab software and applied to the 4D PET dynamic images (the originally reconstructed 4D PET images with voxels size of 2.5x2.5x4.25 mm).

The functional parametric images are processed as follows:

1. All parametric images (K_R, k_2, k_3) are "cleaned" in order to have only reliable estimates.
2. Images from step 1 are then smoothed using a median filter.

3. Smoothed parametric images undergoes step 3 to step 7 presented in chapter 3 for dynamic image processing: normalization to PET-FDG template (SPM2), coregistration to the single-subject canonical template(SPM2), extraction of quantitative information applying the masks ROIs generated with Marina software.

The flowchart of functional parametric images generation and processing is shown in figure 4.3. Two tailed unpaired t-test was applied to quantify the differences in k3 estimates at pixel level obtained by each procedure between the two groups of subjects. The value of p for which the differences were considered significant is $p<0.05$.

Functional Parametric Image Processing

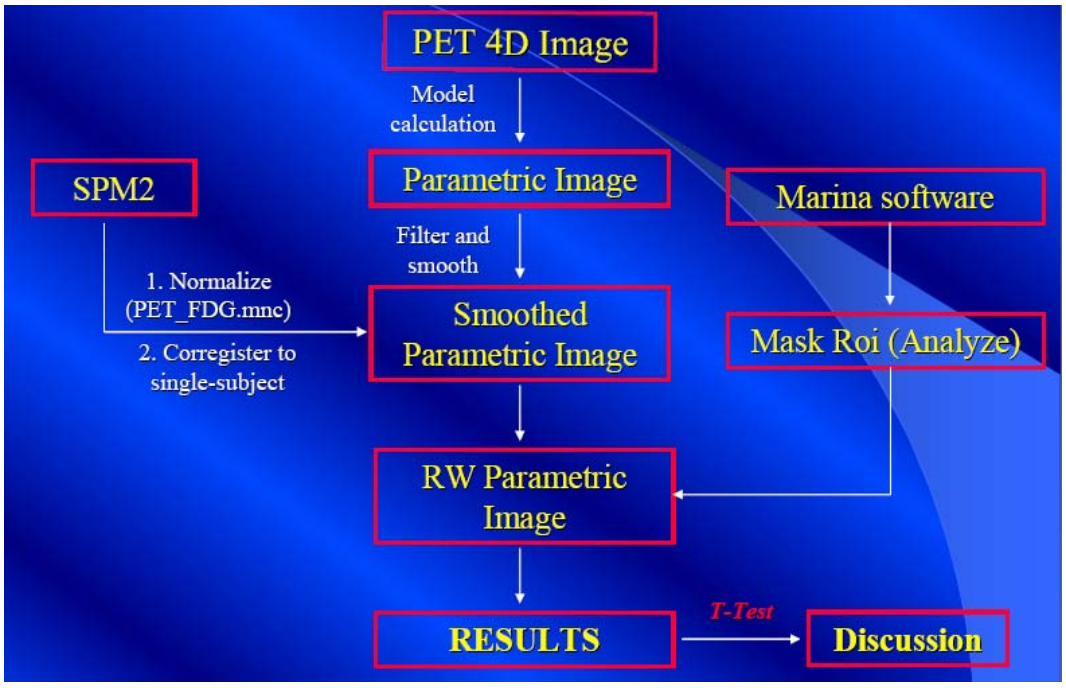

FIGURE 4.3 The flowchart of 4D ^{11}C-MP4A PET images processing at pixel-by-pixel level

Chapter 5

Results

AChE activity was measured in terms of the rate constant for hydrolysis of ^{11}C-MP4A, k_3. In particular, the methods described in the previous chapter are used in order to determine the quantitative kinetics indexes without arterial blood sampling and are as follows: the method proposed in the literature: reference tissue linear least squares (RLS) proposed by Blomqvist [46] and validated by Nagatsuka et al 2001 [12], reference ratio exponential (RRE) approach proposed by Herholz and coworkers in 2001 [13], Zundorf et al that used a modified simplification hypothesis of Herholz approach in order to reduce unnecessary bias and implemented a basis function approach in order to estimate the parameters of interest [14]; the new proposed approaches based on reference tissue nonlinear least squares (R-NLLS) and reference maximum a posteriori method (MAP).

5.1. RLS results and discussion

RLS approach was applied at both pixel (pTAC) and ROI (TAC_ROI) level in order to obtain k_3 estimates. Precision of estimates was measured in terms of variation coefficient (CV) described in section 4.1. Parametric images of K_R, k_2 and k_3 of the entire dataset were filtered for the pixels estimated with precision higher than 300 and k_3 values higher than 0.95 min-1. Thus were obtained only reliable parametric images of the indexes

describing tracer kinetics that undergoes parametric images processing flowchart presented in section 4, figure 4.3.

AChE activity is measured in terms of tracer hydrolysis rate constant k_3. Average k_3 parametric images for both groups of subjects are shown in figure 5.1: in panel A are represented the lower slices of the brain containing anatomical structure like cerebellum, hippocampus (HP), temporal (TE) and frontal (FR) lobe, while in panel B are represented brain structure like thalamus (TH), basal ganglia (GB), TE, FR, occipital (OC), insula (I) and initial of parietal (PA) lobe. Each panel represents the mean k_3 parametric image of the NC in the top line and AD in the bottom line. All images are represented using the same image scale: [0, 0.4] min^{-1}.

Two tailed t-test was applied in order to identify differences in k_3 estimates between the two groups of subjects.

Despite the small group of dataset – 4NC and 7AD – RLS method applied at pixel level identify significant reduction of AChE activity in AD patients respect to normals in area with low enzyme expression like FR, TE, PA, OC (Table 5.1) with $p<0.005$. However, no differences were identified applying the same mathematical approach at TAC_ROI level except the Rolandic operculum region (R).

	RLS pixel-by-pixel			RLS TAC_ROI		
ROI	NC MEAN ± SD	AD MEAN ± SD	p	NC MEAN ± SD	AD MEAN ± SD	p
FR	0.0726 ± 0.005	0.0566 ± 0.006	0.002	0.0837 ± 0.010	0.0788 ± 0.008	0.387
OC	0.0648 ± 0.005	0.0512 ± 0.007	0.009	0.0772 ± 0.008	0.0691 ± 0.011	0.233
PA	0.0687 ± 0.007	0.0552 ± 0.004	0.003	0.0747 ± 0.010	0.0677 ± 0.008	0.225
TE	0.0747 ± 0.008	0.0599 ± 0.006	0.006	0.0806 ± 0.011	0.0692 ± 0.009	0.098
TH	0.0771 ± 0.024	0.0396 ± 0.012	0.007	0.2312 ± 0.031	0.1403 ± 0.079	0.060
HP	0.0752 ± 0.010	0.0561 ± 0.011	0.022	0.1194 ± 0.024	0.1365 ± 0.041	0.470
I	0.0834 ± 0.006	0.0590 ± 0.009	0.001	0.1154 ± 0.014	0.0973 ± 0.016	0.093
R	0.0854 ± 0.007	0.0679 ± 0.006	0.002	0.0959 ± 0.010	0.0810 ± 0.006	0.012

TABLE 5.1 RLS k_3 indexes obtained at pixel-by-pixel level and TAC_ROI level in brain area with low enzyme activity (neocortex) and low to moderate (HP, R, I) and moderate (TH) enzyme expression in both group of subjects and the respective p value.

RLS method is not able to give reliable estimates of k_3 indexes when applied at pixel level in area with moderate enzyme activity like thalamus and low to moderate as hippocampus (see Table 5.1 and FIGURE. 5.2) even if identifies a significant difference in k_3 values between the groups of subjects (p=0.007 for TH) (Table 5.1).

k_3 estimates obtained at TAC_ROI level show a mean variation of +11% in NC and +22% in AD respect to k_3 estimates at pixel level for the neocortex area and a higher variation of estimates in TH and HP regions: +67% in NC and +72% AD for TH and +37% in NC and +59% in AD respect to k_3 index estimated in the same areas at pixel level. (FIGURE 5.2). The variation between the pixel and TAC_ROI estimates was calculated as ($1\text{-}pixel\_k_3 / TAC\_ROI\_k_3$)$*100$.

Namba and his colleagues [8] identify k_3 estimates in neocortex area in 20 normals subjects using the standard quantification model at TAC_ROI level and arterial input function. The mean value identified on neocortex – as mean of k_3 estimates in FR, OC, TE, PA lobes – was 0.076 ± 0.008 that was considered the "true" k_3 value in NC. Bias of mean k_3 values estimated in neocortex area at pixel and TAC_ROI level was calculated respect to the considered "true" value as follows:

$$\%bias = \left(\frac{estimated\_k_3}{true\_k_3} - 1 \right) * 100 \qquad (5.1)$$

The results obtained applying RLS mathematical approach at pixel level underestimates about 7% the "true" k_3 while there is an overestimation of 4% of k_3 index in case of TAC_ROI approach in cortex area with low enzyme expression. Considering the high variation between pixel and TAC_ROI of k_3 estimates in neocortex area in AD subjects (22%, Table 5.1), RLS might be a good model to be applied at pixel-by-pixel level in order to preserve all the information of tracer kinetics in case of neurodegeneration and to estimate k_3 in area with low enzyme activity.

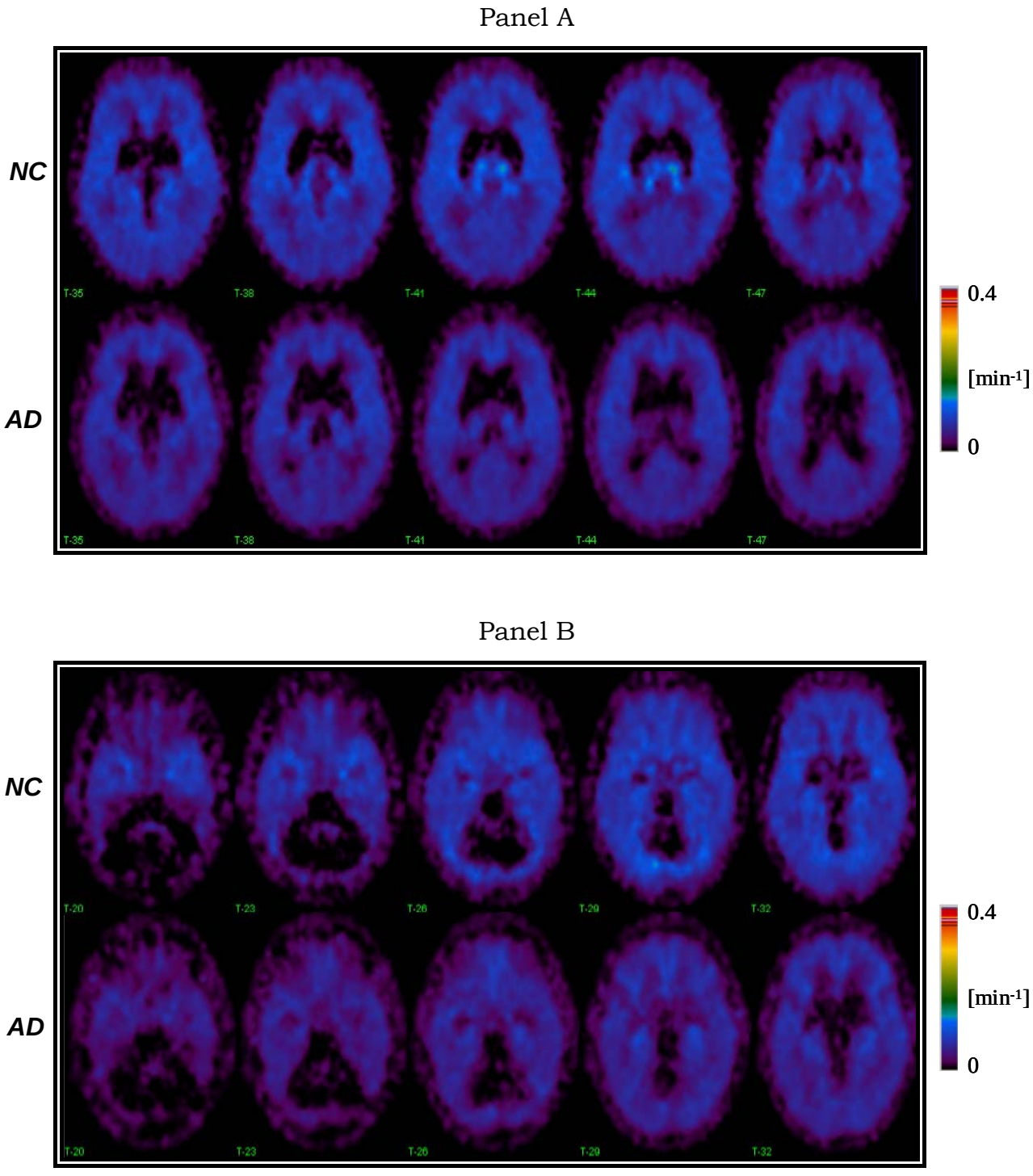

FIGURE 5.1 Average of normalized and co-registered parametric image of k_3 obtained with RLS mathematical procedure for both groups of subjects: NC upper line and AD bottom line in Panel A and Panel B. Image scale: [0, 0.4] min^{-1}.

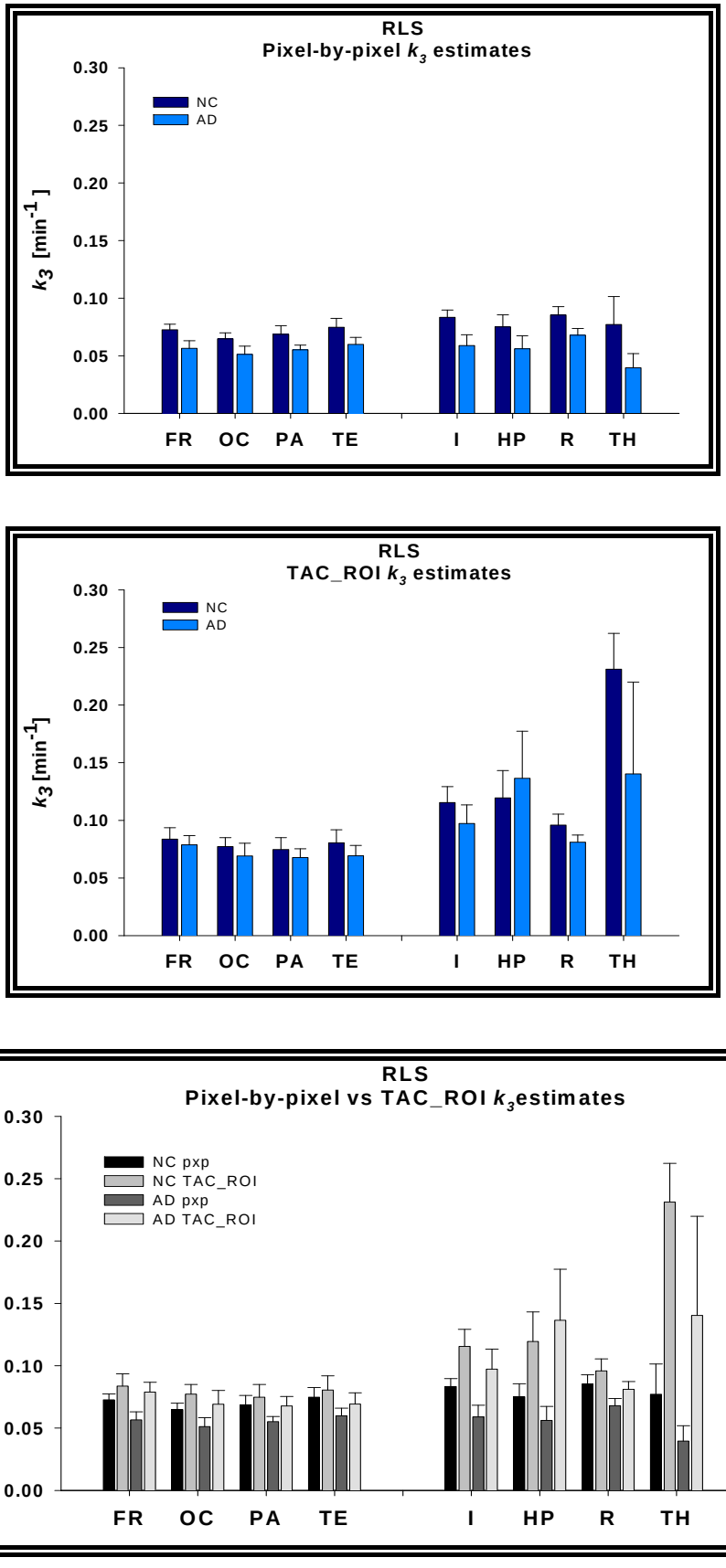

FIGURE 5.2 RLS k_3 estimates at pixel-by-pixel (pxp) level (top panel), TAC_ROI level (middle panel) and comparison pixel vs TAC_ROI estimates (bottom panel).

5.2. RRE results and discussion

Parametric images of k_3 obtained with the ratio approach [13] undergoes the steps for image processing described in the flowchart from Figure 4.3 in order to have reliable filtered, normalized and corregistered images (Figure 5.3).

Two tailed t-test was applied in order to identify differences in k_3 estimates between the two groups of subjects.

RRE method applied at pixel level identify significant reduction of AChE activity in AD patients respect to normals only in FR lobe from the neocortex area, $p<0.05$. In the TH, I, and R area were also identify significant differences between the studied groups (table 5.2). However, no significances were identified applying the same mathematical approach at TAC_ROI level in the neocortex area as shown in table 5.2.

	RRE pixel-by-pixel			RRE TAC_ROI		
ROI	NC	AD		NC	AD	
	MEAN_NC	MEAN ± SD	p	MEAN_NC	MEAN ± SD	p
FR	0.0844 ± 0.008	0.0737 ± 0.005	0.026	0.0703 ± 0.009	0.0631 ± 0.007	0.173
OC	0.0643 ± 0.007	0.0559 ± 0.011	0.215	0.0642 ± 0.007	0.0553 ± 0.010	0.161
PA	0.0639 ± 0.009	0.0560 ± 0.009	0.173	0.0624 ± 0.009	0.0546 ± 0.008	0.161
TE	0.0721 ± 0.010	0.0602 ± 0.011	0.107	0.0683 ± 0.010	0.0564 ± 0.009	0.064
TH	0.1777 ± 0.023	0.1140 ± 0.045	0.029	0.1977 ± 0.023	0.1458 ± 0.080	0.245
HP	0.1128 ± 0.017	0.1067 ± 0.021	0.639	0.1040 ± 0.013	0.1108 ± 0.031	0.686
I	0.1011 ± 0.009	0.0821 ± 0.011	0.015	0.1013 ± 0.008	0.0809 ± 0.014	0.029
R	0.0814 ± 0.008	0.0657 ± 0.006	0.005	0.0809 ± 0.008	0.0655 ± 0.006	0.005

TABLE 5.2 RRE k_3 indexes obtained at pixel-by-pixel level and TAC_ROI level in brain area with low enzyme activity (neocortex) and low to moderate (HP, R, I) and moderate (TH) enzyme expression in both group of subjects and the respective p value.

The brain areas where the model seemed to be conservative in identifying significant differences between normals and AD patients, no matter if applied at pixel or TAC_ROI level are represented by insula and Rolandic operculum (R).

k_3 estimates obtained at TAC_ROI level show a mean variation of -7% in NC and AD respect to k_3 estimates at pixel level for the neocortex area and a higher variation of estimates in TH and HP regions: +10% in NC and +22% AD for TH and -8% in NC and +4% in AD respect to k_3 index

estimated in the same areas at pixel level. (FIGURE 5.4). The variation between the pixel and TAC_ROI estimates was calculated as *(1-pixel_k_3/TAC_ROI_k_3)*100*.

Panel A

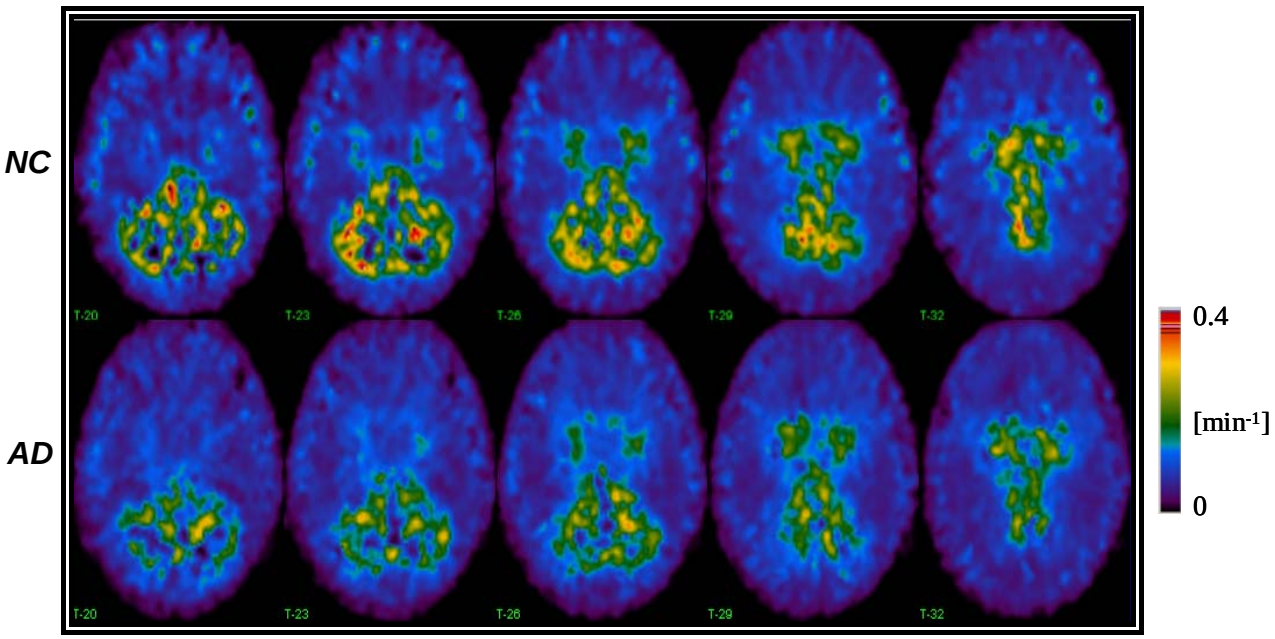

Panel B

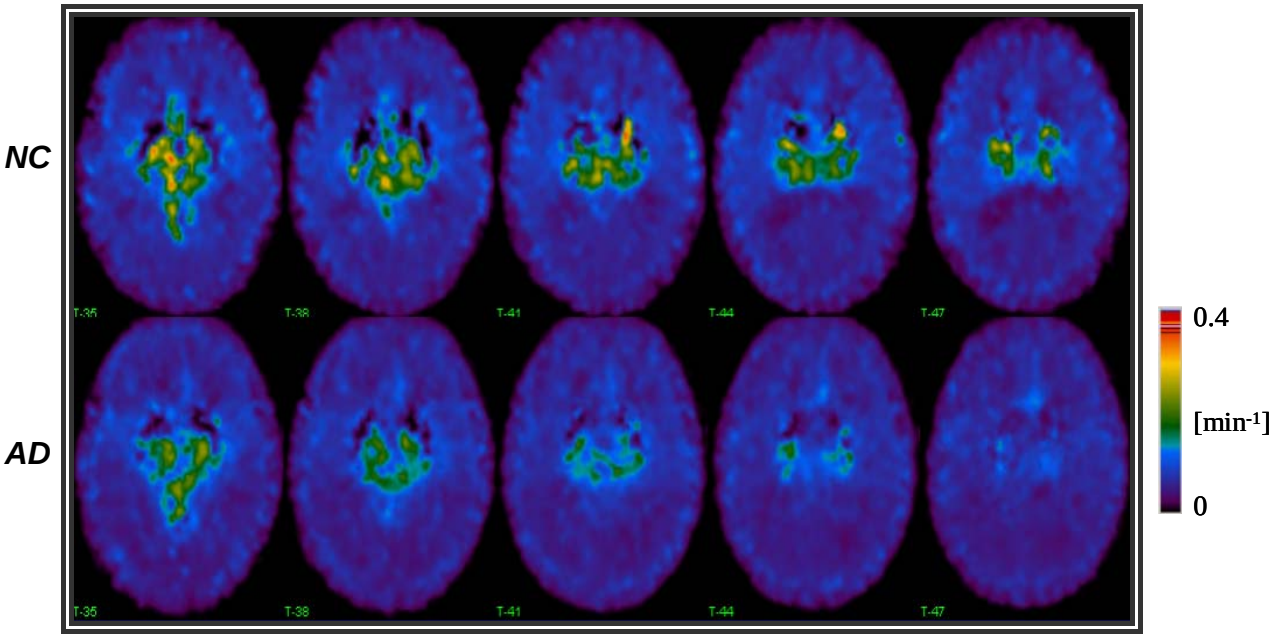

FIGURE 5.3 Average of normalized and co-registered parametric image of k_3 obtained with RRE mathematical procedure for both groups of subjects: NC upper line and AD bottom line in panel A and panel B. Image scale: [0, 0.4] min-1.

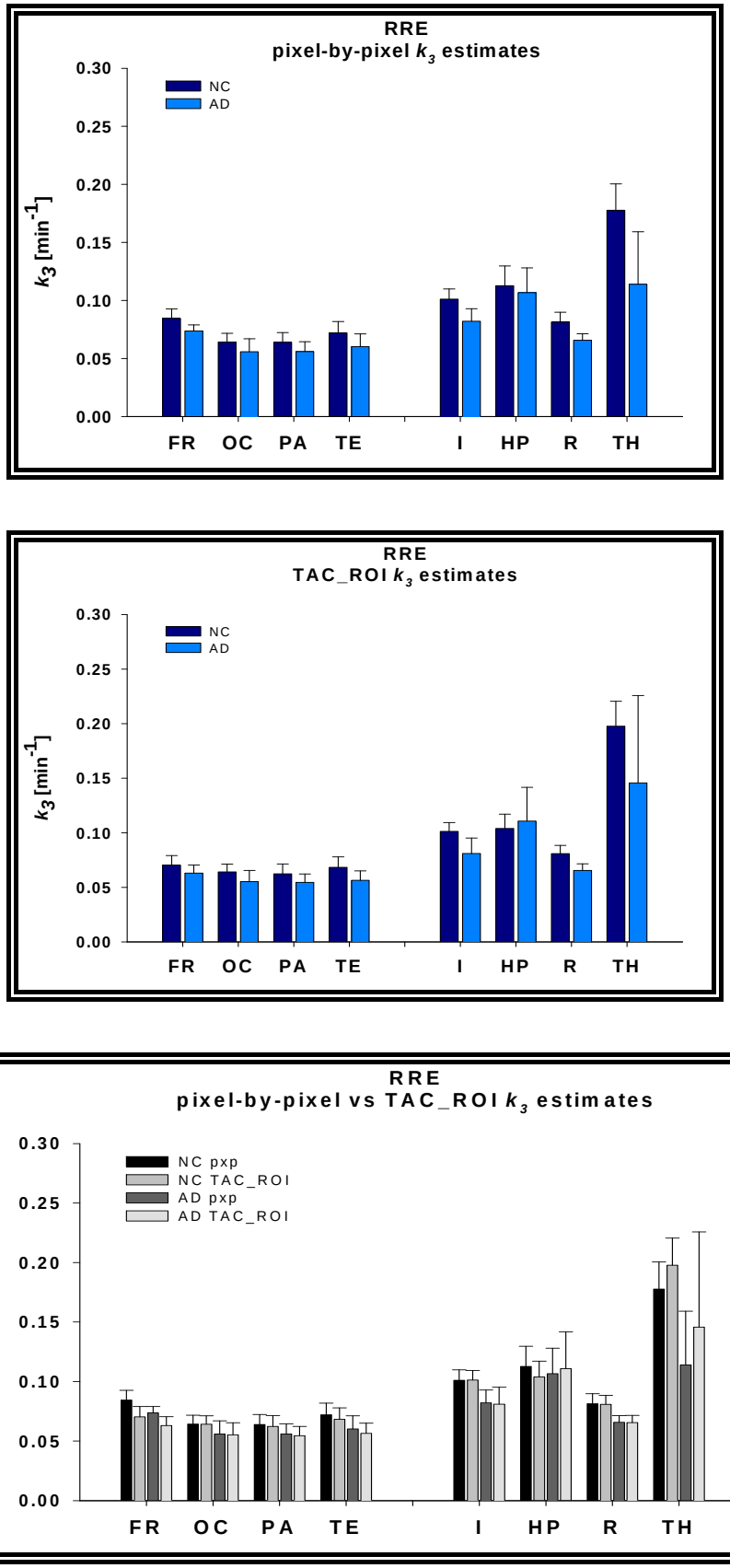

FIGURE 5.4 RRE k_3 estimates at pixel-by-pixel (pxp) level (top panel), TAC_ROI level (middle panel) and comparison pixel vs TAC_ROI estimates (bottom panel).

However, the results obtained applying the model at pixel level presented in Table 5.2 are not in good agreement with the published data in the literature [13, 19].

Therefore we verify the performance of RRE in estimating k_2 and it was observed inaccurate estimates of this parameter. In order to consider only reliable parameter estimates, RRE parametric images have been filtered by calculate a threshold for k_2 estimates. The threshold was estimated in each subject from the k_2 parametric image as the mean k_2 value to which wad added twice the standard deviation. A uniform k_2 threshold of 2 min^{-1} was obtained for each person participated in the study. In this way, only pixels having reliable estimates for RRE model parameters are taken into account. The new k_3 estimates obtained by RRE corrected for the threshold (RRE_t) are reported in table 5.3.

	RRE pixel-by-pixel			RRE_t pixel-by-pixel		
ROI	NC	AD		NC	AD	
	MEAN_NC	MEAN ± SD	p	MEAN_NC	MEAN ± SD	p
FR	0.0844 ± 0.008	0.0737 ± 0.005	0.026	0.0703 ± 0.011	0.0471 ± 0.020	0.067
OC	0.0643 ± 0.007	0.0559 ± 0.011	0.215	0.0594 ± 0.007	0.0388 ± 0.019	0.069
PA	0.0639 ± 0.009	0.0560 ± 0.009	0.173	0.0609 ± 0.009	0.0399 ± 0.020	0.077
TE	0.0721 ± 0.010	0.0602 ± 0.011	0.107	0.0686 ± 0.010	0.0437 ± 0.022	0.065
TH	0.1777 ± 0.023	0.1140 ± 0.045	0.029	0.1206 ± 0.0329	0.0655 ± 0.045	0.062
HP	0.1128 ± 0.017	0.1067 ± 0.021	0.639	0.0820 ± 0.0189	0.0639 ± 0.035	0.375
I	0.1011 ± 0.009	0.0821 ± 0.011	0.015	0.0866 ± 0.0109	0.0511 ± 0.023	0.019
R	0.0814 ± 0.008	0.0657 ± 0.006	0.005	0.0789 ± 0.0082	0.0513 ± 0.023	0.049

TABLE 5.3 RRE k_3 indexes obtained at pixel-by-pixel level before (RRE) and after threshold correction (RRE_t) in brain area with low enzyme activity (neocortex) and low to moderate (HP, R, I) and moderate (TH) enzyme expression in both group of subjects and the respective p value.

The mean k_3 estimates at pixel level corrected for the threshold (RRE_t), in neocortex area are 10% lower in NC and 45% decreased in AD. The TH and HP corrected k_3 indexes showed a higher decrease of 47% in NC and 74% in AD for TH and 30% in normals and 67% in pathologic subjects for HP region respect to non corrected k_3 indexes for the same brain areas. Corrected parametric images of k_3 in both group of subjects showed significant differences respect to non corrected parametric images of the same study groups (FIGURE 5.5). Anyway, the k_3 estimates

corrected for the threshold are to be considering reliable for further comparison.

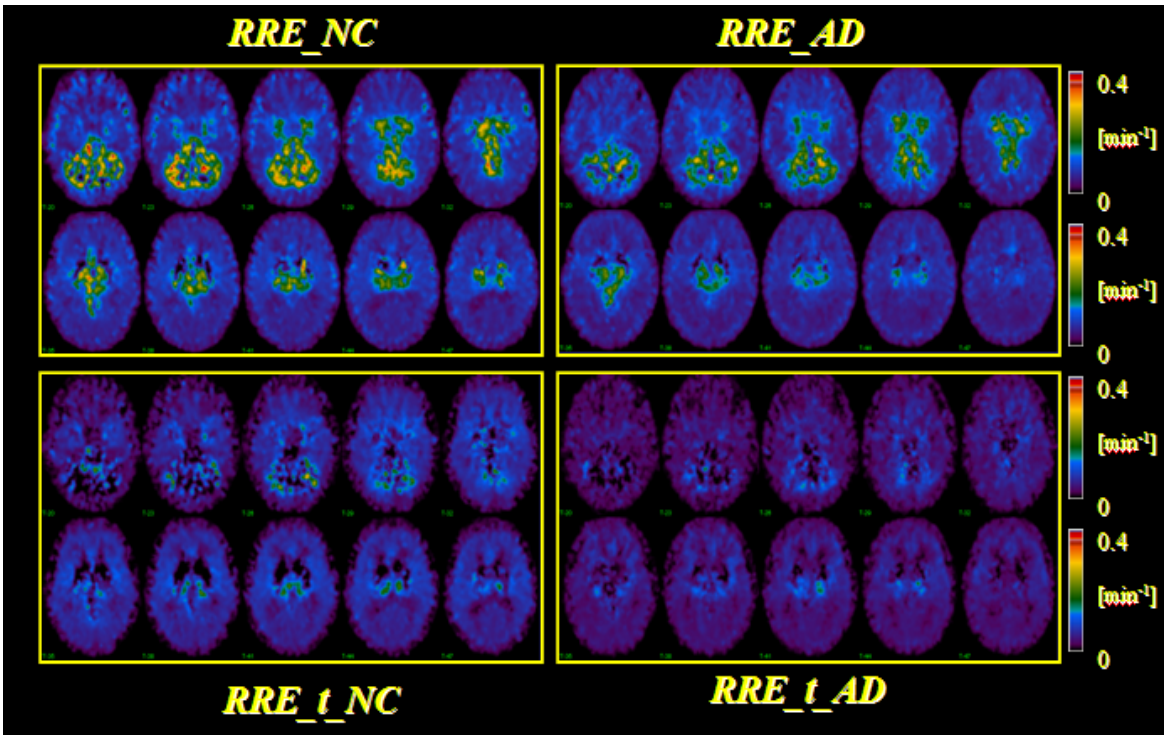

FIGURE 5.5 Average of normalized and co-registered parametric image of k_3 obtained with RRE mathematical procedure not corrected (RRE) and corrected with the threshold (RRE_t) for both groups of subjects: NC (RRE_NC, RRE_t_NC) left part of the panel and AD (RRE_AD, RRE_t_AD) located on the right part of the panel. Images scale: [0, 0.4] min^{-1}.

Bias of mean k_3 values estimated in neocortex area at pixel (RRE_t) and TAC_ROI level was calculated respect to the considered "true" value identified by Namba [8] as follows:

$$\%bias = \left(\frac{estimated\_k_3}{true\_k_3} - 1 \right) * 100 \qquad (5.1)$$

The results obtained applying RRE mathematical approach with the correction for the threshold at pixel level underestimates about 14% the "true" k_3 while there is an underestimation of 12% of k_3 index in case of TAC_ROI approach in neocortex area.

We also consider the "true" values of k_3 index in TH (0.266 min^{-1}) and HP (0.11 min^{-1}) region as the ones identified by Nagatsuka and his

colleagues [12] in normal subjects, using the standard non linear estimation method with arterial input.

The bias calculated with equation 5.1 revealed an underestimation of pixel-by-pixel k_3 indexes in NC of 55% for TH and 25% for HP. In case of TAC_ROI k_3 estimates the identified bias for both TH and HP revealed an underestimation of 26% respect to the considered "true" k_3 values.

RRE_t is not a reliable method for the estimation of k_3 index in area with low to moderate and moderate AChE activity, and proved to have difficulties in giving reliable estimates even in brain area with low enzyme expression.

5.3. RRE_BF results and discussion.

Recently, Zundorf and his colleagues [14] extended and modified the non-invasive technique proposed by Herholz [13] based on reference ratio exponential (RRE) for the quantitation of AChE activity by MP4A PET.

We applied this new proposed technique at pixel-by-pixel level, without applying the smooth of 10 mm FWHM Gaussian filter to the PET dynamic image as described [14]. We also considered in the analysis – as shown in flowchart presented in figure 4.2 - all brain pixels in order to calculate k_3 and k_2 (Eq. 4.32) by estimation of A, B, and K from the weighted linear procedure previously described (See chapter 4, subsection 4.3). As in the RRE approach, k_3 parametric images are filtered for the value k_2 threshold of 2 in order to consider only reliable estimates. Striatum was used as reference region.

Three different assumptions for K have been made:

4. K range between 0.05 and 0.5 with NBF=100 (C1).
5. K range between 0.01 to 1 with NBF=100 (C2).
6. K range between 0.01 to 1 with NBF=200 (C3).

Groups mean has been compared by applying two tailed sample t-test on the mean cortical k_3 values of the subjects. The mean k_3 values were calculated by averaging all voxels of the parametric image within the

standard ROI masks generated with Marina software as already described (flowchart in figure 4.3).

Mean, normalized and co-registered k_3 parametric image for both groups of subjects (NC and AD), obtained applying RRE_BF technique considering the three different conditions (C1, C2, C3) are shown in FIGURE 5.6.

RRE_BF method applied at pixel level identify significant reduction of AChE activity in AD patients respect to normals only in PA lobe from the neocortex area, in the TH, I, and R area, with $p<0.05$, when assuming condition C1 for K index; in TH, I, R in case of C2 condition and at I and R area level for C3 (see TABLE 5.4).

No improvement in model performance is observed when consider the other two assumption, for K, C2 and C3, in order to calculate k_3 index at neocortex level. A slight improvement in the performance of the procedure is identifying in case of C2 condition for TH (Table 5.4, Figure 5.7).

The variation of k_3 estimates when considering the three conditions for K are calculated as follows:

(1-C1_estimate/C2_estimate)*100 for NC and respectively AD.

(1-C2_estimate/C3_estimate)*100 for NC and respectively AD.

The variation analysis on k_3 estimates obtained with basis function approaches revealed that when K range is increased (from C1 to C2 with constant NBF) at neocortex level we have a decreased in estimates of 2% in NC and 5% in AD subjects, in TH this variation is higher: +14% in NC and +5% in AD while at HP level we have a variation of +5% in both groups.

In case of the same K interval but a doubled increased NBF (C2 to C3) the variation of k_3 estimates at neocortex level is around 3% in NC and less than 1% in AD. A higher variation was identified in case of TH: a decreased in k_3 estimates of 13% for NC and a little variation of less than 1% in AD.

ROI	RRE_BF b=[0.05;0.5], NBF=100			RRE_BF b=[0.01;1], NBF=100			RRE_BF b=[0.01;1], NBF=200		
	NC	AD		NC	AD		NC	AD	
	MEAN ± SD	MEAN ± SD	p	MEAN ± SD	MEAN ± SD	p	MEAN ± SD	MEAN ± SD	p
FR	0.0823 ± 0.016	0.0707 ± 0.006	0.121	0.0816 ± 0.019	0.0690 ± 0.010	0.168	0.0929 ± 0.029	0.0690 ± 0.010	0.069
OC	0.0695 ± 0.009	0.0593 ± 0.007	0.068	0.0675 ± 0.010	0.0565 ± 0.008	0.073	0.0570 ± 0.023	0.0565 ± 0.008	0.954
PA	0.0711 ± 0.013	0.0584 ± 0.005	0.044	0.0676 ± 0.016	0.0530 ± 0.007	0.055	0.0607 ± 0.022	0.0530 ± 0.007	0.406
TE	0.0810 ± 0.014	0.0664 ± 0.009	0.059	0.0801 ± 0.014	0.0634 ± 0.012	0.063	0.0770 ± 0.016	0.0633 ± 0.012	0.128
I	0.1019 ± 0.017	0.0799 ± 0.010	0.025	0.1055 ± 0.018	0.0801 ± 0.013	0.024	0.1073 ± 0.019	0.0800 ± 0.013	0.019
HP	0.1096 ± 0.029	0.0902 ± 0.020	0.217	0.1178 ± 0.031	0.0948 ± 0.028	0.245	0.1135 ± 0.034	0.0948 ± 0.028	0.354
R	0.0894 ± 0.013	0.0719 ± 0.008	0.020	0.0893 ± 0.014	0.0693 ± 0.011	0.026	0.0877 ± 0.014	0.0693 ± 0.011	0.036
TH	0.1522 ± 0.032	0.0984 ± 0.032	0.024	0.1768 ± 0.035	0.1035 ± 0.040	0.014	0.1566 ± 0.061	0.1034 ± 0.040	0.112

TABLE 5.4 RRE_BF mean k_3 indexes obtained at pixel-by-pixel level (considering the three assumptions of range(b) and number of basis function (NBF)) in brain area with low enzyme activity (neocortex) and low to moderate (HP, R, I) and moderate (TH) enzyme expression in both group of subjects and the respective p value.

Mean k_3 values estimated in neocortex area at pixel level for normal subjects were also compare to the considered "true" value identified by Namba [8] for NC .

A bias was calculated as follows:

$$\%bias = \left(\frac{estimated\_k_3}{true\_k_3} - 1 \right) * 100 \qquad (5.1)$$

The results obtained applying RRE_BF mathematical approach at pixel level while considering the three different assumption (C1, C2 and C3) give good mean estimates in C1 condition (bias 0.3%), underestimates about 2% the "true" k_3 when considering C2 and there is an underestimation of 5% of k_3 index in case of C3 approach in neocortex area.

We also consider the "true" values of k_3 index in TH (0.266 min^{-1}) and HP (0.11 min^{-1}) region as the ones identified by Nagatsuka and his colleagues [12] in normal subjects, using the standard non linear estimation method with arterial input.

The bias calculated with equation 5.1 revealed an underestimation of pixel-by-pixel mean k_3 indexes in NC for TH of 43% , 34% and 41% when consider assumption C1, C2 and respectively C3. A lower variation in mean k_3 estimates was revealed for HP respect to the considered "true" k_3 values: -0.4% for C1, +7% case C2 and 3% for assumption C3.

Basis function approach [14] of Herholz method [13] was developed in order to obtain k_3 index in area with low enzyme activity. The results obtained applying RRE_BF technique to our data set is not in good agreement with the already published results [14]: in our case the method does not indicate a high sensitivity in detecting mild reduction of AChE activity early in the course of AD. However, since k_3 estimates in neocortex area calculated in case of C1 assumption for K showed the smallest bias respect to the considered true k_3 value, these indexes are going to be used in further models performance comparison.

Panel A

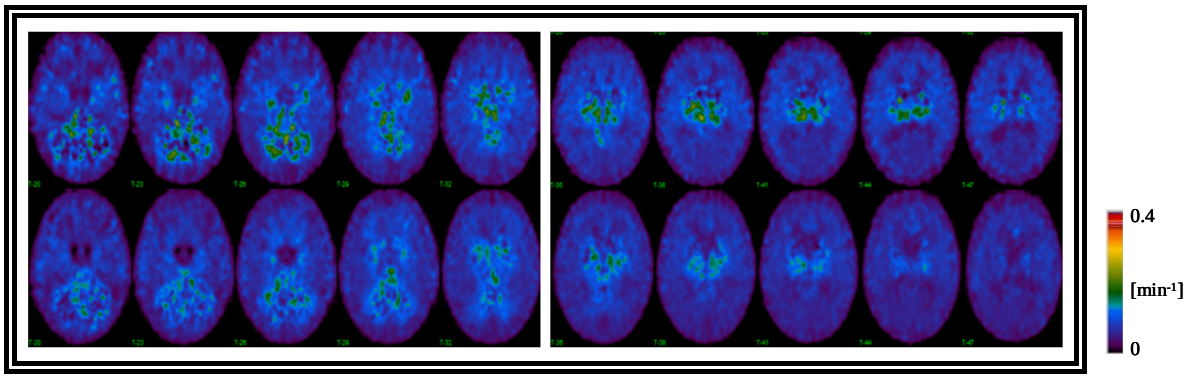

Panel B

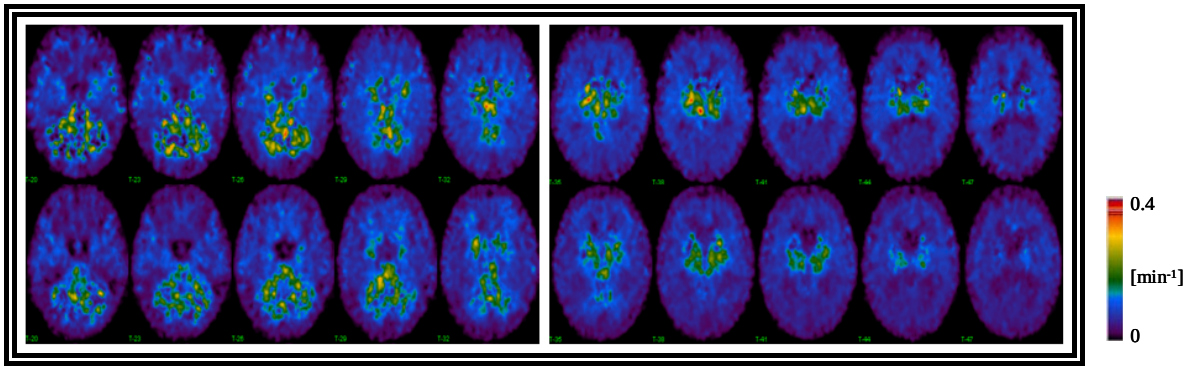

Panel C

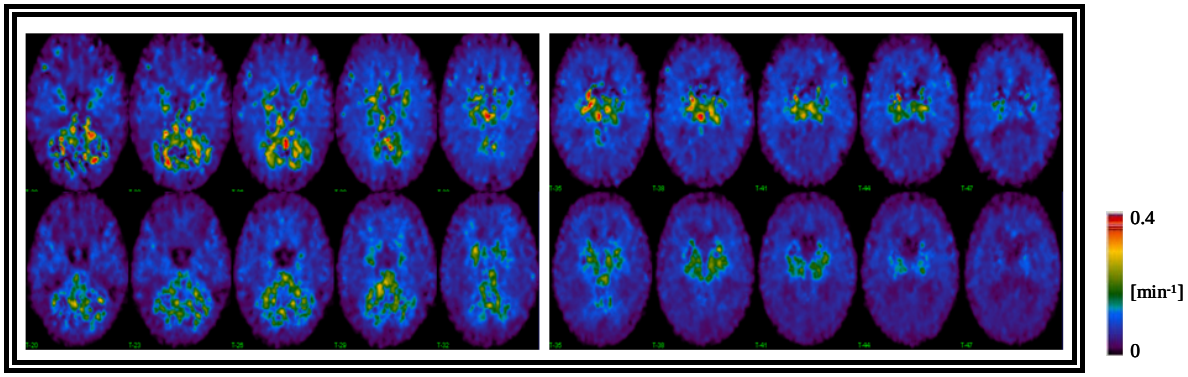

FIGURE 5.6 Average of normalized and co-registered parametric image of k_3 obtained with RRE_BF mathematical procedure for both groups of subjects: NC upper line and AD bottom line in each panel considering the assumption on K index: C1 in panel A, C2 in panel B and C3 in panel C. Images scale: [0, 0.4] min^{-1}.

Panel A

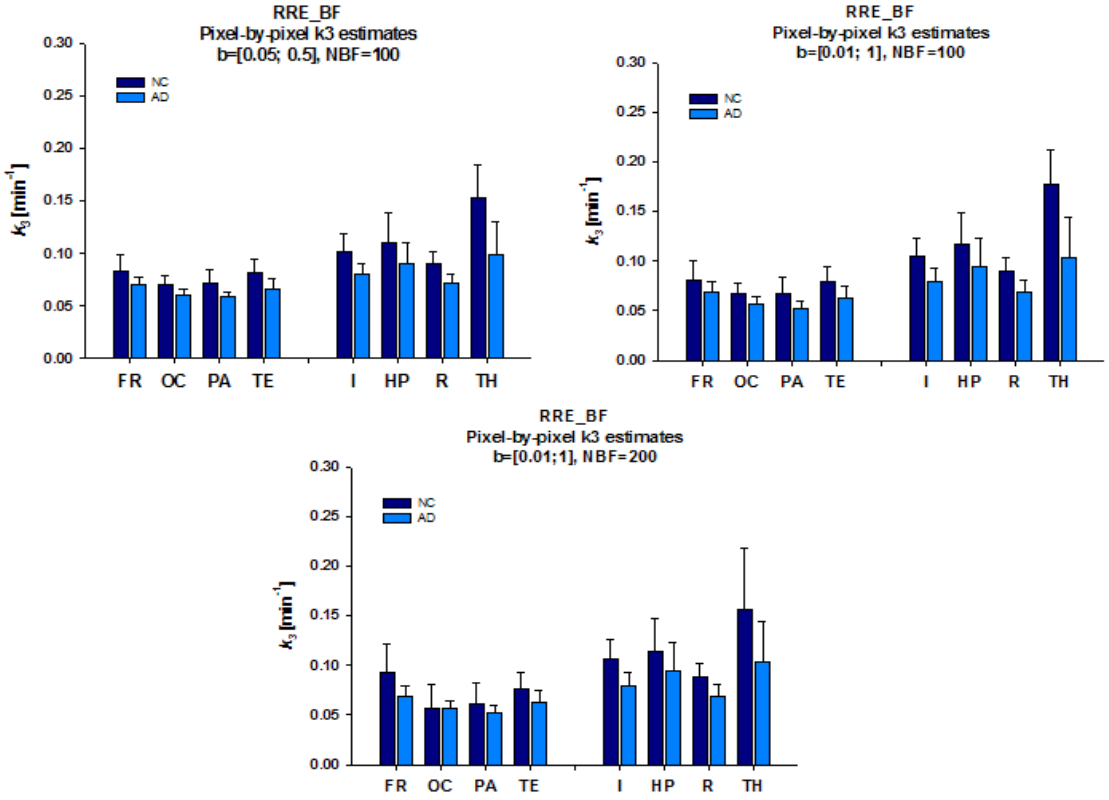

Panel B

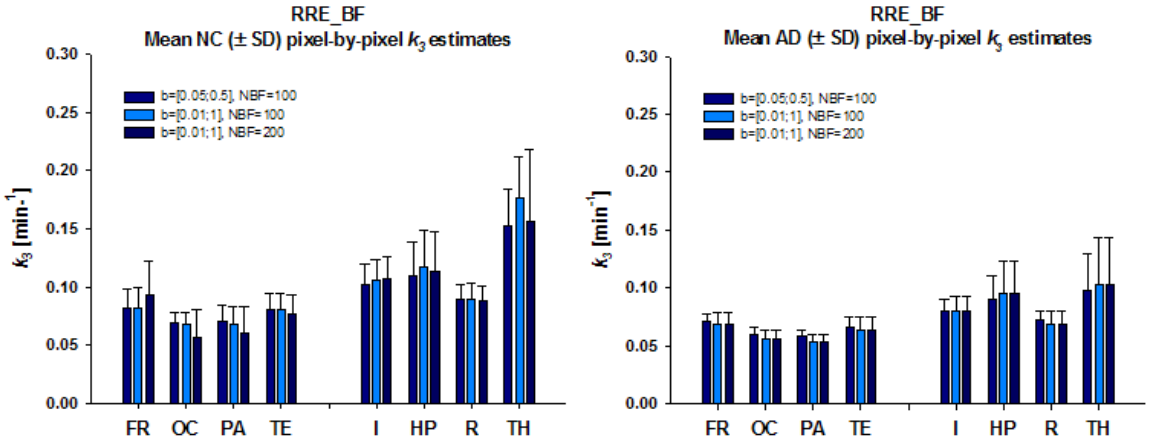

FIGURE 5.7 RRE_BF k_3 estimates at pixel-by-pixel level in NC vs AD when consider the different assumption for K (panel A) and the variation of the mean estimates within subject group (NC and respectively AD group) in Panel B.

5.4. R-NLLS results and discussion.

The R-NLLS algorithm was applied at both pixel and ROI level. Parametric images were filtered and then transformed in order to the scheme presented in figure 4.3 presented in section 4 of this work in order to have reliable estimates.

Mean image of k_3 estimates obtained with the reference tissue based non linear technique are shown in FIGURE 5.8 for both groups of subjects.

Two tailed t-test was applied in order to identify differences in k_3 estimates between the two groups of subjects.

R-NLLS method applied at pixel level identify significant reduction of AChE activity in AD patients respect to normals in all the neocortex area, $p<0.05$. In the TH, I, and R area were also identify significant differences between the studied groups (Table 5.5). However, no significances were identified applying the same mathematical approach at TAC_ROI level in the neocortex area neither in TH or HP as shown in table 5.5.

k_3 estimates obtained at TAC_ROI level show a mean variation of +11% in NC and +20% in AD respect to k_3 estimates at pixel level for the neocortex area and a higher variation of estimates in TH and HP regions: +54% in NC and +76% in AD for TH and +29% in NC and +48% in AD respect to k_3 index estimated in the same areas at pixel level (FIGURE 5.9). The variation between the pixel and TAC_ROI estimates was calculated as *(1-pixel_k_3/TAC_ROI_k_3)*100*.

	R-NLLS pixel-by-pixel			R-NLLS TAC_ROI		
ROI	NC	AD		NC	AD	
	MEAN ± SD	MEAN ± SD	p	MEAN ± SD	MEAN ± SD	p
FR	0.0728 ± 0.006	0.0587 ± 0.006	0.004	0.0818 ± 0.008	0.0760 ± 0.008	0.284
OC	0.0628 ± 0.006	0.0498 ± 0.007	0.010	0.0742 ± 0.007	0.0669 ± 0.012	0.300
PA	0.0650 ± 0.007	0.0531 ± 0.006	0.012	0.0723 ± 0.008	0.0649 ± 0.009	0.188
TE	0.0720 ± 0.010	0.0572 ± 0.008	0.023	0.0788 ± 0.011	0.0670 ± 0.010	0.099
TH	0.0863 ± 0.039	0.0396 ± 0.024	0.034	0.1866 ± 0.019	0.1665 ± 0.104	0.715
HP	0.0833 ± 0.012	0.0667 ± 0.017	0.116	0.1168 ± 0.019	0.1292 ± 0.042	0.596
I	0.0894 ± 0.010	0.0643 ± 0.010	0.003	0.1139 ± 0.014	0.0941 ± 0.017	0.078
R	0.0825 ± 0.010	0.0659 ± 0.005	0.004	0.0935 ± 0.009	0.0787 ± 0.006	0.009

TABLE 5.5 R-NLLS k_3 indexes obtained at pixel-by-pixel level in brain area with low enzyme activity (neocortex) and low to moderate (HP, R, I) and moderate (TH) enzyme expression in both group of subjects and the respective p value.

Panel A

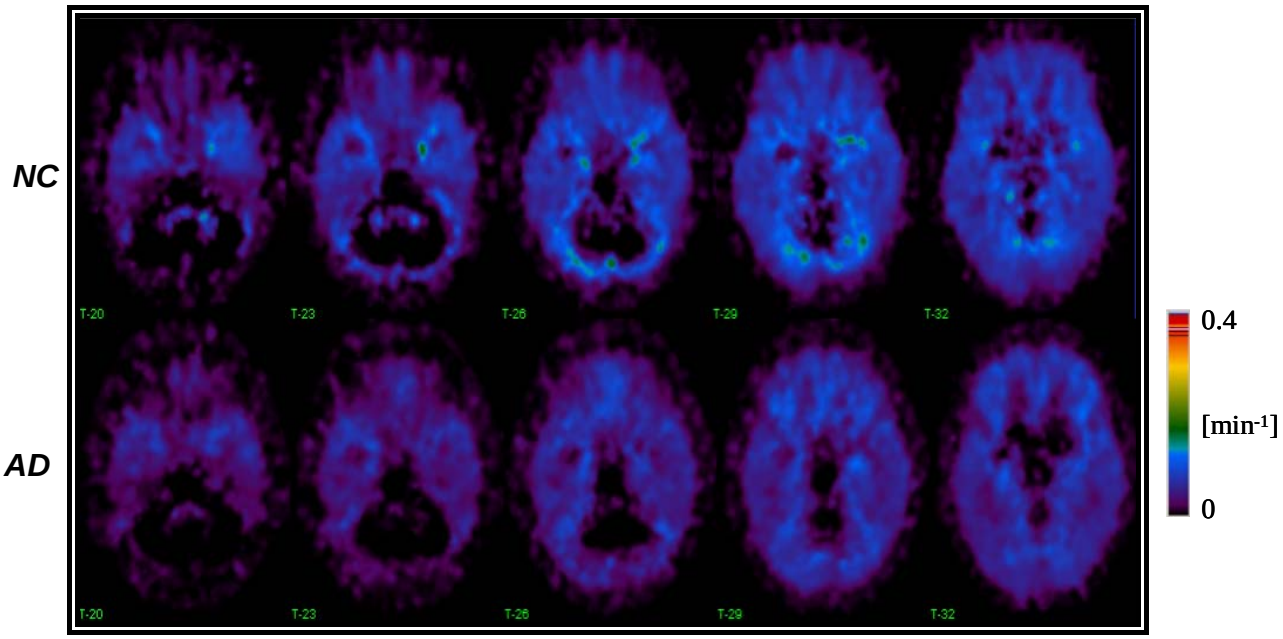

Panel B

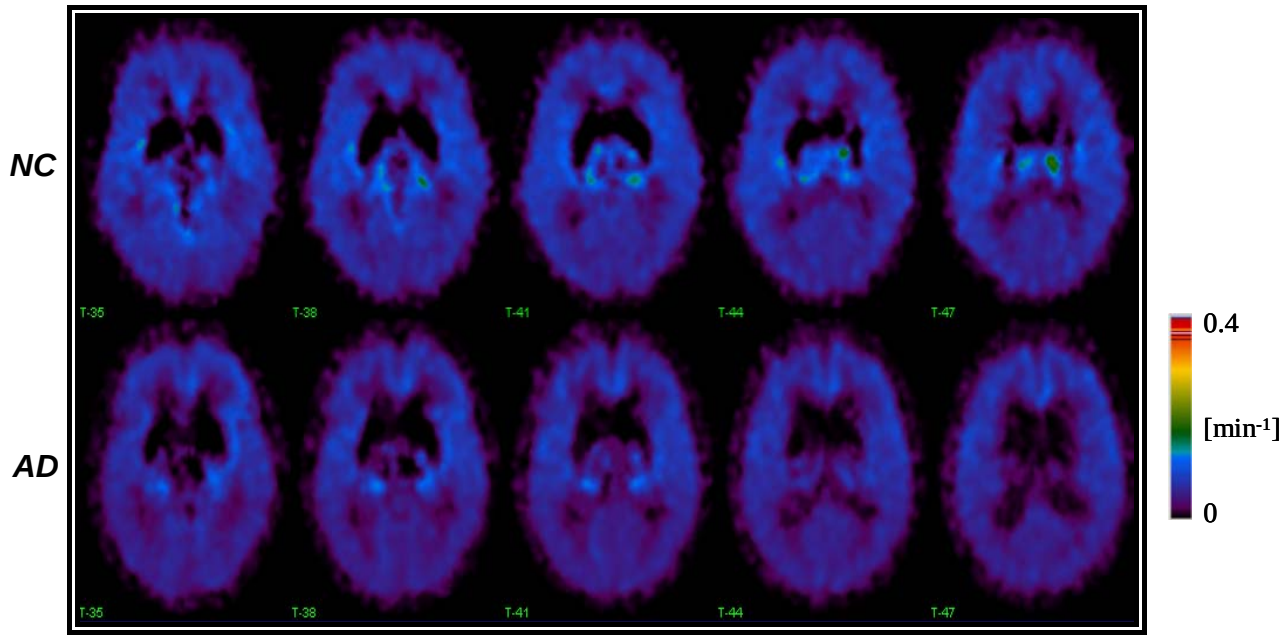

FIGURE 5.8 Average of normalized and co-registered parametric image of k_3 obtained with R-NLLS mathematical procedure for both groups of subjects: NC upper line and AD bottom line in panel A and panel B. Image scale: [0, 0.4] min^{-1}.

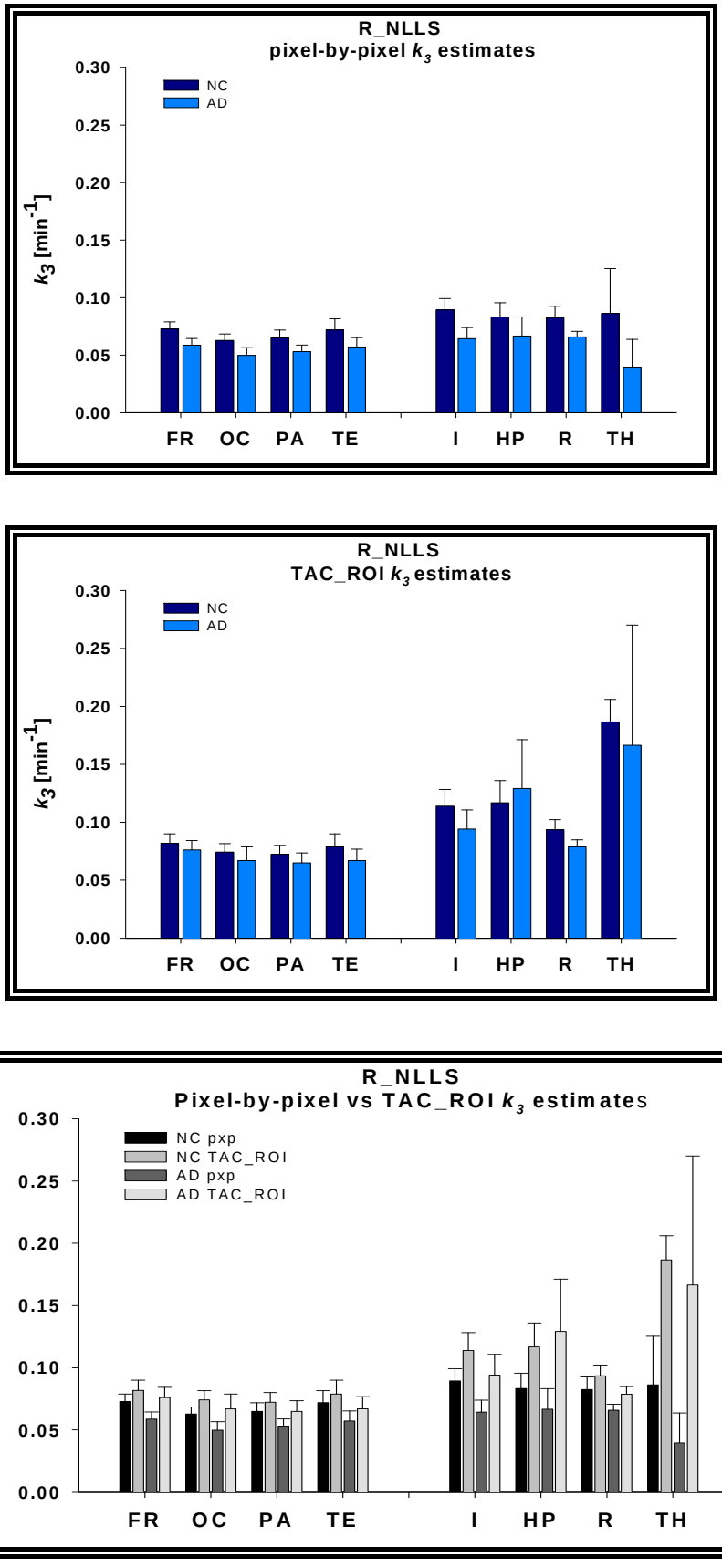

FIGURE 5.9 R-NLLS k_3 estimates at pixel-by-pixel level (top panel), TAC_ROI level (middle panel) and comparison pixel vs TAC_ROI estimates (bottom panel).

Bias of mean k_3 values estimated in neocortex area at pixel and TAC_ROI level was calculated respect to the considered "true" value identified by Namba [8]. We also consider the "true" values of k_3 index in TH (0.266 min^{-1}) and HP (0.11 min^{-1}) region as the ones identified by Nagatsuka and his colleagues [12] in normal subjects, using the standard non linear estimation method with arterial input.

The bias values was calculated as presented in equation 5.1:

$$\%bias = \left(\frac{estimated\_k_3}{true\_k_3} - 1 \right) * 100 \tag{5.1}$$

The results obtained applying R-NLLS technique at pixel level underestimates about 10% the "true" k_3 while a low underestimation of 1% was revealed for k_3 index in case of TAC_ROI approach in neocortex area.

The bias calculated with equation 5.1 showed an underestimation of pixel-by-pixel k_3 indexes in NC of 68% for TH and 24% for HP. In case of TAC_ROI k_3 estimates the identified bias for TH was -30% while for HP revealed a variability of +6% respect to the considered "true" k_3 values.

R-NLLS procedure revealed also a variation between k_3 estimates at pixel-by-pixel level respect to TAC_ROI level. However, k_2 indexes show a very low inter-variability within subject at both level analysis. Therefore k_2 will be used as *a priori* information in the new proposed mathematical approach in order to improve the precision of k_3 estimates.

5.5. MAP results and discussion.

Bayesian algorithm (MAP) was applied at both pixel and ROI level. Parametric images were filtered and then transformed as described in section 4 of this work (FIGURE 4.3) in order to be considered only reliable estimates of all indexes.

Mean image of k_3 estimates obtained with the reference tissue based MAP approach are shown in Figure 5.10 for both groups of subjects.

Two tailed t-test was applied in order to identify differences in k_3 estimates between the two groups of subjects.

Despite the small group of dataset – 4NC and 7AD – MAP method applied at pixel level identify significant reduction of AChE activity in AD patients respect to normals in area with low enzyme expression like FR, TE, PA, OC (Table 5.6) and also in area with moderate enzyme expression as TH and HP, with a $p<0.05$. However, no differences were identified applying the same mathematical approach at TAC_ROI level except the Rolandic operculum region (R) as it revealed in table 5.6.

k_3 estimates obtained at TAC_ROI level show a mean variation of -10% in NC and +0.4% in AD respect to k_3 estimates at pixel level for the neocortex area and a higher variation of estimates in TH and HP regions: -4% in NC and +25% in AD for TH and -15% in NC and +14% in AD respect to k_3 index estimated in the same areas at pixel level (FIGURE 5.11). The variation between the pixel and TAC_ROI estimates was calculated as *(1-pixel_k_3/TAC_ROI_k_3)*100*.

	R-MAP pixel-by-pixel			R-MAP TAC_ROI		
ROI	NC MEAN ± SD	AD MEAN ± SD	p	NC MEAN ± SD	AD MEAN ± SD	p
FR	0.0935 ± 0.010	0.0748 ± 0.010	0.016	0.0785 ± 0.009	0.0731 ± 0.009	0.353
OC	0.0735 ± 0.006	0.0599 ± 0.010	0.033	0.0711 ± 0.005	0.0631 ± 0.011	0.225
PA	0.0717 ± 0.006	0.0608 ± 0.008	0.047	0.0688 ± 0.008	0.0623 ± 0.007	0.194
TE	0.0828 ± 0.008	0.0666 ± 0.011	0.029	0.0746 ± 0.011	0.0646 ± 0.010	0.156
TH	0.2209 ± 0.041	0.1181 ± 0.044	0.004	0.2118 ± 0.022	0.1567 ± 0.085	0.245
HP	0.1340 ± 0.021	0.1012 ± 0.021	0.033	0.1163 ± 0.022	0.1175 ± 0.031	0.945
I	0.1162 ± 0.011	0.0876 ± 0.015	0.008	0.1098 ± 0.012	0.0916 ± 0.014	0.061
R	0.0904 ± 0.007	0.0736 ± 0.006	0.003	0.0887 ± 0.010	0.0748 ± 0.005	0.012

TABLE 5.6 MAP k_3 indexes obtained at pixel-by-pixel and TAC_ROI level in brain area with low enzyme activity (neocortex) and low to moderate (HP, R, I) and moderate (TH) enzyme expression in both group of subjects and the respective p value.

Namba [8] and Nagatsuka [12] estimated k_3 for normal subjects in neocortex area and respectively in TH and HP by using the standard method with arterial input function in order to calculate MP4A kinetic indexes. The mean value identified on neocortex – as mean of "true" k_3 estimates in FR, OC, TE, PA lobes – was 0.076 ± 0.008, while the

estimates for TH and HP are 0.266 min^{-1} and 0.11 min^{-1} respectively. Bias of mean k_3 values estimated in neocortex area and TH and HP at pixel and TAC_ROI level was calculated respect to the considered "true" value as follows:

$$\%bias = \left(\frac{estimated\_k_3}{true\_k_3} - 1 \right) * 100 \quad (5.1)$$

The results obtained applying MAP technique at pixel level overestimates about 6% the considered "true" k_3 while there is an underestimation of 3% of k_3 index in case of TAC_ROI approach. The bias calculated for TH and HP revealed an underestimation of pixel-by-pixel k_3 indexes in NC of 17% for TH and an overestimation about 22% for HP. In case of TAC_ROI k_3 estimates the identified bias for both TH revealed an underestimation of 20% while for HP the estimated value was increase about 6% respect to the considered "true" k_3 values.

Our method based on the automatic extraction of anatomical areas and on the use of MAP estimator allows the quantification of AChE activity in regions with low and medium enzyme expression at both pixel and ROI level. The general agreement between pixel and ROI k_3 estimates in both NC and AD groups support this finding.

The differences between pixel and ROI k_3 Bayes estimates observed in area with medium AChE activity in AD subjects and in cortex area with small volume (HP) might be caused by partial volume effect or by the selection method used to accept estimates at pixel level.

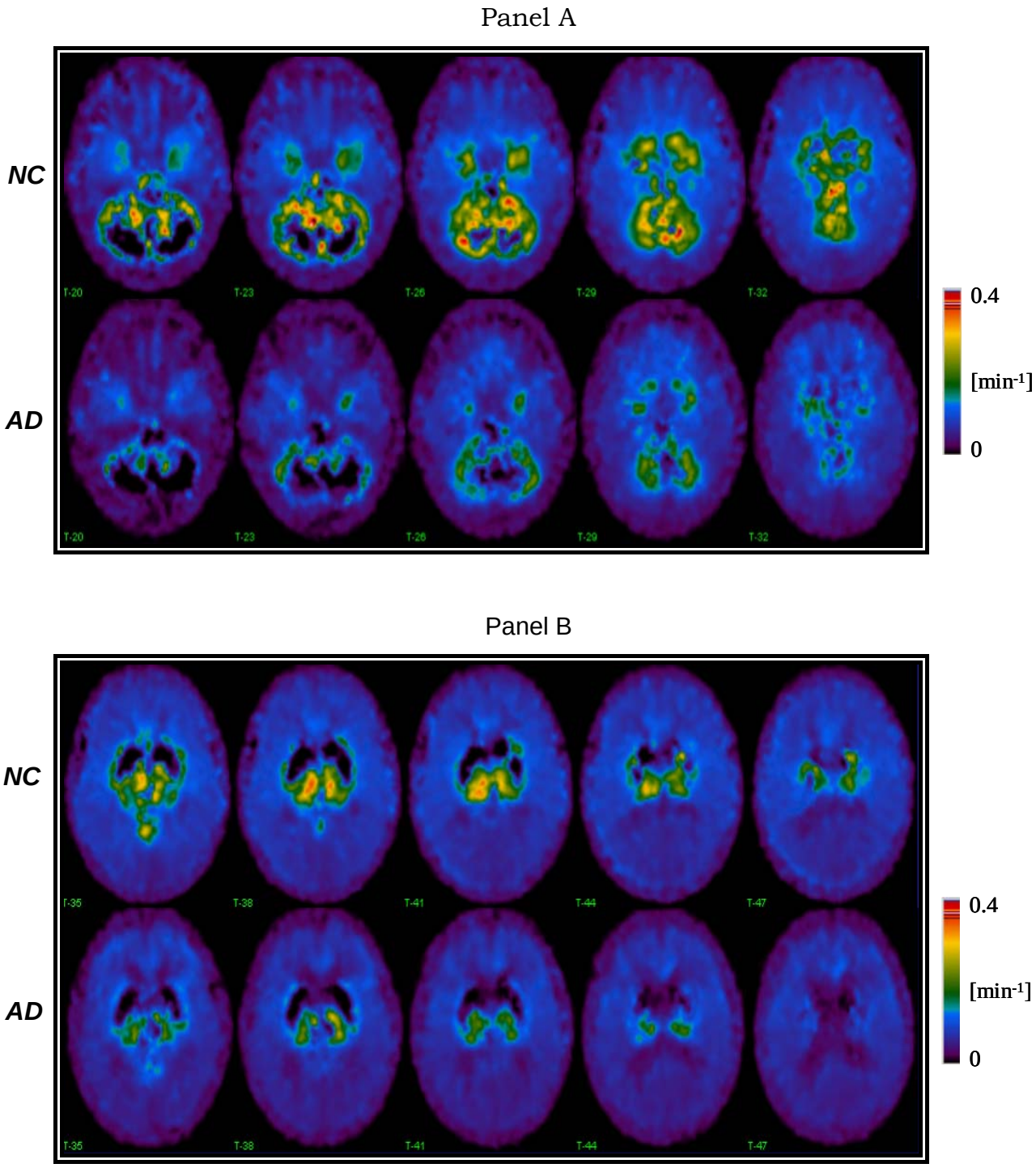

FIGURE 5.10 Average of normalized and co-registered parametric image of k_3 obtained with MAP mathematical procedure for both groups of subjects: NC upper line and AD bottom line in Panel A and Panel B. Image scale: [0, 0.4] min^{-1}.

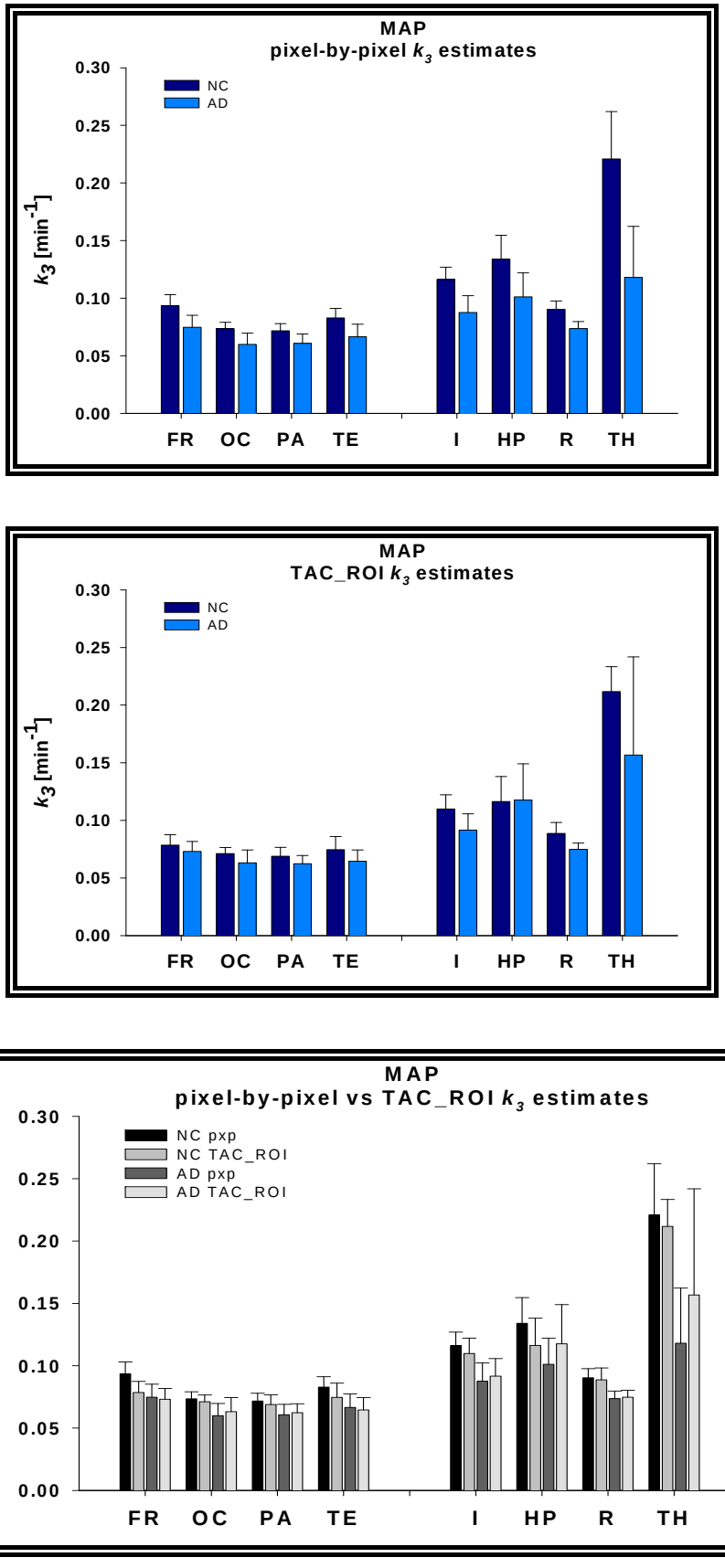

FIGURE 5.11 . MAP k_3 estimates at pixel-by-pixel (pxp) level (top panel), TAC_ROI level (middle panel) and comparison pixel vs TAC_ROI estimates (bottom panel).

Chapter 6

MP4A Functional Parametric Images: Assessment and Models Comparison.

All parametric images obtained in the present study were filtered for CV>300 and k_3>0.95 and then smoothed performing a two dimensional median filter as described in image processing flowchart 4.3. RRE and RRE_BF k3 parametric images were also "cleaned" for a threshold value of k_2 in order to have reliable estimates.

Individual k_3 values were calculated by generating 58 region of interest (ROI) with MARINA software. A Matlab program was developed in order to allow an operator independent quantification of the k_3 values in the 58 region of interest generated as mask_ROI with MARINA software.
The final results are presented in terms of average value among main neocortex area like temporal (TE), frontal (FR), occipital (OC) and parietal (PA) lobe. Regions as thalamus (TH), hippocampus (HP), insula (I), Rolandic operculum (R) and brainstem nuclei are also presented during the analysis.

Non invasive k_3 obtained with the mathematical methods: RLS, RRE, RRE_BF, R-NLLS and MAP were compared between groups using two tailed t test statistic analysis.

The ^{11}C-MP4A normalized and coregistered - as described in flowchart from figure 3.4 - mean uptake images recorded 10 minutes after injection revealed no difference between normal controls and Alzheimer

patients in terms of perfusion. However, higher tracer accumulation is revealed in both group of subjects in cortex area with high (cerebellum, striatum) and moderate (thalamus and brainstem nuclei) AChE activity (FIGURE 3.1). The accumulation of radioactivity reflects regional AChE activity as well as regional cerebral blood flow.

AChE activity was measured in terms of rate constant for hydrolysis of ^{11}C-MP4A (k_3), which is the parameter of interest in this study.

Average parametric images of k_3 were derived for both groups of subjects: NC left image and AD right image in each panel (A, B, C, D, E corresponding to each mathematical procedure: RLS, RRE, RRE_BF, R-NLLS and MAP respectively) and are shown FIGURE 6.1.

Regional kinetic parameter k_3 estimated by the mathematical analysis described previously are summarized in Table 6.1. The mean k_3, SD and p value of each quantification method for both groups of subjects are shown. Despite the small group of persons participated in this pilot study, all the methods used to generate k_3 parametric images were able to detect reduction of AChE activity in AD brain areas of interest respect to NC. In particular, cortical k_3 values obtained applying RLS, R-NLLS and MAP techniques were reduce significantly in neocortex area in Alzheimer subjects respect to controls (frontal, parietal, occipital, temporal lobe), as it can be observed in Table 6.1; in case of RRE quantification no significant decrease in AD AChE activity respect to normals was identify in neocortex area (Table 6.1). The areas that showed a significant difference ($p<0.05$) in enzyme expression between groups of subjects by RRE approach are represented by insula and Rolandic operculum. The implementation of basis function approach in RRE (RRE_BF) technique [14] identified a significant decrease of enzyme activity in AD respect to normal subject in parietal cortex, Rolandic operculum and thalamus.

k_3 estimated values obtained with all mathematical methods were compared with k_3 values already reported in the scientific publications obtained with the standard analysis: a three compartmental model structured by an arterial blood compartment and a cerebral tissue

compartment comprising of two subcompartments representing unmetabolized and metabolised radiotracer [8, 12]. Biases of the k_3 estimates respect to the "true" k_3 standard values for normal subjects were calculated using equation 5.1 and are shown in TABLE 6.2. k_3 estimates in neocortex area, TH and HP obtain by all mathematical procedure presented in this work are represented in FIGURE 6.2 for both groups of subjects. "True" k_3 estimates reported in the literature for normals are also shown as a constant red line in each plot from FIGURE 6.2.

Significant difference that is in good agreement with published studies [11, 12, 16] was identified by MAP analysis in hippocampus region. Two-tailed unpaired t-test indicated a significant difference ($p<0.005$) of k_3 estimates by MAP in brainstem nuclei: pedunculopontine and laterodorsal tegmentalnuclei (PPT and LDT). The k_3 values in AD (0.09 ± 0.03) patients is two times lower respect to NC (0.18 ± 0.04).

Panel A: RLS

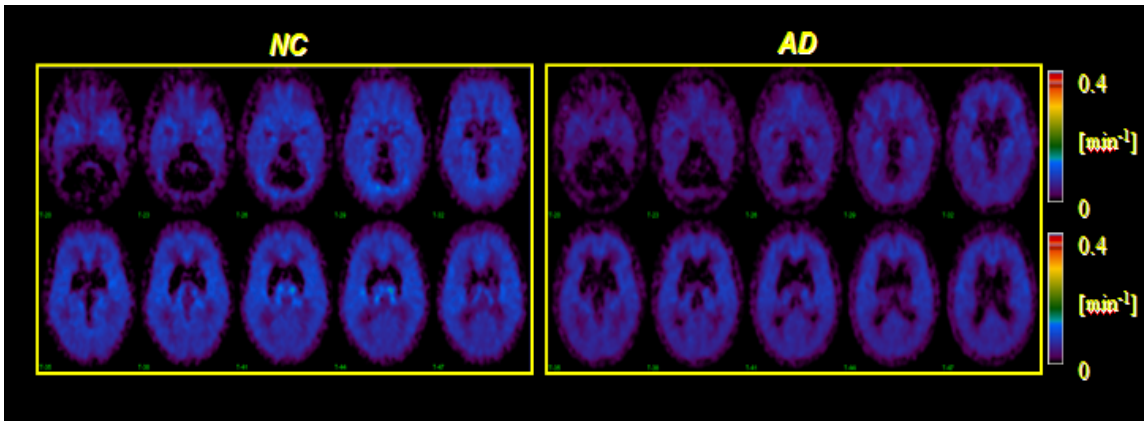

Panel B: RRE

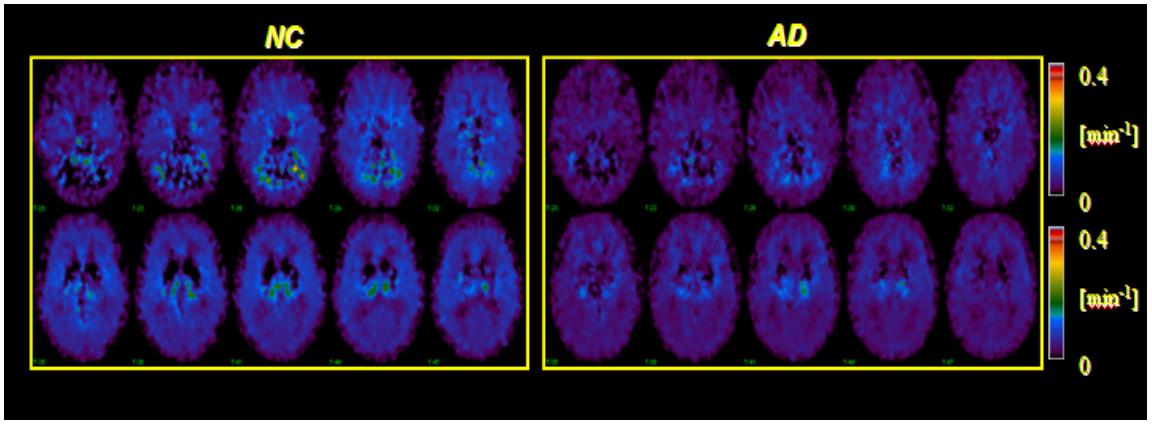

Panel C: RRE_BF

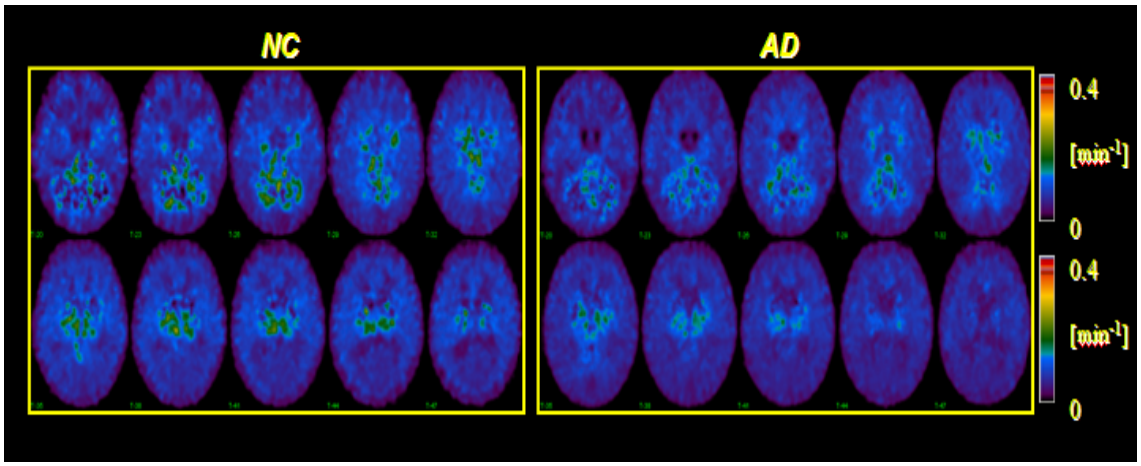

Panel D: R-NLLS

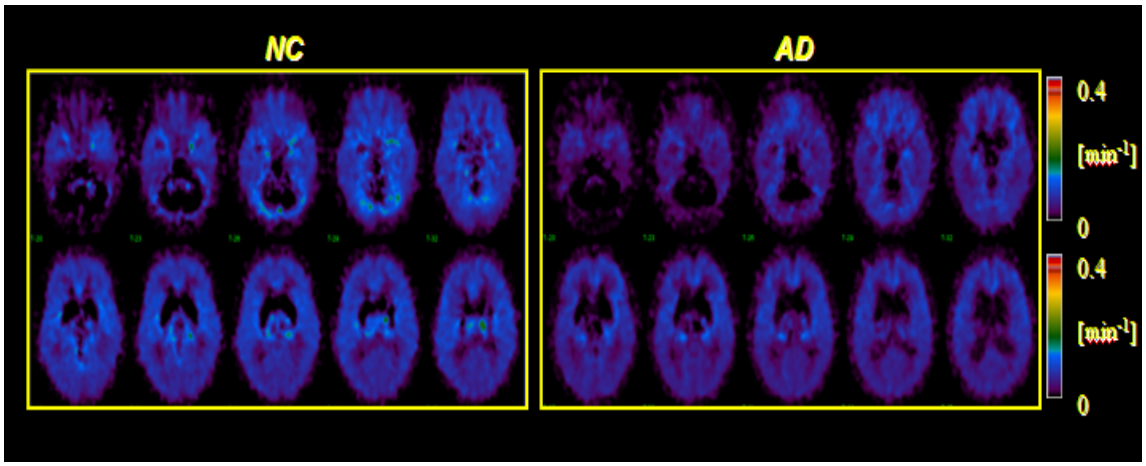

Panel E: MAP

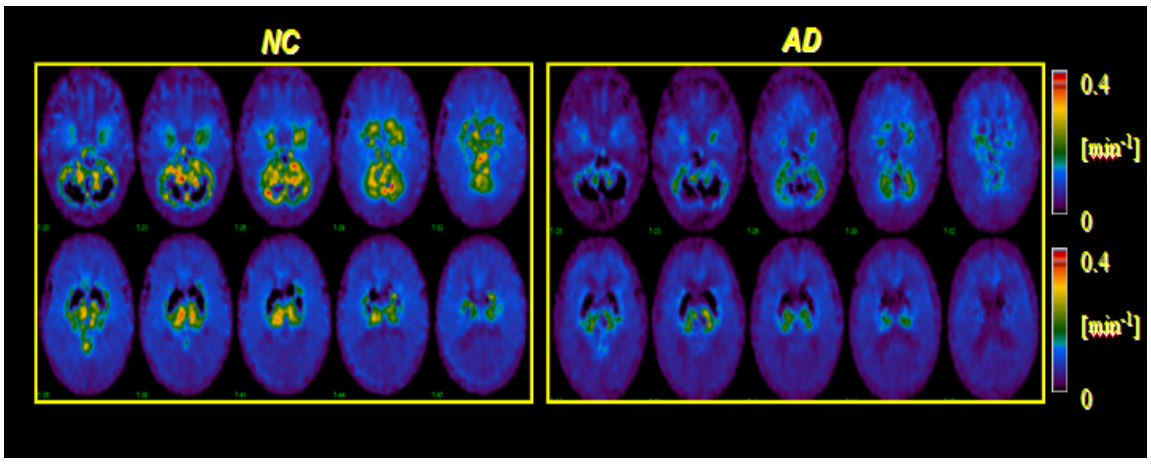

FIGURE 6.1 k_3 mean parametric images for both groups of subjects (NC on the left and AD on the right part of each panel) obtained with all described techniques: RLS, RRE, RRE_BF, R-NLLS, and MAP.

ROI	RLS			RRE *			RRE_BF **		
	NC	AD		NC	AD		NC	AD	
	MEAN ± SD	MEAN ± SD	p	MEAN_NC	MEAN ± SD	p	MEAN ± SD	MEAN ± SD	p
FR	0.0726 ± 0.005	0.0566 ± 0.006	0.002	0.0703 ± 0.011	0.0471 ± 0.020	0.067	0.0823 ± 0.016	0.0707 ± 0.006	0.121
OC	0.0648 ± 0.005	0.0512 ± 0.007	0.009	0.0594 ± 0.007	0.0388 ± 0.019	0.069	0.0695 ± 0.009	0.0593 ± 0.007	0.068
PA	0.0687 ± 0.007	0.0552 ± 0.004	0.003	0.0609 ± 0.009	0.0399 ± 0.020	0.077	0.0711 ± 0.013	0.0584 ± 0.005	0.044
TE	0.0747 ± 0.008	0.0599 ± 0.006	0.006	0.0686 ± 0.010	0.0437 ± 0.022	0.065	0.0810 ± 0.014	0.0664 ± 0.009	0.059
TH	0.0771 ± 0.024	0.0396 ± 0.012	0.007	0.1206 ± 0.033	0.0655 ± 0.045	0.062	0.1522 ± 0.032	0.0984 ± 0.032	0.024
HP	0.0752 ± 0.010	0.0561 ± 0.011	0.022	0.0820 ± 0.019	0.0639 ± 0.035	0.375	0.1096 ± 0.029	0.0902 ± 0.020	0.217
I	0.0834 ± 0.006	0.0590 ± 0.009	0.001	0.0866 ± 0.011	0.0511 ± 0.023	0.019	0.1019 ± 0.017	0.0799 ± 0.010	0.025
R	0.0854 ± 0.007	0.0679 ± 0.006	0.002	0.0789 ± 0.008	0.0513 ± 0.023	0.049	0.0894 ± 0.013	0.0719 ± 0.008	0.020

ROI	R-NLLS			MAP		
	NC	AD		NC	AD	
	MEAN ± SD	MEAN ± SD	p	MEAN ± SD	MEAN ± SD	p
FR	0.0728 ± 0.006	0.0587 ± 0.006	0.004	0.0935 ± 0.010	0.0748 ± 0.010	0.016
OC	0.0628 ± 0.006	0.0498 ± 0.007	0.010	0.0735 ± 0.006	0.0599 ± 0.010	0.033
PA	0.0650 ± 0.007	0.0531 ± 0.006	0.012	0.0717 ± 0.006	0.0608 ± 0.008	0.047
TE	0.0720 ± 0.010	0.0572 ± 0.008	0.023	0.0828 ± 0.008	0.0666 ± 0.011	0.029
TH	0.0863 ± 0.039	0.0396 ± 0.024	0.034	0.2209 ± 0.041	0.1181 ± 0.044	0.004
HP	0.0833 ± 0.012	0.0667 ± 0.017	0.116	0.1340 ± 0.021	0.1012 ± 0.021	0.033
I	0.0894 ± 0.010	0.0643 ± 0.010	0.003	0.1162 ± 0.011	0.0876 ± 0.015	0.008
R	0.0825 ± 0.010	0.0659 ± 0.005	0.004	0.0904 ± 0.007	0.0736 ± 0.006	0.003

TABLE 6.1 Mean ± SD regional values of k_3 parameter extracted from the parametric images obtained with different estimation approaches for both groups participated at the study. * recalls that we considered reliable the RRE estimated cleaned for the k_2 threshold identified for each subject; ** remind that for basis function approach(RRE_BF) were considered more reliable the result obtained with the assumption C1 for K: range from 0.05 to 0.5 and NBF=100.

ROI	"true" k3	Bias RLS (%)	Bias RRE* (%)	Bias RRE_BF ** (%)	Bias R-NLLS (%)	Bias MAP (%)
FR	0.076	-4	-7	8	-4	23
OC	0.067	-3	-11	4	-6	10
PA	0.074	-7	-18	-4	-12	-3
TE	0.086	-13	-20	-6	-16	-4
TH	0.266	-71	-55	-43	-68	-17
HP	0.11	-32	-25	-0.4	-24	22

TABLE 6.2 Bias of the mean k_3 estimates in NC obtained with all mathematical procedures respect to the considered k_3 "true" value. * recalls that were considered reliable the RRE estimated cleaned for the k_2 threshold identified for each subject; ** remind that for basis function approach(RRE_BF) were considered more reliable the result obtained with the assumption C1 for K: range from 0.05 to 0.5 and NBF=100.

The models performance in brain areas with low AChE activity is very similar, as it can be seen in Table 6.2 and figure 6.2. RLS technique is fast at pixel level and the precision of its estimates can be identified as for RRE, R-NLLS and MAP approach. RRE_BF indexes reliability could be questioned as there is an underestimation in identifying the precision of its estimates because of the basis function approach technique (eq. 4.41, section 4). A solution could be if considered the precision of A and B estimates in order to have only reliable k_2 and k_3 index by RRE_BF procedure.

However, in area with moderate enzyme activity (e.g. TH) MAP approach overcomes the drawbacks where the other methods failed [34]: the method is able to recover information and the estimates for this area at pixel level show the smallest bias respect to the considered 'true" k_3 value (-17%, table 6.2). Further work is ongoing in order to test new Bayesian estimation approach for ^{11}C-MP4A.

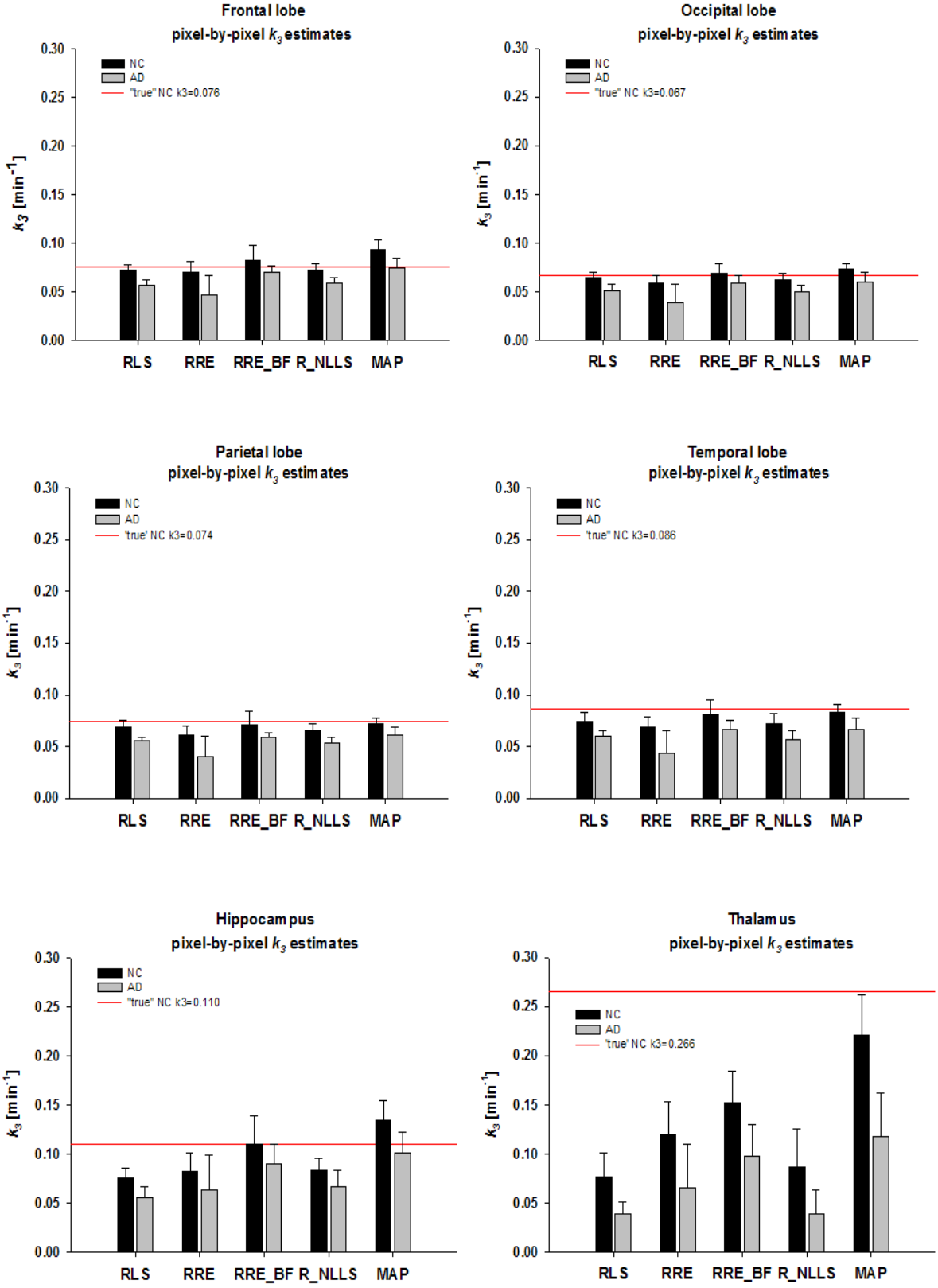

FIGURE 6.2 Mean ± SD k_3 obtained with all applied mathematical procedures at pixel level in both NC and AD groups. The red line represents the considered "true" NC k_3 value for each considered brain area.

Chapter 7

Discussion

Several recent studies have described in vivo study of AChE activity [1-22]. Reduction of AChE activity was also shown in the cerebral cortex of patients with Alzheimer disease by quantitative analysis of PET data using ^{11}C-MP4A as tracer [8, 10-16, 19-22]. ^{11}C-MP4A is a ACh analogue and is specifically hydrolyzed by AChE in the brain to a hydrophilic metabolite, which is irreversible trapped locally in the brain.

In this study we proposed a new pixel by pixel quantification approach of brain AChE by PET without arterial blood sampling: maximum *a posteriori* parametric estimation (MAP). The standard non linear least square method was also consider but using reference region input instead of arterial input function. Comparison with other published methods based on reference region input (RLS, RRE, RRE_BF), that we implemented at pixel level, has also been done. As far as we know, a comparison study at whole brain pixel-by-pixel level for ^{11}C-MP4A quantification method has not been done yet. Namba and his colleagues made a tentative of study comparison at pixel level for a temporal area that covered only 200 pixels for RLS and arterial input NLLS procedure [22].

Despite the small group of subjects, the mathematical methods used to generate k_3 parametric images in this study, were able to detect reduction of AChE activity in different brain areas of interest. In particular, RLS, R-NLLS and MAP analysis identified significant

differences of k_3 estimates between NC and AD in regions with low enzyme expression like temporal, frontal, parietal and occipital cortex, while no significant differences were identify on neocortex area between NC and AD groups by applying RRE technique. The performance of RRE and RRE_BF procedure on our data set is not consistent with that described in the literature [13, 14, 19]. Therefore it was verified the performance of RRE in estimating k_2 and it was observed inaccurate estimates of this parameter. In order to consider only reliable parameter estimates, RRE parametric images have been filtered by calculate a threshold for k_2 estimates. The threshold was estimated in each subject from the k_2 parametric image as the mean k_2 value to which was added twice the standard deviation. A uniform k_2 threshold of 2 min^{-1} was obtained for each person participated in the study. In this way, only pixels having reliable estimates for RRE model parameters are taken into account. In case of RRE_BF model that is based on the same mathematical procedure as RRE but use different estimation approach of its parameters – basis function – the analysis was performed three times considering three different conditions for K parameter (See section 4.3). The k_2 threshold was also considered for RRE_BF analysis in order to have only reliable k_3. The significance of the differences identified in the estimates changes both with K range and basis function number. Finally, for RRE_BF method has been chosen the condition that gives estimates closest with the reported literature values. When applying basis function approach must be considered that for different neurodegenerative disease might be considered different K range and different number of basis function that influence the final estimates; it is also important to be recalled that an underestimation of precision of estimates are encountered for RRE_BF technique. The reliability of A and B estimates might also be considered in order to have more reliability in k_3 estimates by RRE_BF and RRE.

Significant differences between the groups of subjects were identified in cerebral region with moderate AChE activity like thalamus by all mathematical methods. However, if we consider the “true” k_3 value of

thalamus from the literature, MAP k_3 estimate have the smallest bias (17%) respect to the "true" value [33]. Ratios of AChE activity values reported in literature as post mortem human brain ratios were compared with ratios of k_3 values among brain obtained with the analytical methods applied to our data set. The ratio of AChE activity between the temporal cortex and thalamus of normal patients obtained with MAP (1:2.7) are consistent with the same ratio reported in the literature by Arai et al [43] as a result of a post-mortem human brain study (1:2.7). The same ratios obtained with the other techniques are much lower (under 1:2).

Brainstem nuclei k_3 estimate by MAP method indicate a 50% reduction in AD AChE activity respect to NC [33]. This data is consistent with a recently communication in which was reported a reduction of uptake of the ACh analogue tracer ^{11}C-MP4A in AD subjects who complained of sleep disturbance [44]. However, no significance between NC and AD k_3 estimates in brainstem nuclei was identify by RLS, R-NLLS, RRE or RRE_BF analysis.

The automatic extraction of anatomical areas and our comparison study of the different methodologies for AChE activity quantification at pixel level confirm that in cortex area with low enzyme activity the models have similar performances. RRE_BF approach might also be considered with some cautions. However, RLS linear calculation is faster for pixel by pixel parameter estimation respect to non linear quantification methods (R-NLLS, MAP) and the results are in good agreement with cortex values (FR, TE, PA, OC) already published (see table 6.2).

Contrary, RLS approach showed some difficulties in estimating k_3 index in area with moderate enzyme activity. The use of Bayes (MAP) estimator helps to overcome these drawbacks [33, 34] and allows the quantification of AChE activity in regions with moderate enzyme expression at pixel level with results consistent with the scientific literature [12]. MAP techniques is more time consuming respect to the other methods because implicate a previous analysis at TAC_ROI level in order to obtain the *a priori* information on parameter k_2.

The results obtained applying mathematical techniques described in this work at TAC_ROI level showed the smallest differences between TAC_ROI estimates and pixel estimates for MAP procedure as shown in chapter 5. However, further work is needed in order to evaluate the performance of the models on a larger data set. A simulation study based on real plasmatic data would be very useful in identifying the best non invasive quantification method for clinical application.

Chapter 8

Conclusions

^{11}C-MP4A is a PET tracer that is highly specific for AChE and its kinetic properties are favorable for the measurement of cortical AChE activity. Kinetic analysis of ^{11}C-MP4A PET images provides information on the important physiologic parameter like AChE activity (k_3) and about tracer distribution in different brain areas. The parameter estimates can be used to derive physiological information as well as to distinguish differences between various group of subjects, e.g normal and pathological subjects.

The analysis of ^{11}C-MP4A PET images can be performed both at pixel and region of interest level. In this study some of the recent findings and issues relative to ^{11}C-MP4A modeling are discussed.

The goal of this study was twofold: first, it was proposed and developed a Bayesian method (MAP) in order to accurately estimate AChE activity in normal subjects and patients with neurodegenerative disease (e.g. AD). A lot of effort was made to ensure accuracy and reliability of all pixel-level estimates in brain region with low (neocortex) and moderate (thalamus and brainstem) enzyme activity. The second intent of this work was to compare, at pixel level, the performance of the Bayesian approach with the other methods already propose in the literature for AChE activity quantification: RLS [12], RRE [13], RRE_BF [14], reference NLLS. The comparison between methods was based on the precision and reliability of estimates.

In order to avoid errors sampling during a manual position of ROIs

on the dynamic or parametric ^{11}C-MP4A PET images an automatic ROIs extraction was preferred to the often used manual technique.

Despite the low number of subjects who participated in the study, the performance of the various techniques at pixel level showed to be very similar in the brain areas with low enzyme expression (e. g neocortex). However, when considering the reliability and accuracy of each models parameters some issues should be taken into account:

- RLS does not include any information on the measurement error present in the data, thus does not consider much the noisiness of the PET study;
- RRE and RRE_BF approaches applied to our data set do not identified significant differences between NC and AD group and the results obtained are not in good agreement with published data. This might be due to the consideration on error propagation that was implemented in the original methods or by the selection method used to accept estimates at pixel level. Another disadvantage of both technique consisted in inaccurate estimates of the parameter that describe the unmetabolized tracer washout from tissue to blood. It is also important to be recalled that an underestimation of precision of estimates are encountered for RRE_BF technique.

Anyway, from computational point of view, RLS linear calculation is faster for pixel by pixel parameter estimation respect to non linear quantification methods (R-NLLS, MAP) and the results are in good agreement with published neocortex values.

On the contrary, RLS approach shows some difficulties in estimating k_3 index in area with moderate enzyme activity, such as thalamus and brainstem. The use of Bayesian (MAP) estimator helps to overcome these drawbacks and allows the quantification of AChE activity in regions with moderate enzyme expression, like thalamus and brainstem. At pixel level, this procedure presents results consistent with the scientific literature.

MAP technique is more time consuming respect to the other methods because it implicates a previous analysis at ROI level in order to obtain the a priori information, but improve the precision of estimates. Actually, pixel and ROI estimates obtain applying the Bayesian estimator are more similar respect to the ones obtained with published methods. A new Bayesian approach that allows a faster identification of the a priori information is on study. A simulation study based on real plasmatic data would be very useful for the validation of the best non invasive method.

In conclusion, MAP methods provides the most reliable and accurate estimates, even if is the most time consuming among the various procedures.

An European project finalized to validate on a bigger dataset the best method to be applied to 11C-MP4A/PET images is going to start soon. Its aim will be the confirmation of the clinical applicability of the chosen technique in the discrimination of different neurodegenerative pathologies as AD, Lewy body dementia and mild cognitive impairment. MAP procedure and another Bayesian method under development as well as the other non invasive mathematical approach presented in this work will be taken into account. Real plasma data will also be available for a simulation study. Thus, simulation results are going to be considered for best method validation.

Bibliography

[1]. Irie T., Fusushi K., Akimoto Y., Tamagami H., Nozaki T., "Design and evaluation of radioactive acetylcholine analogs for mapping brain acetylcholinesterase (AchE) in vivo" *Nucl.Med.Biol (1994)*, 21:801-808.

[2]. Irie T, Fusushi K, Namba H, Iyo M, et al, "Brain acetylcholinesterase activity: validation of a PET tracer in a rat model of Alzheimers disease", *J Nucl Med* (*1996*), 37: 649-655.

[3]. Namba H, Irie T., Fusushi K, Iyo M, "In vivo measurements of acetylcholinesterase activity in the brain with radioactive acetylcholine analog", *Brain.Res. (1994)*, 667:278-282.

[4]. Kilbourn MR., Snyder SE., Sherman PS., Kuhl DE., " In vivo studies of acetylcholinesterase activity using a labeled substrate N-[^{11}C]methylpiperidin-4-yl propionate ([^{11}C]PMP)", *Synapse, (1996)*, 22 :123-131.

[5]. Frey KA., Koeppe RA., Kilbourne MR., Snyder SE., Kuhl DE., "PET quantification of cortical acetylcholinesterase inhibition in monkey and human", *J. Nucl. Med.*, *(1997)*, 38:146P.

[6]. Koeppe RA., Frey KA., Snyder SE., Meyer P., Kilbourn MR., Kuhl DE., " Kinetic modeling of N-[^{11}C]methylpiperidin-4-yl propionate: alternatives for analysis of an irreversible PET tracer for measurment

of acetylcholinesterase activity in human brain“, *Cereb. Blood Flow Metab., (1999)*, 19:1150-1163.

[7]. Iyo M, Namba H, Fukushi K, et al, “Measurement of acetylcholinesterase by positron emission tomography in the brains of healthy controls and patients with Alzheimer’s disease”, *Lancet* (*1997*), 349: 1805-1809.

[8]. Namba H, Iyo M, Fusushi K, et al., “Human cerebral acetylcholinesterase activity measured with positron emission tomography: procedure, normal values and effect of age”, *Eur.J Nucl Med* (*1999*), 26:135-143.

[9]. Kuhl DE, Koeppe RA, Minoshima S, et al.(Kuhl, D. E. MD; Koeppe, R. A. PhD; Minoshima, S. MD, PhD; Snyder, S. E. PhD; Ficaro, E. P. PhD; Foster, N. L. MD; Frey, K. A. MD, PhD; Kilbourn, M. R. PhD), “In vivo mapping of cerebral acetylcholinesterase activity in aging and Alzheimer’s disease”, *Neurology* (*1999*), 52(4): 691-699.

[10]. Herholz K, Bauer B, Wienhard K, et al., “In vivo measurement of regional acethylcholine esterase activity in degenerative dementia: comparison with blood flow and glucose metabolism”, *J Neural Transm* (*2000*), 107: 1457-1468.

[11]. Shinotoh H, Namba H, Fusushi K, Nagatsuka S, et al, “Progressive loss of cortical acetylcholinesterase activity in association with cognitive decline in Alzheimer’s disease: a positron emission tomography study”, *Ann Neurol* (*2000*), 48: 194-200.

[12]. Nagatsuka S, Fukushi K, Shinotoh H, Namba H, et al., “Kinetic analysis of [11C]MP4A using a high-radioactivity brain region that represents an integrated input function for measurement of cerebral acethylcholinesterase activity without arterial blood sampling”, *JCBFM* (*2001*), 21: 1354-1366.

[13]. Herholz K, Lercher M, Wienhard K, Bauer B, Lenz O, Heiss WD, "PET measurement of cerebral acethylcholine esterase activity without blood sampling", *Eur J Nucl Med* (*2001*), 28:472-477.

[14]. Zundorf G, Herholz K, Lercher M, Wienhard K, Bauer B, Weisenbach S, Heiss WD, "PET functional parametric images of acetylcholine esterase activity without arterial blood sampling" In Senda M et al (eds), Brain Imaging Using PET, Academic Press, San Diego, Ca, USA, pp 41-46, Proceedings for BrainPET2001.

[15]. Namba H, Fukushi K, Nagatsuka S, Iyo M, Shinotoh H, Tanada S, Irie T. "Positron emission tomography: quantitative measurement of brain acetylcholinesterase activity using radiolabeled substrates.", *Methods* (*2002*) Jul;27(3):242-50.

[16]. Rinne JO, Kaasinen V, Jarvenpaa T, Nagren K, Roivainen A, Yu M, Oikonen V, Kurki T., "Brain acetylcholinesterase activity in mild cognitive impairment and early Alzheimer's disease.", *J Neurol Neurosurg Psychiatry* (*2003)* Jan;74(1):113-5.

[17]. Herholz K., "PET studies in dementia", *Ann Nucl Med.* (*2003)* Apr;17(2):79-89.

[18]. Shinotoh H, Fukushi K, Nagatsuka S, Irie T., "Acetylcholinesterase imaging: its use in therapy evaluation and drug design.", *Curr Pharm Des.* (*2004*);10(13):1505-17.

[19]. Herholz K, Weisenbach S, Zundorf G, Lenz O, Schroder H, Bauer B, Kalbe E, Heiss WD, "In vivo study of acetylcholine esterase in basal forebrain, amygdala, and cortex in mild to moderate Alzheimer disease.", *Neuroimage* (*2004) Jan*;21(1):136-43.

[20]. Ota T, Shinotoh H, Fukushi K, Nagatsuka S, Namba H, Iyo M, Aotsuka A, Tanaka N, Sato K, Shiraishi T, Tanada S, Arai H, Irie T., "A simple method for the detection of abnormal brain regions in

Alzheimer's disease patients using [11C]MP4A: comparison with [123I]IMP SPECT.", *Ann Nucl Med*. (*2004*) May;18(3):187-93.

[21]. Tsukada H, Nishiyama S, Fukumoto D, Ohba H, Sato K, Kakiuchi T., "Effects of acute acetylcholinesterase inhibition on the cerebral cholinergic neuronal system and cognitive function: Functional imaging of the conscious monkey brain using animal PET in combination with microdialysis.", *Synapse*. (*2004*)Apr;52(1):1-10.

[22]. Namba Hiroki et al, "Pixel-by-pixel Mapping of AChE Activity in Human Brain with 11C MP4A/PET", In Senda M et al (eds), Brain Imaging Using PET, Academic Press, San Diego, Ca, USA, pp 55-61, Proceedings for BrainPET2001.

[23]. Siegel GJ, Agranoff BW, Albers RW, Fisher SK, Uhler MD, "Basic Neurochemistry: molecular, cellular and medical aspects", (Chapter 11), *LippincottWilliams&Wilkins*, sixth edition, *(1999).*

[24]. http://wiz2.pharm.wayne.edu/biochem/enz.html, *(2007).*

[25]. Tanaka N, Fukushi K, Shinotoh H, Nagatsuka S, Namba H, Iyo M, Aotsuka A, Ota T, Tanada S, Irie T., "Positron emission tomographic measurement of brain acetylcholinesterase activity using N-[(11)C]methylpiperidin-4-yl acetate without arterial blood sampling: methodology of shape analysis and its diagnostic power for Alzheimer's disease.", *J Cereb Blood Flow Metab*. *(2001)* Mar;21(3):295-306.

[26]. Walter, B., Blecker, C., Kirsch, P., Sammer, G., Schienle, A., Stark, R., & Vaitl, D., "MARINA: An easy to use tool for the creation of MAsks for Region of INterest Analyses" [abstract]. Presented at the 9th International Conference on Functional Mapping of the Human Brain, June 19-22, (*2003)*, New York, NY. Available CD-Rom in *NeuroImage*, Vol. 19, No. 2.

[27]. Sato K, Fukushi K, Shinitoh H, Nagatsuka S, Tanaka N, Aotsuka A, Ota T, Shinraishi T, Tanada S, Iyo M, Irie T, "Evaluation of simplified kinetic analysis for measurement of brain acetylcholinesterase activity using N-[11C]Methylpiperidin-4-yl propionate and positron emission tomography", *JCBFM*, *(2004)*, 24:600-611.

[28]. Cobelli C, Carson E, Finkelstein L. "The mathematical Modeling of Metabolic and Endocrine System". New York, Wiley (*1983)*.

[29]. http://en.wikipedia.org/wiki/Maximum_a_posteriori,(*2007)*

[30]. Bertoldo, A., Sparacino, G., Cobelli, C., "Population approach improves parameter estimation of kinetic models from dynamic PET data", *IEEE Trans.Med.Im*, *(2004)*; 23(3):297-306.

[31]. Sparacino, G., Tombolato, C., Cobelli, C, "Maximum Likelihood versus Maximum a posteriori parameter estimation of physiological system models:the C-peptide impulse response case study"., *IEEE Trans.BioMed.Eng*, *(2000)*; 47(6):801-811.

[32]. Callegari, T., Caumo A., Cobelli, C., "Generalization of Map estimation in SAAM II: validation against ADAPT II in a glucose model case study", *Ann.BioMed.Eng.*, *(2002)*; 30:1-8.

[33]. Florea I., Bertoldo A., Moresco RM, Carpinelli A, Panzacchi A, Garibotto V, Perani D, Gilardi MC, Fazio F, Cobelli C., "[^{11}C] MP4A Bayesian quantification of AChE activity at pixel and ROI level in normals and Alzheimer patients.", Proceedings of 2nd European Society of Molecular Imaging, Naples, Italy, 14 - 15 June (*2007)*.

[34]. Florea I., Bertoldo A., Pietra L., Moresco RM, Carpinelli A, Panzacchi A, Garibotto V, Perani D, Gilardi MC, Fazio F, Cobelli C., "Kinetic analysis of [^{11}C]MP4A for measurement of cerebral acetylcholine esterase activity without arterial blood sampling.", Proceedings for

6th International Symposium on Functional Neuroceptor Mapping, Copenhagen – Denmark, 6th - 8th July *(2006)*.

[35]. http:// en.wikipedia.org/wiki/Acetylcholine, *(2007).*

[36]. http://www.pharmacorama.com/en/Sections/Acetylcholine.php, *(2007).*

[37]. http://www.cnsforum.com/imagebank/section/Dementia_Cholinergic/default.aspx, *(2007).*

[38]. www.dns.ed.ac.uk/teaching.html, *(2007).*

[39]. http://www.mrothery.co.uk/studentswork/synapses%20and%20drugs.ppt#260, *(2007).*

[40]. Purves, Dale; Augustine, George J.; Fitzpatrick, David; Katz, Lawrence C.; LaMantia, Anthony-Samuel; McNamara, James O.; Williams, S. Mark., *Neuroscience* Sunderland (MA): Sinauer Associates, Inc. ; (*c2001).*

[41]. Herholz K., Heiss, W.D., "Positron Emission Tomography in Clinical Neurology", *Molecular Imag. Biol*, *(2004)*, 6(4):239-269.

[42]. Carpinelli A, Magni F, Cattaneo A, Matarrese M, Turolla E, Todde S, Bosso N, Galli Kienle M, Fazio F., "Improved synthesis and radiolabeling of [11C]MP4A, a suitable ligand for the investigation of the cholinergic system using PET", *Appl Radiat Isot. (2006)* Feb;64(2):182-6.

[43]. Arai H., Kosaka k., Muramoto O., Moroji T., Iizuka R., "A biochemical study of cholinergic neurons in the post mortem brains from the patient with alzheimer-type dementia." *Clin Neurol* (Tokyo*)(1984)*; 24:1128-1135.

[44]. Eggers C, Szelies B, Bauer B, Wienhard K, Schroder H, Herholz K, Heiss WD., "Imaging of acetylcholine esterase activity in brainstem nuclei involved in regulation of sleep and wakefulness", *Eur J Neurol. (2007)* Jun;14(6):690-3.

[45]. Lammertsma A. and Hume S. P., "Simplified reference tissue model for pet receptor studies", *NeuroImage*, *(1996)* 4, 153-58.

[46]. Blumqvist G., " On the construction of functional maps in positron emission tomography", *J. Cereb. Blood Flow Metab*, *(1984),* 4:629-632

[47]. Carson E., Cobelli C "Modelling methodology for physiology and medicine", Academis Press, San Diego, CA, USA, *(2001).*

[48]. Koeppe RA, Frey KA, Snyder SE, Kuhl DE, "Kinetic modeling of N-[11C]methylpiperidin-4-yl propionate: alternatives for analysis of an irreversible positron emission tomography trace for measurement of acetylcholinesterase activity in human brain", *J Cereb Blood Flow Metab.*, (1999) ,19(10):1150-63.

[49]. Mesulam MM, Geula C, "Acetylcholinesterase-rich neurons of the human cerebral cortex: cytoarchitectocnic and ontogenetic patterns of distribution", *J. Comp Neurol* (1991), 306: 193-220.

[50]. Mesulam MM, Geula C, "Overlap between acetylcholinesterase-rich and cholin acetyltransferase-positive (cholinergic) axons in human cerebral cortex", *Brain Res*, (1992), 577: 112-120.

[51]. Geula C, Mesulam MM, "Cholinergic systems and related neuropathological predilection patterns in Alzheimer disease", in Terry RD, et al(eds) Alzheimer Disease, Raven Press, New York, (1994), pp 263-291.

Acknowledgments

It was a pleasure for me to work with all the wonderful people from Padua University and from PET Unit of San Raffaele Hospital in Milan.

First of all, I would like to thank Prof. Claudio Cobelli and Prof. Maria Carla Gilardi for their support and for giving me the chance to visit several interesting conferences.

A special thank to Dr. Alessandra Bertoldo. Her ideas and support had a major influence on this thesis. She spent a lot of time advising me: I learned a lot during this time and I am convinced that this knowledge will help me in the future.

Many thanks to Dr. Rosamaria Moresco that was so kind during my permanence in Milan group. I am happy to have had such a supportive collaborator.

I would like to thank Karl Herholz, MD for reviewing my thesis. I enjoyed his interest in my research as well as his useful suggestion.

My thanks to Dr. Andrea Caumo, a wonderful friend and collaborator: thank you for sharing with me the wonderful world of mathematical modeling for biological system.

My thanks to my friends and colleagues from Padua for the great time I had in the group. I enjoyed the atmosphere, their friendship, and their

support. Thank you all. A special thank to my dear friend Giulia for her friendship, hospitality and almost daily sharing.

My thanks to my friend and colleagues from Milan for the great collaboration over the years (especially for your understanding in the last month of my PhD). It was a pleasure to work with all these people and to benefit from their knowledge. Especially, I would like to thank Giovanna for the “brainstorming” in moments of engineering doubts. Many thanks to Lorena, for the wonderful technical support and for lifetime discussion. And thank you Deby, Dany and all of you guys that shared lunch, coffee/tea break and for the cool time we had at LITA.

Additionally, I would like to thank several people that encourage me always: my friends Anna and Marco(*2), Andreia and Tudor.

My grateful thanks to my family who supported me with all I have done during my life. Thank you Mama, Toto, Mami, Tati: you are always in my thoughs and heart. My thanks for my parents in low for their love and support.

Last but not least, I wish to thank my husband Anto for always loving, supporting me and for enjoying life together with me.